

**POLITECNICO DI TORINO**

Collegio di Ingegneria Chimica e dei Materiali

**Corso di Laurea Magistrale  
in Ingegneria Chimica e dei Processi Sostenibili**

Tesi di Laurea Magistrale

**VOC Abatement with Mixed Oxide  
Catalysts**



**Academic Tutors**

prof. Marco Piumetti  
prof. Samir Bensaid  
prof. Nunzio Russo

**Candidate**

MARIN FIGUEREDO, Miguel José

March 2018

## DEDICATION

*Above everything I dedicate this work to God for allowing me to be in this world, being my companion and guide into every challenge I take and for surrounding me with the most amazing family and friends someone could ask for. With you by my side everything in life is possible.*

*To Maritza and Ivan, my mom and dad, who brought me into this world and were always there for me in the best and in the hardest of times. You both are who have always given me the strength and inspiration to keep working for my dreams. Your love and help has been infinite, always encouraging me to success in everything I start. I love you with all my heart.*

*To Bella, Ryan and Carlianys. All the work I do, and everything I put my mind into is always in the desire of helping to build a better and a fair world for angels like you. I hope you apologize me if this work has kept me apart from you.*

*To Ivan Jose. You have always been more than my brother, you have been a counselor and an example for me to follow. This work is also for you for believing in me and helping me to reach it from the very beginning.*

*Miguel J Marin F*

*March 14<sup>th</sup>, 2018*

## ACKNOWLEDGEMENTS

Thank you, God. For giving me patience, strength and wisdom along my life and in this academic path.

Thank you, mom. You have always been my mentor, an example to follow, a great woman and even more than what I my words can express. Saying “I love you” is nothing compared to what I feel for you.

Thank you, dad. You have always been supportive, loving and a great father. This achievement is also yours for all the effort you put all these years into raising me and Ivan Jose. I love you so much dad.

Thank you, Ivan Jose. You helped me in everything and your support and love have been essential. There are not enough words to tell you how grateful I am.

To the Universidad Central de Venezuela and the Politecnico di Torino, for giving me excellent studying conditions, the best professors and mentors and for giving me the opportunity to grow up personally and meet friends that will surely last a lifetime. Additionally, for giving me the opportunity of being part of the Double Degree Agreement and representing the good talent that Venezuela has to offer and to learn about the Italian culture.

To my tutor Marco Piumetti for giving me this great opportunity, of making research on such an amazing thesis topic. I learned much more than what I could have imagined.

I thank my co-tutor Samir Bensaid as well and the PhD students, particularly Tahrizi, for helping and supporting me through the realization of this work.

To Gabriela, Luis and Ivonne. You have been my brother and sisters through all these years, my companions, my friends, mostly everything. When things were good, when things were not so good, every time you were there for me since our childhood. Maritza one, you also helped in this path of becoming and engineer. I thank you all for that. I love you so much.

To all my cousins, specially to Johanlyb and Johanna. You were all like my brothers and sisters and I am sure that who I am right now is because you were more than inspiring to me, you were the best example to follow.

To Roxana and Maria, you were the best friends that the UCV gave me, I love you so much and I hope that we can reunite soon.

To Gabriel, Barbara, Alexander and Victor. You, and many others were more than supportive and good friends in this path, I hope our friendship will last for long.

To my aunts and uncles, all of you put a little piece on me to build this dream and who I am. I thank you dearly for that and for the love you always gave me. Parties, meetings, dinner with all of you may have remained in the past, but is very alive in my memory, and even more now that I am far away from you.

*Miguel Marin*

## ABSTRACT

A set of binary and ternary (Cu and Mn) cerium mixed oxide catalysts with different Ce-to-metal ratios were prepared via Solution Combustion synthesis using urea as the fuel for the reaction. The catalysts were characterized using different physicochemical techniques such as N<sub>2</sub> physisorption at -196 °C, x-ray diffraction (XRD), field-emission scanning electron microscopy (FESEM) and H<sub>2</sub>-temperature-programmed reduction (H<sub>2</sub>-TPR). Catalytic activity testing with VOC oxidation reactions was performed in a classical temperature-programmed oxidation (TPO) setup. Ethylene and propylene were used as the probe molecules for the VOC abatement. The test was carried out isothermally at various temperatures between ambient temperature and 350 °C. The gas hourly space velocity (GHSV) was maintained at 20,000 h<sup>-1</sup> and the amount of catalyst embedded in the reactor was 0.1 g. A mixture of 500 ppm-vol of VOC and 10%-vol of O<sub>2</sub> in N<sub>2</sub> was continuously flowed through the reactor during the test. It has been observed that the catalyst containing only MnO<sub>x</sub> clusters interacting with CeO<sub>2</sub> is the most active towards VOC total oxidation, resulting in a total conversion at 250 °C. The ternary oxide catalyst (Ce-Mn-Cu oxide) has demonstrated a higher catalytic activity than the binary copper oxide one, thus confirming the synergy between manganese and cerium. In addition, tests with lower concentration of oxygen (1%-vol) were carried on using the most active sample of every set, and the results showed that the performance of the trinary oxide and the copper binary remained almost unchanged, while the manganese binary oxide's activity had been affected.

# SOMMARIO

1. Introduzione	1
2. Sintesi dei catalizzatori e procedura	2
3. Caratterizzazione dei catalizzatori	4
3.1 Diffrazione di raggi-X	4
3.2 Morfologia e spettroscopia EDS	5
3.3 Fisisorbimento di N <sub>2</sub> a 77 K	6
3.4 Riduzione a temperatura programmata (H <sub>2</sub> -TPR)	6
4. Test catalitici	8
4.1 Ossidazione a temperatura programmata (10%-vol di O <sub>2</sub> )	8
4.1.1 Catalizzatori “freschi”	8
4.1.2 Catalizzatori “invecchiati”	10
4.2 Ossidazione a temperatura programmata (1%-vol di O <sub>2</sub> )	11
5. Conclusioni	12

## 1. Introduzione

Nell'attualità in diversi contesti, ad esempio automotive, petrolchimico, gestione rifiuti, alimentare e tante altre industrie, si sviluppano processi fisici e chimici. Ogni uno di questi si eseguono con obiettivi specifici ed è inevitabile produrre delle sostanze che possano essere dannose, tossiche o anche pericolose per quelli che stanno in contatto con loro. È questo il motivo per cui diventa sempre necessario ridurre o eliminare l'emissione di questi tipi di sostanze, attraverso sia processi fisici che chimici, e di questo modo evitare causare qualsiasi tipo di danno alla società in generale.

Tra le varie classificazioni di inquinanti che ce ne sono, c'è un gruppo di composti i quali dovuto a le loro caratteristiche fisiche e chimiche sono classificati come composti organici volatili. Secondo la nazione presa conto, quando si fa riferimento ai composti organici volatili, ogni legislazione stabilisce una descrizione particolare per questi. Ad esempio, la legislazione europea indica una definizione basata sulle caratteristiche fisiche del composto, e dice *“Composto organico volatile (COV), qualsiasi composto organico avente un punto di ebollizione iniziale pari o inferiore a 250 °C misurato ad una pressione standard di 101.3 kPa”* [2]. Così la legislazione europea considera un ampio gruppo di composti organici che potrebbero essere presenti in qualsiasi processo, caratterizzandoli attraverso una proprietà diversa dalla composizione chimica o reattività, ma attraverso una proprietà che può essere sia misurata che calcolata.

Il cerio è un elemento delle terre rare ed è stato utilizzato ampiamente nella catalisi dovuto a le sue proprietà redox quando si trova nella sua forma ionica nell'ossido di cerio (IV). Queste proprietà gli permettono di avere difetti di ione ossigeno, e questi nello stesso tempo danno alla struttura della ceria la proprietà denominata capacità d'immagazzinamento di ossigeno. Detta proprietà permette alla ceria di accumulare ossigeno quando questo si trova in elevate quantità nell'intorno reattivo, ed usarlo quando questa condizione cambia. È conosciuto che la ceria funziona attraverso il meccanismo di reazione di tipo Mars-van Krevelen, e di conseguenza è conveniente migliorare la capacità della ceria di donare gli ossigeni contenuti dentro il suo reticolo (creando dei difetti puntuali), ed anche la sua capacità di ri-ossidazione. Questo può essere raggiungibile attraverso l'aggiunta di metalli dentro del reticolo cristallino, e di quel modo inducendo i disequilibri elettronici.

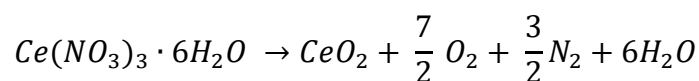
In questo lavoro si è svolto lo studio dell'attività catalitica di catalizzatori di cerio binari e ternari nell'ossidazione completa di due composti organici volatili diversi. Le molecole sonda

usate per lo studio catalitico sono state l'etilene e il propilene. Questi composti sono stati scelti come rappresentativi di un ampio gruppo di COV. Detto studio è stato fatto realizzando delle ossidazioni a temperatura programmata, stabilendo un set d'isoterme di temperatura. Questo set di catalizzatori misti, ossidi binari e ternari (Cu and Mn) di cerio, sono stati preparati utilizzando diversi rapporti Ce/metallo per svolgere lo studio della variazione dell'attività catalitica in funzione della composizione di dopaggio. I catalizzatori sono stati fatti attraverso il metodo Solution Combustion Synthesis, usando urea come combustibile per la reazione, visto che questa tecnica permette di produrre catalizzatori in tempi ridotti ed attraverso una procedura semplice.

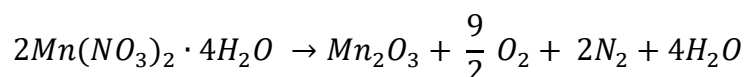
## 2. Sintesi dei catalizzatori e procedura

Le reazioni implicate nel processo sono due. La prima è la decomposizione del nitrato, la quale è caratteristica per ogni nitrato. Queste sono le seguenti:

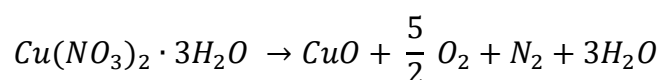
- Per il cerio



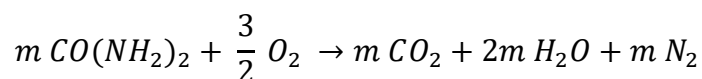
- Per il manganese



- Per il rame



La seconda reazione implicata nel processo è l'ossidazione dell'urea, descritta così:



In entrambi delle equazioni lo stato di ossidazione dell'azoto viene ridotto a zero. Il coefficiente  $m$  introdotto nell'equazione precedente definisce l'equilibrio tra le due reazioni. Questo coefficiente è allora il rapporto stechiometrico fra l'urea e il nitrato. Così, il valore di  $m$  è uguale a 15/6 quando avviene l'ossidazione del cerio o del rame, mentre che lo stesso valore nell'ossidazione del manganese diventa uguale a 10/6. Conoscendo tutti i parametri stechiometrici, sono state calcolate le quantità di reagenti necessarie per svolgere ogni sintesi, usando un eccesso di urea del 200%.

La lista seguente mostra i catalizzatori misti di cerio che sono stati sintetizzati e il corrispondente rapporto Ce/metallo utilizzato:

- Ossidi binari cerio-manganese,  $Ce_xMn_{100-x}O_y$ 
  - Dopato al 5% di Mn,  $Ce_{95}Mn_5O_y$
  - Dopato al 15% di Mn,  $Ce_{85}Mn_{15}O_y$
  - Dopato al 55% di Mn,  $Ce_{55}Mn_{45}O_y$
- Ossidi binari cerio-rame,  $Ce_xCu_{100-x}O_y$ 
  - Dopato al 5% di Cu,  $Ce_{95}Cu_5O_y$
  - Dopato al 15% di Cu,  $Ce_{85}Cu_{15}O_y$
  - Dopato al 55% di Cu,  $Ce_{55}Cu_{45}O_y$
- Ossidi ternari cerio-manganese-rame,  $Ce_xMn_{(100-x)/2}Cu_{(100-x)/2}O_y$ 
  - Dopato al 5% di Mn+Cu,  $Ce_{95}Mn_{2.5}Cu_{2.5}O_y$
  - Dopato al 15% di Mn+Cu,  $Ce_{85}Mn_{7.5}Cu_{7.5}O_y$
  - Dopato al 45% di Mn+Cu,  $Ce_{55}Mn_{22.5}Cu_{22.5}O_y$

Calcolate le quantità di nitrati necessarie per la produzione di ogni ossido, e la massa necessaria corrispondente a 200% di eccesso, la procedura svolta comprende i seguenti passi:

- a) Pesata l'urea ed il/i nitrato/i corrispondente/i usando la bilancia analitica.
- b) Dissoluzione dei reagenti in acqua deionizzata dentro un beaker, usando un agitatore magnetico e una piastra di riscaldamento con agitazione magnetica per 5 minuti a temperatura ambiente.
- c) Riscaldamento della miscela di reazione dentro un crogiolo usando un forno elettrico a muffola, stabilendo una rampa di temperatura di 10 °C, passando nella temperatura di auto ignizione della polvere e portandola fino a 650 °C.
- d) Fare la calcinazione del campione per una durata di 30 minuti a 650 °C.
- e) Raffreddamento fino a temperatura ambiente.
- f) Frantumazione e macinazione del campione con mortaio e pestello.

Dopo che sono state svolti i test catalitici ed i campioni più attivi sono stati identificati, si è realizzato un invecchiamento dei suddetti campioni, per verificare se alcun cambiamento nell'attività catalitica veniva rilevato. Questo è stato realizzato in un forno elettrico a muffola, usando una rampa programmata di 10 °C/min, partendo dalla temperatura ambiente fino a 750°C and mantenendo la temperatura per 4 ore.

### 3. Caratterizzazione dei catalizzatori

Una discussione breve delle tecniche di caratterizzazione utilizzate e i risultati ottenuti è la seguente:

#### 3.1 Diffrazione di raggi-X

Per la ceria sintetizzata, i picchi della diffrazione ottenuti evidenziano una struttura di fluorite  $Fm\bar{3}m$  caratteristica dell'ossido di cerio (IV). Questi picchi corrispondono a una struttura cubica a facce centrate (FCC), contenente di buchi ottaedrici ed esaedrici riempiti con ioni ossigeno [13].

Per la ceria dopata con manganese, nella Figura 4.1 si può vedere che mentre che il dopaggio di manganese è aumentato, i picchi più intensi rimangono rappresentativi della struttura cristallina corrispondente alla ceria. Si può anche notare che le linee di diffrazione di raggi-X si sono amplificate con l'aumento della percentuale di dopaggio, questo atteggiamento potrebbe essere legato al fatto che la quantità di cristalliti piccoli e pieni di difetti nel campione sia aumentata [17]. Una fase nuova è stata trovata per il catalizzatore dopato con manganese al 45%, il quale ha mostrato un picco a  $38.17^\circ$ . Questa fase nuova è stata associata al  $Mn_2O_3$ , il quale potrebbe essere presente dentro del campione.

La Figura 4.2 evidenzia che i campioni dopati con rame con una percentuale di dopaggio di 5% and 15% sono ancora caratterizzati dalla struttura cristallina della ceria. Invece i picchi rilevati del catalizzatore dopato al 45% mostrano la presenza di cristalli di  $CuO$ , due di questi picchi sono infatti i picchi più intensi dell'ossido di rame (II) puro. Questo risultato può indicare che potrebbe essere avvenuta la segregazione delle specie di rame nel bulk.

Nella Figura 4.3 è possibile notare che nel caso degli ossidi ternari la situazione è più complessa rispetto a quella dei catalizzatori binari. Nel catalizzatore dopato al 5% di  $Mn+Cu$  ed anche quello al 15% la struttura generalmente corrisponde a la fluorite della ceria, senza altre fasi identificabili, mostrando che entrambi i dopanti si sono integrati nel reticolo. Nel caso del campione dopato al 45% i picchi rappresentativi sono ancora quegli corrispondenti alla struttura della ceria, tuttavia picchi corrispondenti ad altri ossidi sono stati trovati. Picchi corrispondenti ad un ossido misto di rame e manganese sono stati trovati a  $35.94^\circ$  e  $63.51^\circ$ , questo fatto indica che il manganese e rame possono reagire anche fra di loro, e non solo con il cerio. Inoltre, si è trovato un picco a  $38.87^\circ$ , questo corrisponde all'ossido di rame (II). Questo ultimo risultato

suggerisce che anche le specie CuO potrebbero aversi formato durante la sintesi. Invece, nel caso dei catalizzatori invecchiati non si è rilevata nessuna nuova fase presente.

Le lunghezze di cristallo sono state calcolate usando l'equazione di Scherrer. Queste lunghezze hanno evidenziato generalmente una tendenza decrescente della lunghezza di cristallo dei catalizzatori quando la percentuale di dopaggio viene aumentata. Questo atteggiamento, accanto ai modelli ottenuti dal XRD, conferma che gli ioni  $Mn^{+3}$  and  $Cu^{+2}$  individualmente, vengono aggiunti nel reticolo della ceria di modo effettivo. Questo può essere legato a i suoi raggi ionici (0.064 nm and 0.073 nm rispettivamente) i quali sono più piccoli rispetto al raggio del  $Ce^{+4}$  (0.114 nm) [23]. Tuttavia, si è visto anche che quando i dopanti vengono introdotti insieme al 5% di concentrazione, la lunghezza di cristallo ha un atteggiamento diverso a quello generale. Detto risultato suggerisce che quando i dopanti vengono introdotti nella struttura della ceria in quelle condizioni, i rispettivi difetti di ossigeno diminuiscono e la cristallinità del campione è aumentata durante la calcinazione a cui è stato soggetto durante la sintesi. [24].

### *3.2 Morfologia e spettroscopia EDS*

La Figura 4.5 evidenzia che la  $CeO_2$  sintetizzata presenta una forma globulare di tipo spugnosa. L'immagine mostra le discontinuità presenti nel materiale ed i pori di lunghezza variabile, in tal modo la struttura del campione può essere classificata come porosa. Il diametro delle forme globulari presenti nella superficie del solido sembra di aumentare quando il dopaggio di manganese viene aumentato. Inoltre, l'immagine mostra che la struttura globulare base corrispondente alla ceria si mantiene nonostante venga aumentata la percentuale di manganese, e solo nel caso della concentrazione di Mn più elevata, le forme presenti nella struttura diventano più piane.

Le immagini dei campioni dopati con il rame che sono state analizzate mostrano che anche in questo caso la struttura principale di tipo globulare viene mantenuta, e che le forme presenti hanno anche diametri variabili come nel caso della ceria dopata al 5%. Quindi, questa struttura e atteggiamento generale, anche visto in lavori precedenti [25] si sono assunti costanti per gli altri campioni sintetizzati.

La spettrometria di raggi-X praticata ai campioni prima menzionati ha dimostrato che in ogni caso la concentrazione definita nel processo di sintesi si è raggiunta, cioè viene è concordante con la composizione atomica voluta dall'inizio.

### 3.3 Fisisorbimento di $N_2$ a 77 K

La Figura 4.10 mostra che la ceria sintetizzata ha un'isoterma di adsorbimento di tipo IV. Questo tipo è corrispondente ad adsorbenti mesoporosi, per i quali il primo adsorbimento avviene sulle pareti dei mesopori, seguito dalla condensazione capillare [17]. Inoltre, l'isoterma di adsorbimento non è limitata quando la pressione uguaglia la tensione di vapore, atteggiamento caratteristico di particelle di forma piatta con pori di forma tipo *slit*. Questo atteggiamento come adsorbente si è rilevato costante per tutti i campioni ed anche le lunghezze medie dei pori sono sempre state nel range dei mesopori.

In generale dall'andamento dell'area superficiale dei catalizzatori, si può capire che questa generalmente incrementa quando il dopaggio di manganese, rame o entrambi viene aumentato, però quando il dopaggio cresce ancora di più, il valore dell'area superficiale scende anche sotto quello della ceria. L'unico caso in cui l'andamento generale non è stato rispettato è stato nel campione dopato da Mn e Cu al 5%, atteggiamento possibilmente collegato ad una eventuale elevata cristallinità del campione.

Sono state ricavate anche le distribuzioni dei pori di ogni campione e la lunghezza di questi, e si è visto che non seguono nessun atteggiamento particolare, alcuni campioni hanno avuto distribuzioni di tipo normali, avendo la maggior parte dei pori di una stessa lunghezza, ed altri distribuzioni totalmente a caso, quindi non permettendo associarle ad alcuna condizione particolare.

Questa caratterizzazione è stata svolta anche ai campioni che sono stati invecchiati, cioè quelli dopati al 45% di ogni serie. Questo con l'obiettivo di evidenziare eventuali cambiamenti dell'area superficiale specifica, causate dal trattamento subito ad alta temperatura e lungo tempo (750 °C, 4 ore). L'informazione messa nella Tabella 4.7 conferma che l'area superficiale dai catalizzatori potrebbe essere ridotta quando vengono soggetti a temperature elevate per tempi lunghi.

### 3.4 Riduzione a temperatura programmata ( $H_2$ -TPR)

La ceria ha mostrato un ampio picco di riduzione a 548 °C, il quale può essere attribuito alla riduzione di ossigeno superficiale e sub superficiale ed alla riduzione di cerio superficiale ( $Ce^{4+} \rightarrow Ce^{3+}$ ) [26], mentre che il picco crescente localizzato oltre 700 °C è attribuito alla riduzione del cerio nel bulk.

La deconvoluzione statistica fatta per la ceria dopata di manganese al 45% mostra due picchi. Il primo centrato a 357 °C può essere associato alla riduzione dell'ossigeno adsorbito nella superficie dell'ossido misto Ce-Mn, ed il secondo centrato a 430 °C potrebbe essere attribuito alla riduzione dell'ossigeno nella superficie del reticolo dello stesso ossido misto. Inoltre, sopra i 700 °C si sviluppa un altro picco di riduzione, e questa potrebbe essere associata alla riduzione dell'ossigeno nel bulk [28].

Nel caso del catalizzatore dopato con il rame al 45%, l'approssimazione statistica evidenzia due picchi interagendo a 253 °C ed a 334 °C. Il picco a bassa temperatura potrebbe essere legato alla riduzione di cristalli di CuO, interagenti con la struttura mista della ceria, mentre che il secondo picco che avviene a temperatura più alta viene attribuito alla riduzione dell'ossido di rame ben disperso nella struttura. Osservando l'area corrispondente ai cristalli di ossido di rame, è possibile accorgersene che il loro consumo d'idrogeno è più alto rispetto quello legato alla riduzione dell'ossigeno del reticolo [25].

La ceria con dopanti misti ha mostrato un insieme di picchi attorno 200 °C. Dopo la deconvoluzione, il picco è stato separato in tre, quello che accade a bassa temperatura a 193 °C può essere attribuito alla presenza di cristalli di ossido di rame che interagiscono con le specie presenti nel campione, questo fatto fa che lo stesso ossido venga ridotto ad una temperatura più bassa rispetto all'ossido di rame puro [25]. Il secondo picco può essere legato alla presenza di cristalli d'ossido di rame-manganese ( $\text{Cu}_{1.5}\text{Mn}_{1.5}\text{O}_4$ ) presenti dentro il campione, questa specie interagendo con la struttura mista di ceria mostra il suo picco attorno ai 221 °C [29]. Finalmente, il picco centrato a 260 °C potrebbe essere legato alla riduzione dell'ossigeno presente nel reticolo della struttura mista di ceria.

**Tabella 4.8** H<sub>2</sub>-TPR consumo d'idrogeno dei catalizzatori

Catalyst	Temp. Peak 1 (°C)	Peak 1 H <sub>2</sub> -Uptake (mmol/gcat)	Temp. Peak 2 (°C)	Peak 2 H <sub>2</sub> -Uptake (mmol/gcat)	Temp. Peak 3 (°C)	Peak 3 H <sub>2</sub> -Uptake (mmol/gcat)	Total H <sub>2</sub> -uptake (mmol/gcat)
CeO <sub>2</sub>	548	0.18					0.18
Ce55Mn45	357	0.93	430	0.93			1.86
Ce55Cu45	253	2.17	334	0.83			3.01
Ce55Mn22.5Cu22.5	193	0.29	221	0.31	260	1.74	2.33
Mn <sub>2</sub> O <sub>3</sub>	365	1.81	463	4.17			5.98
CuO	308	12.57					12.57

La Tabella 4.8 mostra il consumo d'idrogeno corrispondente al campione dopato al 45% di ogni serie, ed i rispettivi ossidi base. Questa evidenza l'ordine di riducibilità dall'ossigeno presente nel bulk dei campioni, il quale secondo al tipo di dopanti segue il trend di riduzione seguente: catalizzatori ternari > catalizzatori dopati con Mn > catalizzatori dopati con Cu.

## 4. Test catalitici

Questi test consistevano nella realizzazione di una classica ossidazione a temperatura programmata (TPO), utilizzando un microreattore tubolare Quartz-U a letto fisso. Il reattore è stato messo dentro un forno a controllore PID e la temperatura è stata misurata usando una termocoppia di tipo K. Per ogni esperimento la massa usata di catalizzatore è stata di 0.1 g.

Un pretrattamento degassante è stato svolto. Questo è stato realizzato usando una portata d'elio di 15 mL/min, mantenendo una temperatura costante di 150 °C per 1 ora.

La velocità spaziale oraria (GHSV) del gas è stata di 20000 h<sup>-1</sup>, si è mantenuta identica per tutti i test. La quantità di VOC inviata nel reattore è stata 500 ppm-vol e la percentuale volumica d'ossigeno è stata mantenuta a 10% in azoto. Le stesse condizioni si sono preservate nello svolgimento dai test catalitici fatti ai catalizzatori invecchiati a 750 °C per 4 ore.

I test catalitici si sono svolti in un set di temperature, cominciando dalla temperatura ambiente, alzando fino a 50 °C e realizzando un'isoterma. In seguito, si sono realizzati ulteriori di 50 °C. In ogni gradino si sono mantenute condizioni isotermali, fino che l'equilibrio termodinamico veniva raggiunto e la conversione del composto organico volatile era stabile. Queste condizioni si sono ripetute fino ad arrivare a 350 °C, condizione nella quale si svolgeva l'ultima isoterma. Dopo questa il test catalitico veniva fermato.

Inoltre, test catalitici a bassa concentrazione d'ossigeno sono stati realizzati ai catalizzatori che hanno mostrato nella fase precedente l'attività ossidativa più elevata. Durante questi test la percentuale volumica d'ossigeno è stata mantenuta ad 1% in azoto, invece da 10%.

### 4.1 Ossidazione a temperatura programmata (10%-vol di O<sub>2</sub>)

#### 4.1.1 Catalizzatori "freschi"

Quando l'etilene è stato usato come molecola sonda, la prestazione catalitica dei campioni è stata qualitativamente simile all'ossidazione del propilene, ma questa prestazione è stata in generale ridotta, dovuto alla natura chimica dell'etilene che dà alla molecola una reattività minore in confronto con il propilene. Per questo l'andamento generale analizzato in questo riassunto è quello delle prove con l'etilene.

L'atteggiamento catalitico visto nella Figura 4.21 mostra un andamento crescente quando il dopaggio di manganese è incrementato. Mostrando che il dopaggio di manganese

migliora l'attività catalitica della ceria verso l'ossidazione d'etilene, raggiungendo il 100% di conversione a 300 °C solo con l'aumento di 5% di dopaggio con manganese.

Nella Figura 4.22 è evidenziato lo stesso andamento crescente precedente dell'attività catalitica, ma quando il contenuto di rame viene aumentato, raggiungendo per il migliore catalizzatore la conversione totale del VOC attorno a 300 °C invece che 250 °C.

La Figura 4.23 mostra che anche nel caso dei catalizzatori ternari, l'ossidazione catalitica d'etilene viene migliorata quando la percentuale di dopanti è più grande. I catalizzatori dopati al 45% mostrano di essere i più attivi in questo set di campioni. Questo atteggiamento indica che le specie presenti in questo campione potrebbero migliorare l'attività catalitica, dovuto alle interazioni che avvengono tra di loro e la struttura mista di ceria. Così, dopo ulteriore analisi delle Figure 4.21, 4.22, 4.23 si è osservato che il catalizzatore più attivo nell'ossidazione d'etilene è quello ternario dopato al 45%. Sapendo questo si può affermare che la presenza della coppia di cristalli di ossido di rame-manganese, con quelli d'ossido di rame migliorano l'attività della ceria nell'ossidazione d'etilene.

I dettagli più rilevanti delle prestazioni catalitiche per i migliori campioni sono mostrati nella seguente figura.

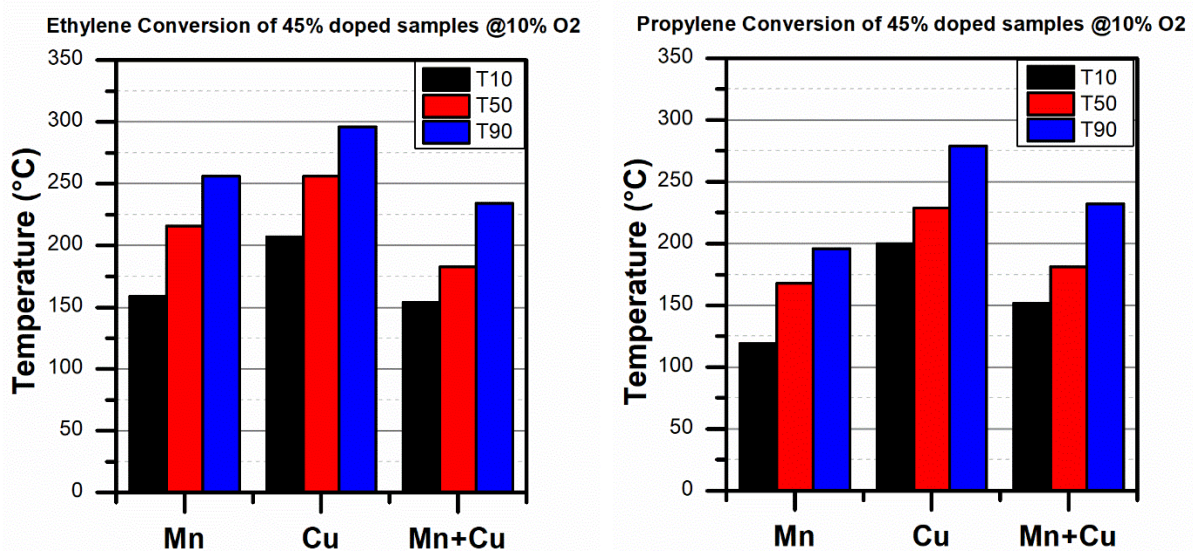


Figura 4.24 T<sub>10</sub>, T<sub>50</sub> and T<sub>90</sub> dai campioni dopati al 45% at. nell'ossidazione di COV

La Figura 4.24 evidenzia che i catalizzatori più attivi sono quelli contenenti specie di ossidi di manganese, perché il manganese riesce ad aumentare l'attività catalitica del reticolo della ceria quando vengono coppiati, ed anche quando interagisce con il rame e/o il cerio, quando stanno tutti insieme in una singola struttura.

Le velocità di reazione mostrate nella Tabella 4.9 evidenziano sono le velocità medie di reazione delle polveri sintetizzate, normalizzate in funzione della loro area superficiale specifica. Prendendo l'etilene come una molecola rappresentativa dai COV, si può dire che la presenza delle specie di manganese nel reticolo della ceria migliora effettivamente l'attività catalitica, e quando forma delle specie miste con rame, queste migliorano ancora di più le proprietà redox del catalizzatore [25,27,29].

#### 4.1.2 Catalizzatori “invecchiati”

La figura seguente mostra l'attività catalitica dei catalizzatori più attivi durante lo svolgimento delle prove termiche catalitiche.

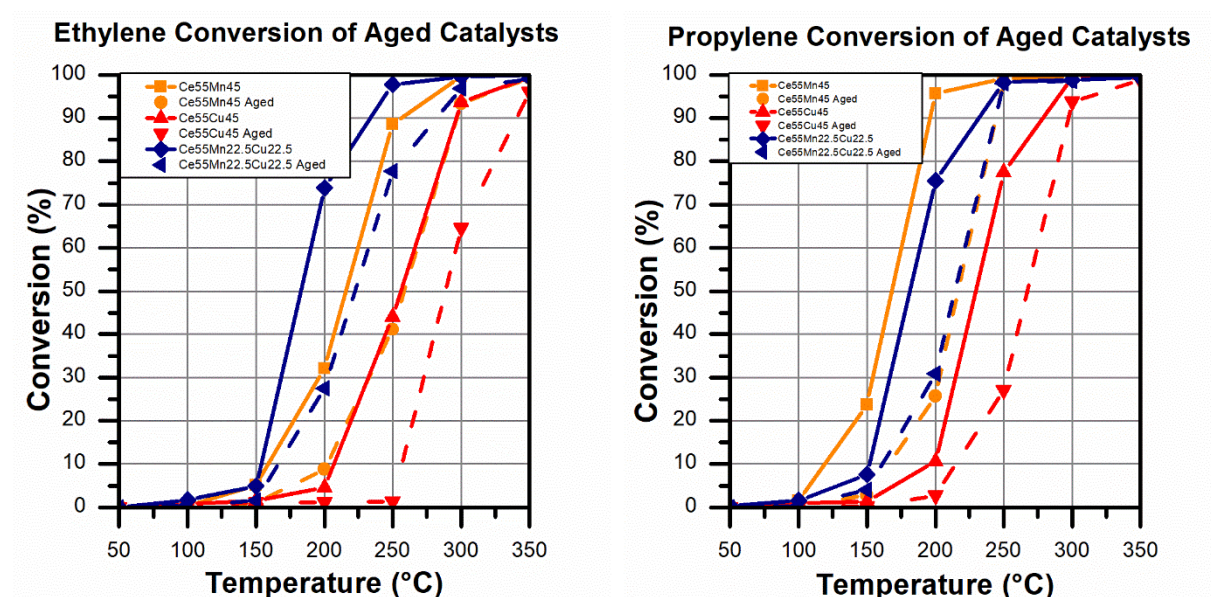


**Figura 4.25** Confronto della conversione dei catalizzatori invecchiati dopati al 45% at., durante i test per l'ossidazione dei COV a 10%-vol di O<sub>2</sub>

Gli andamenti catalitici osservati nella Figura 4.25 evidenziano che l'attività nell'ossidazione catalitica dei COV viene ridotta. Tutti i catalizzatori hanno evidenziato una diminuzione importante delle conversioni raggiunte alle stesse temperature per l'ossidazione d'etilene che per il propilene. Questo può essere attribuito alla riduzione dell'area superficiale specifica dopo l'invecchiamento. Queste area si sono ridotte di almeno 56%, come è stato evidenziato nella sezione 4.2.3 di questo lavoro. Detta riduzione diminuisce i siti attivi disponibili nel campione per svolgere l'ossidazione dei COV.

Questo andamento può essere anche legato alla sinterizzazione che potrebbe esser capitato dovuto alle elevate temperature durante il processo d'invecchiamento. Questo causerebbe un incremento nella cristallinità e una riduzione dei difetti d'ossigeno come infatti

indicano i picchi più stretti visti nello studio XRD praticato ai campioni invecchiati, e così causare anche una riduzione della capacità d'immagazzinamento d'ossigeno del catalizzatore [13,24].

#### 4.2 Ossidazione a temperatura programmata (1%-vol di O<sub>2</sub>)

Le conversioni risultanti, ottenute durante le ossidazioni catalitiche svolte ad una concentrazione di ossigeno del 1% sono mostrate nella seguente figure.

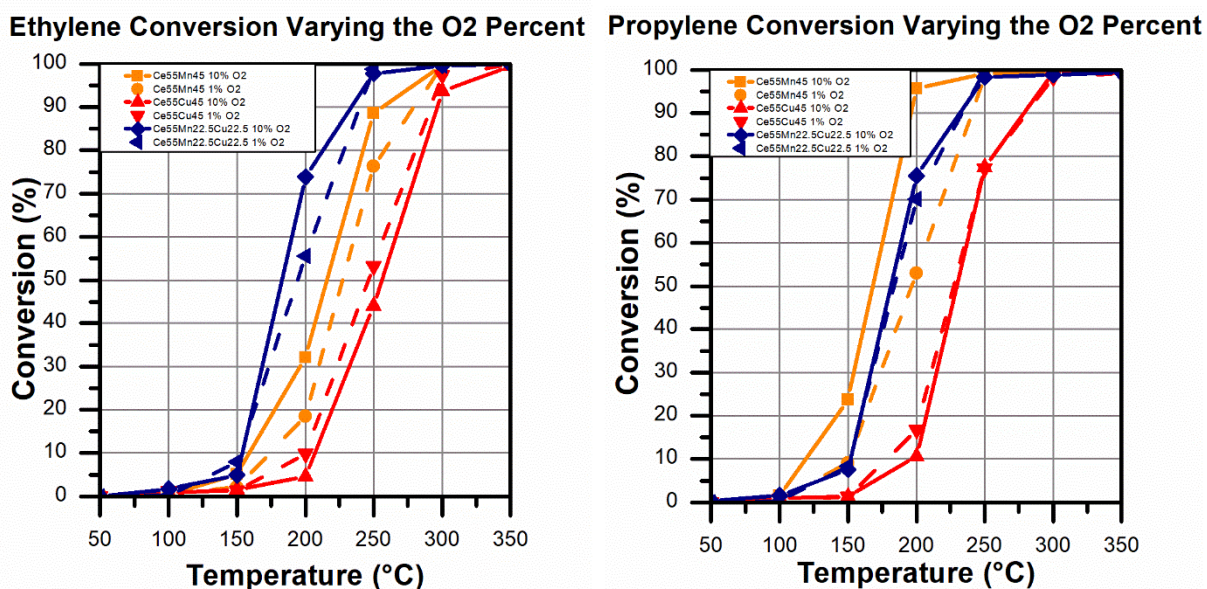


**Figura 4.26** Confronto della conversione dei catalizzatori dopati al 45% at., durante i test per l'ossidazione dei COV a 1%-vol di O<sub>2</sub>

Le conversioni mostrate nella Figura 4.26 evidenziano un trend generale, nel quale le attività dei catalizzatori viene leggermente ridotta quando l'ossigeno disponibile nella miscela reattiva è ridotto al 1% in volume. Siccome il meccanismo di reazione per la ceria pura e dopata è stato definito come quello proposto da Mars-van Krevelen in ricerche precedenti e bibliografie [25,28,29], una spiegazione a detto atteggiamento sarebbe che la specifica pressione parziale d'ossigeno in questo sistema influenza la sua incorporazione nella struttura cristallina [13], riducendo così la capacità d'immagazzinamento d'ossigeno e il suo rilascio quando l'ossidazione catalitica si svolge.

Nel caso dell'ossidazione del propilene, un cambio sostanziale dell'attività è verificato solo nel caso della ceria dopata al manganese, mentre che per gli altri catalizzatori l'attività rimane praticamente immutata. Perciò, l'analisi dell'influenza della concentrazione d'ossigeno, per i COV in generale è stata basata sui risultati ottenuti per l'ossidazione d'etilene.

Solo in un caso c'è un leggero miglioramento dell'attività catalitica, questo è per il campione dopato solo con rame. Questo fatto indica che in condizioni di bassa concentrazione d'ossigeno il reticolo misto cerio-rame potrebbe facilitare il rilascio dell'ossigeno rispetto a quando questo è in eccesso. Detto atteggiamento potrebbe essere associato coi risultati ottenuti nello studio di riduzione a temperatura programmata, nel quale il campione dopato con rame ha mostrato essere uno di quelli più riducibili sotto condizioni altamente riducenti.

## 5. Conclusioni

Dopo studio, ricerca, e analisi degli atteggiamenti catalitici e la loro relazione con le principali caratteristiche chimico-fisiche dei catalizzatori, le conclusioni di questo lavoro sperimentale sono le seguenti:

- Il manganese e/o il rame sono stati effettivamente introdotti nel reticolo della ceria attraverso la “solution combustion synthesis”
- L'aggiunta di manganese e/o rame nel reticolo della ceria potrebbe ridurre la lunghezza dei cristalliti del catalizzatore ed aumentare la sua quantità di difetti ossigeno.
- L'incremento del dopaggio di rame e/o manganese potrebbe favorire la formazione di cristalli d'ossidi puri e misti durante la sintesi.
- Dopaggio di manganese e/o rame migliora la riducibilità della struttura della ceria.
- L'incremento della percentuale di dopaggio di metalli migliora l'attività della ceria nell'ossidazione catalitica dei COV.
- Secondo la percentuale di dopante, i catalizzatori binari di Ce-Mn hanno mostrato di essere i più attivi nell'ossidazione del propilene.
- Secondo la percentuale di dopante, i catalizzatori ternari Ce-Mn-Cu hanno mostrato di essere i più attivi nell'ossidazione dell'etilene.
- I catalizzatori contenenti manganese hanno mostrato miglior prestazione catalitica rispetto quelli dopati con il rame.
- Gli ossidi misti sintetizzati potrebbero non essere stabili in ambienti con condizioni di temperatura elevata per tempi prolungati.
- L'attività catalitica degli ossidi dopati con manganese sembra ridursi in condizione di bassa concentrazione di ossigeno.
- L'attività catalitica dei catalizzatori dopati con il rame sembra migliorare in condizione di bassa concentrazione di ossigeno.

# **VOC Abatement with Mixed Oxide Catalysts**

# LIST OF CONTENTS

<b>CHAPTER I: INTRODUCTION</b>	1
1.1 Introduction	2
1.2 General Objective	4
1.3 Specific Objectives	4
<b>CHAPTER II: THEORETICAL ASPECTS</b>	5
2.1 Volatile organic compounds (VOC)	6
2.2 VOC abatement methods	7
2.3 Catalysis	11
2.3.1 Heterogeneous catalysis	11
2.4 Pure metal oxides as catalysts	15
2.5 Pure and doped ceria as catalyst	17
2.6 Catalyst characterization techniques	18
2.6.1 Surface area and porosity (BET and BJH method)	18
2.6.2 X-ray diffraction (XRD)	21
2.6.3 Field emission scanning electron microscopy (FESEM)	23
2.6.4 Temperature programmed reduction (H <sub>2</sub> -TPR)	23
2.7 Solution combustion synthesis	25
<b>CHAPTER III: EXPERIMENTAL PROCEDURE</b>	27
3.1 Introduction	28
3.2 Synthesis of catalysts	29
3.2.1 Solution Combustion Synthesis	29

3.2.2 Required materials	30
3.2.3 Synthesis procedure	31
3.3 Characterization of catalysts	33
3.4 Catalytic tests	36
<b>CHAPTER IV: RESULTS AND DISCUSSION</b>	<b>38</b>
4.1 Introduction	39
4.2 Characterization of catalysts	41
4.2.1 X-ray diffraction	41
4.2.2 Morphology and energy dispersive X-ray spectrometry	45
4.2.3 Surface area and porosity	52
4.2.4 Temperature programmed reduction (H <sub>2</sub> -TPR)	60
4.3 Catalytic oxidation tests	64
4.3.1 Temperature programmed oxidation at 10%-vol of O <sub>2</sub>	64
4.3.1.1 “Fresh” catalysts	64
4.3.1.2 “Aged” catalysts	71
4.3.2 Temperature programmed oxidation at 1%-vol of O <sub>2</sub>	72
<b>CONCLUSIONS</b>	<b>74</b>
<b>APPENDIX</b>	<b>75</b>
<b>BIBLIOGRAPHY</b>	<b>83</b>

# **CHAPTER I: INTRODUCTION**

## 1.1 Introduction

Currently in several different contexts, such as automotive, petrochemical, waste management, food and many other industries, chemical and physical processes take place. Each one of them is performed with specific objectives, and it is inevitable to produce substances which could be harmful, toxic or even dangerous for those who are in contact with them. In this sense, it is always necessary to reduce or eliminate the emission of this type of substances using either physical or chemical processes, and in that way avoid causing any kind of damage to society in general.

Between the many classifications made to all pollutants in existence, there is a group of compounds which due to their physical and chemical characteristics are classified as volatile organic compounds. At European level, and in other places of the world as well, there are already legal regulations and control over the industrial production of these substances. These are yet widely produced and usually cannot be neither easily metabolized by the human system, nor be naturally transformed into harmless substances at room conditions. That is the reason why if these substances are produced, there will always be the need of converting them into others which represent a lower risk for the people, or also reducing the emissions may be a suitable control for them.

From the ensemble of physical or chemical processes that could be used to control the VOCs, a path frequently taken to perform the abatement of volatile organic compounds is through catalytic oxidation. The utilized solid catalyst should be conveniently active, this means that it must be able to easily convert the unwanted pollutant, selective to the desired reaction and stable under working conditions for a long time. According to this, catalysts are produced to work under specific operative conditions and allow to accomplish the abatement.

Each material is adequate for specific uses, this means that it will be active, resistant, or selective in different operating conditions. Therefore, it is very important to develop new materials, which should gather the best characteristics to allow the effective conversion of the pollutants, in this case, the volatile organic compounds, in an easy, economic, and safe way.

In the past the catalytic performance of materials such as platinum, silver and other precious metals was studied because of their high catalytic activity towards different reactions,

and also because they were able to convert at low temperatures. However, their high costs and risk of poisoning by the effect of specific atoms of molecules, made compulsory the study and development of non-precious metal catalysts such as cobalt, titanium, nickel, manganese, copper, cerium and so on. Even if these might not be as active as the precious metals, these have demonstrated to be conveniently useful in the performance of different reactions, and not less importantly, they have demonstrated to be fairly resistant in a range of operative conditions.

Cerium is a rare earth element and is the most abundant of these in the earth's crust. It is an element widely studied in catalysis because of its redox properties when it is in its ionic form in the cerium (IV) oxide. Such properties eventually let it have oxygen ion defects, and these at the same time give the ceria's structure the so-called property, oxygen storage capacity. Such property allows ceria to accumulate oxygen when this is present in high quantities in the reactive environment, and to use it when such condition changes. Ceria is known to work through the Mars-Van Krevelen reaction mechanism, consequently it is desired to enhance ceria's ability to give up its lattice oxygen (creating point defects) and also its re-oxidizing capacity. Such task may be achievable through the addition of metals inside the lattice, and thereby inducing such electronic misbalances.

In this work there was performed the study of the catalytic activity of binary and ternary cerium catalysts towards the oxidation of two different volatile organic compounds. The probe molecules used for the catalytic study were the ethylene and propylene. These compounds were chosen as representatives of a wide group of VOCs. Such study was made through the realization of temperature-programmed oxidations, establishing a set of temperature isotherms. This set of binary and ternary (Cu and Mn) cerium mixed oxide catalysts were prepared with different Ce-to-metal ratios to study the catalytic activity variation in function of the doping composition. The utilized catalysts were prepared via Solution Combustion Synthesis using urea as the fuel for the reaction, since this is a technique that allows to produce catalysts in reduced time and through a simple procedure.

## **1.2 General Objective**

Evaluate the catalytic activity of mixed cerium oxides towards the oxidation of ethylene and propylene.

## **1.3 Specific Objectives**

Synthesize mixed oxide catalysts through the solution combustion synthesis.

Perform the physicochemical characterization of mixed oxide catalysts.

Study the activity of the catalysts in an oxygen reduced environment.

Evaluate the activity of mixed oxide catalysts subject to aging treatment.

## **CHAPTER II: THEORETICAL ASPECTS**

## 2.1 Volatile organic compounds (VOCs)

Through the years the term volatile organic compound has been progressively adapted with the objective of considering a group of specific substances, which are present in the atmosphere and take part in an ensemble of processes. A large number of these substances are considered to be important air pollutants, and some have also the ability of reacting in the presence of light.

Depending on the country taken in account, when making reference to volatile organic compounds, each legislation states a particular description for them. For example, the United States Environment Protection Agency (EPA), defines these compounds as follows, “*Volatile organic compounds (VOC) means any compound of carbon, excluding carbon monoxide, carbon dioxide, carbonic acid, metallic carbides or carbonates and ammonium carbonate which participates in atmospheric photochemical reactions*” [1]. In this sense, the VOC are described principally by their chemical composition and reactivity under specific conditions. Instead, the European legislation gives a definition based on physical characteristics of the compound, it states “*Volatile organic compound (VOC) means any organic compound having an initial boiling point less than or equal to 250 °C measured at a standard pressure of 101,3 kPa*” [2]. This way the European legislation gets to consider a wide group of organic compounds which could be present mainly in any process, characterizing them with a property beyond their chemical composition or reactivity, but with a property that can be either measured or calculated.

The volatile organic compounds could be classified upon two different sources, anthropogenic and biogenic. The anthropogenic VOCs are every compound produced from any activity humans related, for example industrial activities, like the exploitation of fossil fuels and their usage for transport. When talking about biogenic VOCs it means the organic compounds emitted from the Earth’s surface to the atmosphere, as a result of several process at which soil, vegetation and the oceans are involved. The common set of compounds emitted from both of these sources include many alkanes, alkenes, alkynes, aromatics, isoprenoids, terpenoids, oxygenated organic compounds, and so on [3].

## 2.2 VOC abatement methods [4][5]

There are two different approaches on which VOCs can be controlled, this could be through the installation of control equipment that allows to recover or destroy off-gas pollutants, or it could also be done by making changes to the process and/or changing the used raw materials, with the objective of eliminating or reducing drastically the generation of pollutants.

Some techniques that involve adding new equipment to the process are the following:

### 2.2.1 Thermal Oxidation

This is the technique at which combustible materials are oxidized by taking them above their autoignition temperature. In this process, enough time and oxygen are mandatory to perform a complete oxidation of the combustible to carbon dioxide and water.

The equipment used in this case is a thermal incinerator. Inside it, the combustible VOC's source is sent together with enough air (as source of oxygen), and in case it is needed, supplementary fuel. These are meant to feed a stable flame that, ensures a complete conversion to carbon dioxide and water. The four basic parameters taken in account when designing this equipment is the operative temperature, turbulence, amount of oxygen and contact time. These parameters should be optimized to destroy the pollutants with an efficiency of minimum 98%.

In a specific process, depending on the compound implied and the reaction time, the operative temperature could change. For example, when dealing with halogenated compounds the process temperature may reach 1100 °C, and a scrubber might be needed, in order to remove acid gases. To maintain this condition, it is likely the usage of high quantities of supplementary fuel, which implies an extra economic cost. This, and other reasons encourages the finding of adequate catalysts to perform this abatement at a low temperature condition.

### 2.2.2 Catalytic Oxidation

The process carried on in this case is still an oxidation analogous to the one previously described, but the main difference is that the pre heated gases are sent into a catalyst bed, which

increases the reaction rate at a lower operative temperature, fact that allows the reactors to reduce the size of the oxidizer needed.

In this case, the pollutant and the oxygen must reach the catalyst's surface through diffusion and adsorb on its active sites, afterwards the reaction occurs through a specific mechanism depending on the catalyst's nature, and then, the reaction products desorb and diffuse back into the bulk.

Depending on the compounds that must be abated, a different catalyst could be more suitable for the task than other. Generally, noble metals like platinum or palladium can be used to perform this process, because of their high activity and stability towards fouling, but when poisoning components are present in the reaction mix or if the process expenses are too high, there the use of metal oxides becomes more interesting.

### *2.2.3 Adsorption*

In this type of process, a solid is used to retain the pollutant reaching minimum capture efficiencies of 95% depending on the used adsorbent. The objective is achieved through physical adsorption, thanks to the adsorbate-adsorbent Van der Waal's forces that occur on the solid's surface, or also through chemical adsorption in the case when chemical bonds are established. Subsequently, the pollutant can be recovered from the adsorbent through several techniques.

The recovery of the pollutant from the adsorbent can be made through three different regeneration methods. When the bond established is not very strong a vacuum system could be used in order to perform the separation. It is also possible to use the denominated pressure swing method, at which two columns operate simultaneously one of the adsorbing, while the other is being regenerated using a low-pressure stream. Finally, when the bond between the species is strong the regeneration method would be to use a high temperature stream causing what is defined thermal swing and desorbing the pollutant from the solid.

The solid used for this abatement should have affinity with the pollutants molecule for their interaction to occur. In addition, the adsorbent usually is highly porous, characteristic that ensures a high rate of adsorption inside internal cavities, at which not only physical adsorption occurs, but capillary condensation as well, having then a second capture mechanism.

The most common solid used in the industry to perform the adsorption of VOCs is the activated carbon, logically because of its low cost, high surface area, and also because the low cost of regeneration through heating, respect to the costs of supplementary fuel that must be used in the thermal oxidation method. The disadvantage of activated carbon is that it is not completely hydrophobic nor hydrophilic, and that is why often its saturates with water and needs to be replaced. At industrial level also hydrophobic zeolites or polymeric adsorbents could be used, this due to their low sensitivity to humidity, that makes them less vulnerable than activated carbon.

#### *2.2.4 Absorption*

To perform the absorption of a pollutant the removing media is a liquid, which traps the pollutant through physical dilution, or via chemical reaction. In the light of this, the solvent used in an absorption system must have affinity with the pollutant. When designing such system, it is necessary the availability of the equilibrium data of the solute/solvent system, which may be scarce for unusual organic solvents.

It must be taken into consideration, that when the concentration of the pollutant on the stream is fairly low, long contact times and high quantities of adsorbent are necessary, raising the costs to carry on this separation technique, and therefore making mandatory to contemplate the need of regenerating the adsorbent.

#### *2.2.5 Condensation*

As the title indicates, in this process the objective is to liquefy the organic pollutant from a vapor phase stream. This may be performed at constant pressure by reducing the temperature of the stream that contains the pollutant until its liquefaction is achieved, process which is commonly defined as refrigerated condensation. Also, the process can be accomplished by incrementing the system's pressure at a given temperature, process defined as compression condensation.

To perform the separation of a condensable substance, it is necessary to bring the steam's temperature to the dew point, at which the partial pressure of the pollutant is equivalent

to its vapor pressure. This means that in the presence of low boiling point substances, a refrigeration system is needed to reach inferior temperatures, and therefore fulfill the separation.

### *2.2.6 Flares*

When no supplementary fuel is needed, it is common to use a flare to perform the oxidation of organic pollutants. It is a technique typically used in safety systems designed to incinerate large volumes of gas and it is able to control mostly any volatile organic compound, except from the halogenated substances. The device must every time have a turned-on flame pilot, and the precise dimensions to facilitate the correct operation when an emergency shows up.

An industrial example where flares are the typical safety device to prevent emergencies is the petroleum refineries or the petrochemical facilities, where flares are designed to process the combustible extents inside the productive lines. In this sense, the versatility and simplicity of flares makes them the easiest choice when selecting a VOC controlling system, but the possible production of smoke, heat radiation and light must always be considered.

Briefly resumed the main characteristics of these abatement methods, it becomes evident the necessity of developing new materials used as catalysts, with the objective of encouraging the use and improvement of the catalytic oxidation technique, since it would be able to convert these substances at a lower energy expense if compared with thermal oxidation or without the use of chemical solvents as in the absorption process. Depending on the process and the substances involved, it would likely be required to regenerate an exhausted catalyst, and in this sense, it will be always necessary to develop either optimum materials and operate in the precise conditions to extend the catalyst lifetime.

## 2.3 Catalysis

For centuries, mankind could tell that there existed processes that happened, or others which were fastened, only by ensuring the presence of specific substances with a given composition or surface. These substances could take the shape of atoms or simple molecules, or even complex structures such as enzymes or high surfaced solids like zeolites [6]. This phenomenon, in which a substance acts as a promoter of a chemical reaction, in other words, leading to the decomposition of matter, is the first understanding of catalysis, made by Berzelius in 1835. In that process the promoter, therefore defined as catalyst, remains unaffected in terms of its mass, from the beginning until the end of the process, and accelerates the rate of a reaction; definition given by Ostwald thirty years later [7].

Resuming the steps in which a reaction takes place in the presence of a catalyst, it is always necessary that the reactant gets in contact with the catalyst, establishing a bond with it, and then the transformation occurs. Usually, an intermediate reaction product is formed and then the latter converts to the final product. After this, the product's bond with the catalyst is broken and they separate from each other.

When a compound is decomposed, the atoms of the reactant separate from each other, producing two or more species, and so that occurs when more than one are present in the reaction media, at least one of them should get in contact with the catalyst in order for the reaction to take place.

### *2.3.1 Heterogeneous catalysis*

When a catalytic reaction is occurring, and the present catalyst is on a different state of matter than the one of the reactants, typically gas or liquid-state reactants and solid-state catalyst, there we are before a heterogeneous catalytic system, therefore the case is described as heterogeneous catalysis.

In a catalytic system there are several steps that occur for the reaction to happen, these steps are usually called mechanism. First the reactants contained in the bulk must reach the catalyst's external surface through a diffusive moto. Then the reactants should still diffuse

inside the internal porosity of the catalyst until they reach the catalyst's active sites. These sites are defined active because they represent the available or reachable positions over the catalyst's surface. Subsequently, the reactants adsorb on the active sites and are able to react. After the reaction is finished the product(s) desorb from the surface and diffuse out of the porosities of the catalyst, for then finally diffuse back to the flow's bulk. In the light of this, it is always necessary to identify which one of the steps previously mentioned is the slowest, or in other terms the controlling step, because it will define reaction rate of the global process [8].

As reported in the previous lines, it is possible that the adsorption and desorption of the reactants might be important steps in the reaction mechanism. This process is indeed characteristic of the interaction that occur between the adsorbate and the adsorbent, thereby it is pertinent to categorize the adsorption isotherms. The latter are also interesting because they provide information about the solid's pores.

Porous solids are categorized by their pore length. A microporous solid is one which pores' length doesn't go over 2 nm. Then, a macroporous solid is one which pores' length are superior to 50 nm, and if the size is in between the previously mentioned, the solid is categorized as mesoporous.

The Figure 1.1 shows the classification of the physisorption isotherms according to the International Union of Pure Applied Chemistry (IUPAC)

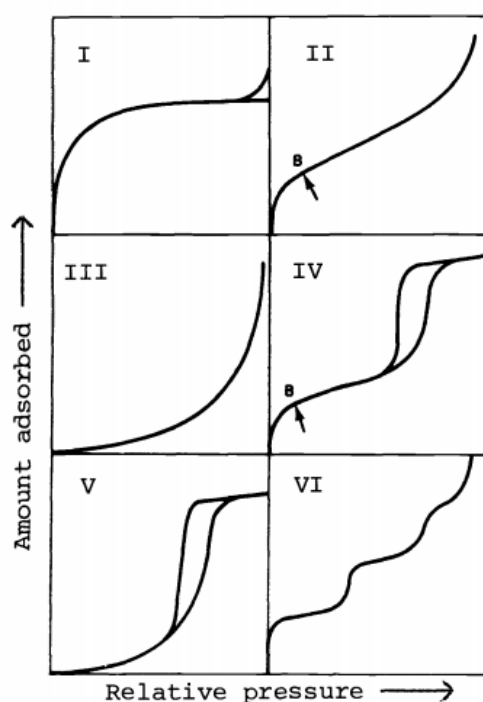


**Figure 1.1** Types of physisorption isotherms [9]

Isotherm type I are obtained for microporous solids with small external surfaces. In this case the limiting uptake is governed by the accessibility to the internal pores.

Isotherm type II is the characteristic behavior of non-porous or macroporous adsorbents. In this case the uptake is unlimited, then the monolayer-multilayer adsorption is very high, and the B point is taken to indicate the moment at which monolayer coverage is full and the multilayer is adsorption is starting.

Isotherm type III is obtained for non-porous solids that exhibit weak adsorbent-adsorbate interactions in comparison with the interactions between the adsorbate's molecules themselves.

Isotherm type IV is related to the isotherm type II and is obtained for mesoporous systems. The characteristic hysteresis loop indicates the limited uptake and is usually with capillary condensation occurring at mesopores.

Isotherm type V is related to the isotherm type III, because the adsorbate-adsorbent interactions are weak and can be obtained with porous adsorbents.

Isotherm type VI are typical of a homogeneous surface solid, because it shows the stepwise formation of the adsorption layers. The height of the steps is then representative of the capacity of each adsorbed layer.

There are several industrial processes which without the action of a catalyst possibly would not be carried on. This could be due to necessary severe operative conditions related to the implied reactions, or also because the selectivity to desired products is low and instead, the production goes towards byproducts or wastes. These catalytic processes are present for example in the petroleum or petrochemical industry, naming the catalytic cracking of crude oil, for which zeolites could be used, or also the catalytic reforming with platinum as the typical catalyst, and so on.

In any type of industry, it is also very common to produce pollutants that must be controlled under every country's national regulations. As of an example there could be taken the nitrogen oxides, which should be reduced to molecular nitrogen, usually made through selective catalytic reduction, or the carbon monoxide that has to be oxidized to carbon dioxide because of its toxicity. These are both produced in the automotive sector, but talking about general industrial emissions, to these pollutants there could be added the volatile organic

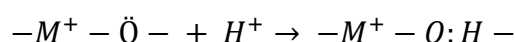
compounds, which are harmful and must be reduced to very low concentrations, and the catalytic oxidation is a common path taken to accomplish this task. For it, several materials are effective, as of an example there are the noble metal catalysts, which are in fact very active and selective, but regrettably feasible to deactivate by poisoning under certain conditions; versus materials based on transition metal oxides that even if they could be quite less active, they are indeed more resistant to poisoning [7].

## 2.4 Pure metal oxides as catalysts [7,10,11,12]

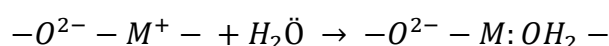
Metal oxides could be either bulk catalysts or catalyst's supports and their activity is related to the acidity behavior of the species in the lattice, these species are the metal itself and the oxygen and they are described as ions. The metal, the cation, surrounds itself with the anions, the oxygen, in order to reduce the repulsion force that exists between same charge particles. Representatively, the formed structure is then as follows:



At each part of the structure's surface there are different acidic behaviors. The oxide ion, by means of its two unpaired electrons is capable of receiving a proton, therefore behaving as a base according to Brønsted-Lowry acidity theory.

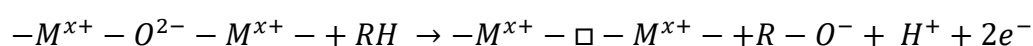


Instead, the metal having an empty space to receive a pair of electrons, behaves as a Lewis acid. As of an example:

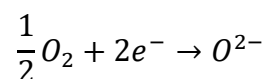


These behaviors are relevant when other compounds adsorb on the solid's surface, for the adsorbate is able to attract oxygen from other molecules to its structural defects, fixing them or also attracting other molecules, and forming coordinate bonds and then splitting the former molecule. This acid-base characteristic is exploited for example for the catalytic cracking at industrial level.

On the other hand, the metal has the ability to be reduced by receiving electrons from the oxide ion. This often occurs in several heterogeneous catalytic reactions and is the basic characteristic in the Mars-Van Krevelen reaction mechanism. It is also defined as the redox mechanism, because it is separated in two steps. First, the nucleophilic oxidation of the adsorbed hydrocarbon by the oxide ion in the lattice takes place, and then it is transferred through the gas/solid interface leaving an empty space in the lattice.



Subsequently, the cycle is closed with the second step, when the empty oxygen space is regenerated with an oxide ion produced by the reduction of the molecular oxygen present in the gas phase as follows:



Catalytic oxidation of several VOCs over different metal oxides has been suggested to occur through the Mars-van Krevelen mechanism, as of an example there a kinetic study of toluene oxidation over Mn<sub>1.5</sub>Cu<sub>1.5</sub>O<sub>4</sub>, where it was demonstrated that the power law model and the Langmuir model do not represent properly the oxidation of toluene over the catalyst's surface.

## 2.5 Pure and doped ceria as catalyst [13,14,15]

Cerium is the most abundant from the rare earth elements in the earth's crust and has two valence states Ce(III) and Ce(IV). Metallic cerium is thermodynamically unstable and in presence of oxygen reacts to form its oxidized forms  $\text{Ce}_2\text{O}_3$  and  $\text{CeO}_2$ . Also,  $\text{Ce}_2\text{O}_3$  is capable of reacting in the presence of an extremely low concentration of oxygen, thereby being the cerium (IV) oxide (ceria) the most stable of the species.

Ceria crystallites have the fluorite structure, characterized by a face-centered unit cell with a cell parameter  $a=0.5411$  nm. In this structure, the cerium cation is placed in the center of the cube surrounded by eight oxygen anions. The extended structure that includes the oxygen cubes at each corner, reveals oxygen cubic cells alternating with centered coordination sites that are empty and then replenished again with a cerium cation, representing consequently point defects or a non-perfect stoichiometry of the structure.

When involved in redox processes ceria is reduced. This aspect has been studied through different techniques, one example is the  $\text{H}_2$ -TPR, which has shown that ceria can be reduced in the presence of hydrogen at high temperature. During the process, the oxygen in the ceria lattice causes an electronic misbalance and then leaves the structure, provoking an oxygen defect. During this process the cerium species are reduced from  $\text{Ce}^{+4}$  to  $\text{Ce}^{+3}$ .

Realizing that the Mars-Van Krevelen reaction mechanism may be the one involved in VOCs oxidation processes, the reducibility of the cations and the oxygen storage capacity become important characteristics for the used catalyst. Studies have found that the rate determining step in oxidation processes is the rate at which oxygen leaves the lattice, thereby if this property is enhanced the catalytic performance may also be improved. Such research has shown that doping ceria with divalent or trivalent cations increase the oxygen defects in the lattice, consequently rising the oxygen storage capacity of the catalyst and improving its reducibility. When this situation occurs between two or more oxides the catalytic activity may improve, showing a synergistic effect between the reduced elements.

## 2.6 Catalyst characterization techniques [7,16,17,18,19]

In catalytic studies it is mandatory to know the main physicochemical characteristics of the catalyst, in order to correlate them with the catalyst's activity. Carrying out this, may allow the optimization of specific characteristics that would enhance the catalyst's performance at given conditions.

One of the characteristics that is often taken into account is the specific surface area (SSA), because of its determining role in the adsorption of the reactants. Together with the latter, morphology and the internal porous structure of the catalyst is examined, to study possible molecular selectivity of the structure, thus the eventual reachability of active sites.

Studying the crystalline structure of the solid is often practiced. A catalyst's crystal planes, and their geometry, is a characteristic that plays an important role in the adsorption and the reactivity of a catalyst.

The following techniques are often utilized to measure and analyze a group of important physicochemical properties:

### 2.6.1 Surface area and porosity (BET and BJH method)

The typical method utilized in order to determine the specific surface area is the low temperature physisorption of a gas. This method follows the theory proposed by Brunauer, Emmett and Teller (BET).

The theory established by BET comprise a group of assumptions to calculate the SSA, then it is necessary to fulfill these conditions before confirming a measured BET surface area. These assumptions are the following:

- The physisorption forces are similar to those responsible of condensation.
- Langmuir's kinetic treatment may be applied to the adsorbed layers.
- Multilayer adsorption. Representing every molecule in the inferior layer the available group of sites of adsorption for the molecules in the superior layer.

- The energy of adsorption in every layer (except the one over the solid) is equal to the energy of liquefaction of the gas, thus in the equilibrium the adsorption (condensation) rate is equal to the desorption (evaporation) rate.

It is necessary to transform the adsorption isotherm into the BET plot. The latter is dependent of the relative pressure and the BET monolayer capacity, and it is this last parameter the one useful to calculate the BET surface area.

In the steady-state each layer is described by the following equation:

$$a_i * p * \theta_{i-1} = b_i * \theta_i * \exp\left(\frac{-E_i}{RT}\right)$$

Where:

$p$ : Equilibrium pressure

$a_i, b_i$ : Adsorption and desorption constants

$\theta_{i-1}$ : Fraction of surface covered by the  $i-1$ th layer

$\theta_i$ : Fraction of surface covered by the  $i$ th layer

$E_i$ : Energy of adsorption of the  $i$ th layer

$R$ : Ideal gas constant

$T$ : Temperature

To simplify the summation of the amounts adsorbed, it was assumed that the layers after the first have the same energy of adsorption, thus the liquefaction energy ( $E_L$ ). Additionally, assuming that the multilayer has an infinite thickness when the pressure ( $p$ ) is equivalent to the saturation pressure ( $p^0$ ), the BET equations was then defined as follows:

$$\frac{\left(\frac{p}{p^0}\right)}{\left[n\left(\frac{1-p}{p^0}\right)\right]} = \left(\frac{1}{n_m C}\right) + \left[\frac{(C-1)}{n_m C}\right]\left(\frac{p}{p^0}\right)$$

Where:

$n$ : Amount of gas adsorbed by unit mass of adsorbent

$n_m$ : Monolayer capacity

$C$ : Empirical constant

The  $C$  constant according to the original theory is related to the energy of adsorption according to the following equation:

$$C = \exp \left[ \frac{(E_1 - E_L)}{RT} \right]$$

Finally, the BET equation plotted versus  $(p/p^0)$  is linear, allowing to find the value of the monolayer capacity, through which the surface area can be calculated assuming the value of the occupied area of each molecule. The equation that expresses this correlation is the next:

$$a_{BET} = n_m * L * \sigma$$

Where:

$a_{BET}$ : Specific surface area

$L$ : Avogadro constant

$\sigma$ : Area occupied by the adsorbate molecule

To study the porosity one of the methods widely used is the one proposed by Barrett, Joyner and Halenda (BJH). The latter is based on the assumption that pores are cylindrical, and that these are filled upon the condensation of the adsorbate. This behavior is based on the Kelvin's equation as follows:

$$r_k = - \frac{2\gamma v_l}{RT} \ln \left( \frac{p}{p^0} \right)$$

Where:

$r_k$ : Kelvin radius

$v_l$ : Molar volume of the condensate

$\gamma$ : Surface tension of the liquid condensate

In the procedure the pores are emptied by a defined reduction of the relative pressure and considering the size variation of the multilayer. Then the pore size distribution is expressed as the variation of the pore volume in function of the variation of the pore radius, versus the pore radius. As of an example, the Figure 1.2 shows the pore distribution of ceria doped with copper at 5%.

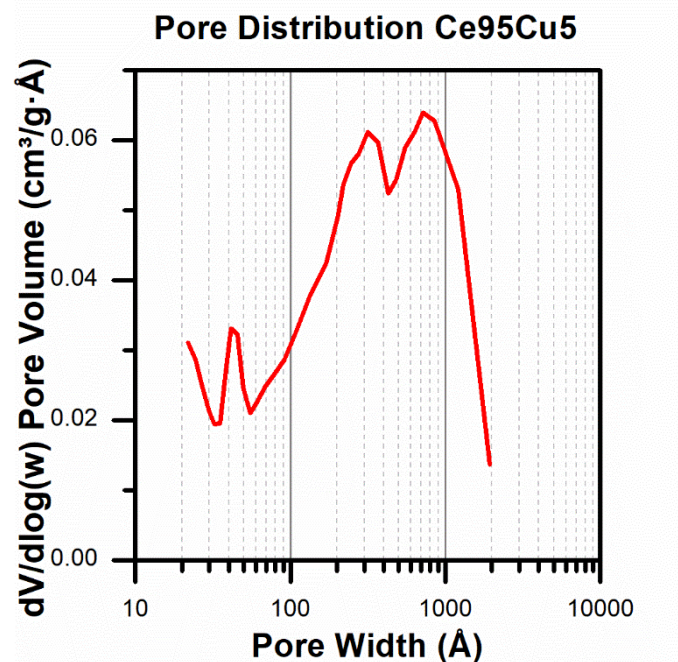


Figure 1.2 Pore distribution of 5% copper doped ceria

### 2.6.2 X-Ray Diffraction (XRD)

This is a characterization technique that provides information about the crystalline structure of the catalyst. It is widely used when any solid is synthesized in order to identify whether the obtained result is what was expected or if the obtained phase is rather something else. This analysis correlates the diffraction of an X-ray beam to the spacing between planes through Bragg's law. The latter is expressed through the next formula:

$$2d \sin \theta = n\lambda$$

Where:

$d$ : Spacing between atomic planes

$\theta$ : Angle of incidence

$n$ : Positive integers

$\lambda$ : Incident wavelength

Each plane present in the crystalline structure is represented with a set of coordinates that indicate the orientation of the planes. Using the d-spacing formulas corresponding to each

structure (such as cubic, tetragonal, orthorhombic, etc.), the cell parameter, and the position of a given peak, it is possible to determine the miller indices of the plane related to that peak.

It is possible to realize a qualitative phase analysis of the sample by making a comparison with a database. In this case, if the atomic composition is known, the phases can be identified by comparing the sample's relative peak intensities and their positions with the reference compounds contained in a commercial database.

When the material set to XRD analysis contains small and defect-rich crystallites the X-ray diffraction lines are subject to an important broadening a qualitative phase analysis is complexed.

As of a quantitative analysis from the collected pattern it is necessary to calculate the scattering power of the diffraction lines of one phase. Thereby, by calculating the area under each peak, the latter is proportional to the scattering power of the diffraction line.

In order to analyze the peaks' profile and quantify the lattice most important parameters, the position of the diffraction line, as well as the location of its maximum are required. Then, the full width of intensity distribution at half maximum  $\Gamma$  (FWHM) is one measure of the peak's breadth. The FWHM can then be used to calculate the crystallite size through the Scherrer formula as follows:

$$\langle L \rangle = \frac{k\lambda}{\Gamma \cos \theta_0}$$

Where:

$\langle L \rangle$ : Average crystallite size

$k$ : Constant dependent of the crystallite's shape

$\lambda$ : X-ray wavelength

$\Gamma$ : Diffraction width

$\theta_0$ : Bragg angle

This equation is based on the assumption that the shape of the peak is dominated by size effects and correlates the diffraction width and the average size of crystallites.

### *2.6.3 Field emission scanning electron microscopy (FESEM)*

When studying a solid's morphology, the field emission scanning electron microscope is capable of supplying high resolution images.

In this technique an electron beam is sent towards the sample's surface. The energy content, thereby the wavelength of these electrons, changes according to the potential difference applied upon them. When the electron beam interacts with the sample, a set of events can take place. As of an example there could be the emission of light, also electrons rejected back from the surface, and so on. One particularly convenient event is the emission of X-rays that can be used to perform an elemental analysis, called energy dispersive X-ray spectrometry (EDS)

When such electron beam interacts with the sample's atoms, secondary electrons are emitted. These are detected and are used to generate the images corresponding to the morphology. Such images provide a set of useful information, like the surface structure, also the shape and size of the features on it.

If the analyzed samples are able to conduct electricity, the resulting images improve, and that is the reason why to improve the obtained results a conductive metal coating may be set on the solid's surface. Such layer is very thin and can be made through several methods.

### *2.6.4 Temperature programmed reduction (H<sub>2</sub>-TPR)*

It is a thermoanalytical technique in which the reducibility of a sample can be studied. In the experiment the sample is put inside a tubular reactor, where it is bound to be reduced by a gas flow, for example H<sub>2</sub>-N<sub>2</sub> or H<sub>2</sub>-Ar, while it is subject to a programmed linear increase of the temperature. In the outlet of the reaction system, there is set a thermal conductivity detector (TCD) that aids in the determination of the outlet gas composition.

Schematically seen, the main event occurring in the process is the reaction that takes place between the hydrogen in the reducing gas flow and the reducible part of the sample at a high temperature. In this sense, if the temperature is raised enough, the moles of reducible species are reduced to zero by the end of the analysis. Then, when the reduction rate of the reducible species reaches its maximum, the signal of the detector also shows the maximum intensity at the same temperature.

When the analyzed sample is a bulk reducible solid, such as metallic oxides, the reductive process can be modelled mathematically as a spherical shaped oxide reacting with gaseous hydrogen as follows:

$$\frac{d\alpha}{dT} = \frac{k_{N_0} A}{\beta} (1 - \alpha) \exp\left(\frac{-E_N}{RT}\right)$$

Where:

$\alpha$ : Degree of reduction

$k_{N_0}$ : Pre-exponential factor

A: Surface area

$E_N$ : Activation energy

This model is controlled by the formation of the first product's nuclei, therefore the formation of the lattice of the reduced oxide, or the pure metal. While these nuclei continue to grow the reaction rate increases as well, and when they are big enough to reach the surface, the reaction rate starts to decrease. Finally, when the metal coat thickness is big enough and the reaction rate is lowering, the last is supposed to be proportional to the specific surface area. This is equivalent to the contracting sphere model as follows:

$$\frac{d\alpha}{dT} = kS$$

Where:

$k$ : Kinetic constant

$S$ : Specific surface area

Then by assuming a geometric relation between the area  $S$  and the degree of reduction with the initial specific surface area, an expression for a dynamic TPR can be obtained, as follows:

$$\frac{d\alpha}{dT} = \frac{S_0 k_0}{\beta} (1 - \alpha)^{\frac{2}{3}} \exp\left(\frac{-E_N}{RT}\right)$$

Where:

$S_0$ : Initial specific surface area

## 2.7 Solution combustion synthesis [20,21,22]

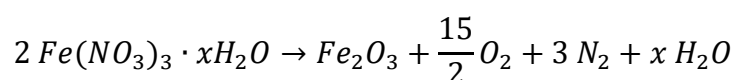
In literature, a combustion synthesis (SC), or also defined self-propagating high-temperature synthesis (SHS), indicates a process at which the reduction of a catalyst precursor is carried on by its self-ignition at high temperature, in the presence of a determined fuel.

The precursor utilized generally is the metal nitrate. The latter is bound to be reduced by the heat generated from the oxidation reaction of an organic molecule. Often the organic fuel selected are either urea or glycine because they act as complexing agents of the metal in solution, besides of generating the needed energy for the combustion of the nitrates.

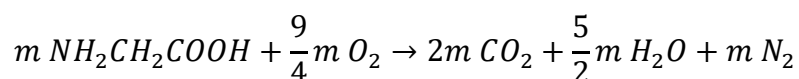
The reaction is highly exothermic, temperatures over 1000 °C are reached in very short times. It also provides the required energy for the oxidation to occur, and more, therefore this is a self-sustainable process that doesn't require external heating. The temperature reached in the system during the combustion is dependent of the used quantity of fuel, since the reaction can be carried out in fuel lean conditions, stoichiometric or fuel rich. The maximum combustion temperature is reached in the condition at which the fuel is fed stoichiometrically.

A suitable example of the reactions implied in this synthesis procedure could be the production of ferric oxide using glycine as follows:

For the iron:



For the glycine:



The coefficient  $m$  must then balance the ensemble of redox equations for the charge of the products must be neutral.

During the synthesis, the metal nitrate and the fuel are dissolved in water with the objective of assuring the mixing at molecular level and the concentration uniformity of the reactive mix. The solution is dried until the reaction mix is crystallized. Such crystallites auto

ignite at a specific temperature depending on the utilized fuel, after which the combustion begins, and the temperature rises rapidly, forming the metal oxide and the gases.

The formed gases can be controlled through the fuel/nitrate ratio, such gases limit the further increase of the temperature, thereby avoiding the sintering possibilities of the early synthesized powder. Additionally, these generate passages inside the material that could increase its porosity and limit the growth of the clusters. Consequently, the gas production is a determining factor that must be taken in account and, if possible controlled, in order to produce an oxide with given characteristics.

Considering that the synthesis technique brings the reaction temperature at such high values allows to obtain a product of high purity and crystalline, avoiding the need of calcination as a post synthesis treatment and that the time required for each synthesis is reduced makes the solution combustion synthesis a remarkable technique to produce nanomaterials useful in catalysis.

## **CHAPTER III: EXPERIMENTAL PROCEDURE**

### 3.1 Introduction

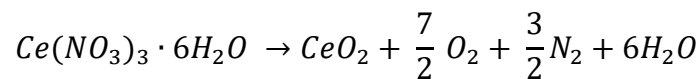
The experimental part of this work may be divided into three main parts. The first part included the synthesis of catalysts that have the ability of oxidizing two probe molecules, ethylene and propylene, since both are representative of a group of volatile organic compounds. Varying the Ce-to-metal ratio, the aim was to produce binary and ternary cerium oxides which can perform the catalytic oxidation of the mentioned molecules at low temperatures, selective towards complete oxidation to carbon dioxide and water, and resistant to fouling by high temperature, and the solution combustion synthesis offers the possibility of producing active catalysts in a reduced time and through a simple process. The second part consisted in the characterization of the produced catalyst's physicochemical properties through four different techniques, the N<sub>2</sub> physisorption at -196 °C, X-ray diffraction (XRD), field-emission scanning electron microscopy (FESEM) and H<sub>2</sub>-temperature programmed reduction. Finally, the third part consisted in the performing of catalytic oxidation tests in a specific temperature range. There was realized the catalytic tests of the fresh catalysts at two different oxygen percentages to evaluate the general performance at either rich or reduced oxygen conditions, using for the oxygen reduced test the most active catalyst of each set. In addition, fouling by temperature was induced to the best catalyst of each set, and they were tested to determine the change in its activity.

## 3.2 Synthesis of Catalysts

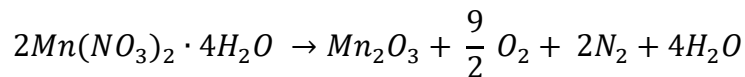
### 3.2.1 Solution Combustion Synthesis

In the synthesis procedure of the oxides, the precursor materials are the corresponding nitrates of each metal, using urea as the fuel for the oxidation. Consequently, the reactions implied in the process are two. The first one is the nitrate decomposition, that is of course characteristic for every nitrate. These are the following:

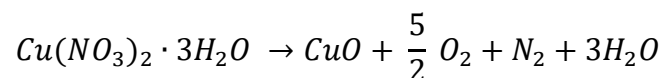
- For the cerium



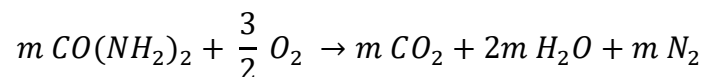
- For the manganese



- For the copper



The second reaction implied in the process is the oxidation of urea, described as follows:



In both equations nitrogen's oxidation states is reduced to zero. The coefficient  $m$  introduced in the former equation defines the equilibrium between the two reactions. Such coefficient is then the stoichiometric ratio between urea and the nitrate. Subsequently, the value of  $m$  is equal to 15/6 when the oxidation of cerium or copper is carried on. Instead the latter value for the manganese oxidation is equal to 10/6. Knowing all the stoichiometric parameters, the quantities of reagent required to perform each synthesis were calculated, and the oxidation were performed with a 200% of fuel excess.

### 3.2.2 Required materials

The following list of materials were used along the synthesis phase of this thesis:

- Glassware
  - Beaker 250 mL.
  - Graduated cylinder 100 mL.
- Miscellaneous
  - Spatula.
  - Deionized water
  - Stir bar.
  - Melting pot.
  - Mortar and pestle
- Chemical reagents
  - Cerium (III) nitrate hexahydrate, REacton; 99.3% (REO)  
Alfa Aesar  
 $\text{Ce}(\text{NO}_3)_3 \cdot 6\text{H}_2\text{O}$
  - Manganese (II) nitrate tetrahydrate  
Sigma-Aldrich  
 $\text{MnN}_2\text{O}_6 \cdot 4\text{H}_2\text{O}$
  - Copper (II) nitrate trihydrate, puriss. p.a.; 99-104%  
Sigma-Aldrich  
 $\text{CuN}_2\text{O}_6 \cdot 3\text{H}_2\text{O}$
  - Urea, ACS reagent; 99.0-100.5%  
Sigma-Aldrich  
 $\text{NH}_2\text{CONH}_2$
- Instruments
  - Electronic analytical balance.
  - Hot plate with magnetic stirrer.
  - Muffle furnace

### 3.2.3 Synthesis Procedure

Calculated the required quantities of nitrates to produce each oxide, and the mass of needed urea corresponding to a 200% excess, the procedure followed involved the next steps:

- g) Weighting of urea and the corresponding nitrate(s) using an electronic analytical balance.
- h) Dissolving the reagents with deionized water inside a beaker, using a stir bar and a hot plate with magnetic stirrer for 5 minutes at room temperature.
- i) Heating the reaction mix inside a melting pot using a muffle furnace, establishing a temperature ramp of 10 °C, passing by the auto-ignition temperature of the powder and bringing it until 650 °C.
- j) Performing the calcination of the sample dwelling for 30 minutes at 650 °C.
- k) Cooling at room temperature.
- l) Crushing and grinding the sample using a mortar and pestle.

Having concluded the synthesis phase the samples were held inside a covered glass bottle, setting them ready to be used for catalytic testing.

After the catalytic tests were performed and the most active samples were identified, an aging process was carried out in order to verify if there would be a catalytic activity change. The latter was realized in a muffled furnace, using a programmed ramp of 10 °C/min, starting from room temperature until 750 °C and dwelling for 4 hours.

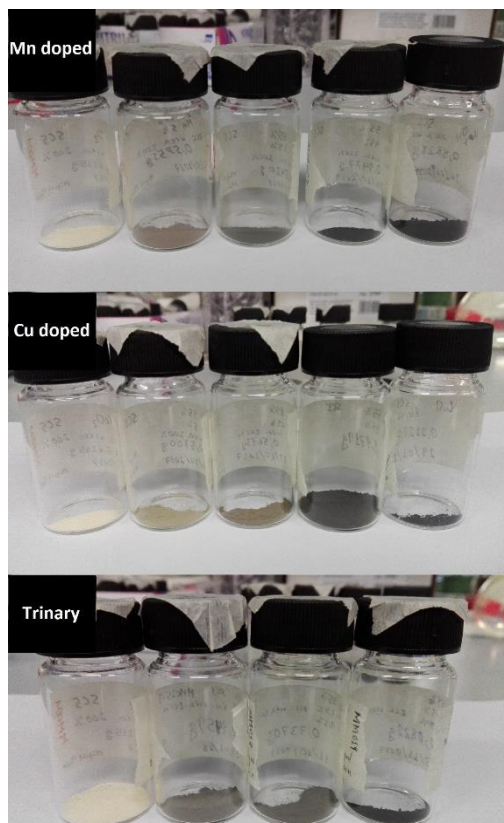


**Figure 3.1** Synthesized catalyst

Figure 3.1 shows the synthesized catalysts. In the manganese-cerium serie the doping percent increases from zero, thereby pure ceria, 5%, 15%, 45% and last 100%, thereby  $Mn_2O_3$ . The same order for the copper, being the 100% doped  $CuO$ , and finally in the bottom the trinary catalysts, where the doping percentages were the same as the binaries, each one equimolar of manganese and copper, as of an example, 5% mix doped means  $Ce_{95}Mn_{2.5}Cu_{2.5}$ .

### 3.3 Characterization of Catalysts

After the synthesis phase, in order to outline the most important characteristic of every synthesized catalyst a characterization of the main physicochemical properties was performed. In this phase the tests that were realized were the physisorption of nitrogen at  $-196\text{ }^{\circ}\text{C}$ , X-ray powder diffraction and field emission scanning electron microscopy. Additionally, after having determined the most active mixed catalysts, the  $\text{H}_2$ -temperature-programmed reduction was performed to these solids, along with the synthesized pure oxides thus cerium (IV) oxide, copper (II) oxide and the manganese (III) oxide.

A brief discussion of the utilized characterization and the conditions are the following:

#### 3.2.4.1 Nitrogen physisorption

This technique was performed with the scope of measuring the specific surface area, the specific pore volume and the pore distribution of the catalysts synthesized in the previous phase.

Before carrying on the measure, the catalyst was subject to an outgassing pretreatment process at  $200\text{ }^{\circ}\text{C}$  for 2 hours, with the objective of removing water and other atmospheric pollutants.

Afterwards, using the Micromeritics TriStar II instrument the physisorption of nitrogen over the catalyst surface was carried on. The method imposed to the machine was the Mesopore and Surface Area Analysis, which sets a pertinent number of measures.

This process was performed inside a necked burette submerged in liquid nitrogen at its boiling point. A flow of nitrogen was sent inside the burette, at a set of pressures below nitrogen's vapor pressure and the quantity adsorbed was measured for each point. With the previous information the instrument's program calculated the specific surface area according to the Brunauer, Emmett and Teller (BET) theory and also calculated the pore-size distribution and the pore volume according to the method proposed by Barrett, Joyner and Halenda (BJH).

The Figure 3.2 is a representative of the equipment used to perform the surface area analysis.



**Figure 3.2** Micromeritics TriStar II [1]

#### 3.2.4.2 X-ray diffraction

To analyze the characteristics of every catalyst's crystalline structure, there was studied how the latter diffracts an X-ray beam. This diffraction is characteristic of the crystalline structure according to Bragg's law and was used to determine the phases of the synthesized material.

The X-ray diffraction parameters were measured on a X'Pert Philips PW 3040 diffractometer using a Cu  $K_{\alpha}$  radiation and analyzing a  $2\theta$  angle range from  $20^{\circ}$  to  $80^{\circ}$ , step= $0.05^{\circ}$   $2\theta$  and time per step equal to 0.2 seconds.

Having measured the samples patterns, these were analyzed using the Powder Data File Database (PDF 2000, International Centre of Diffraction Data, Pennsylvania).

#### 3.2.4.3 Field emission scanning electron microscopy

This technique was utilized with the scope of studying the synthesized catalyst's morphology, and it was performed using a field emission scanning electronic microscope (FESEM) Zeiss Merlin, Gemini-II column. During the analysis an electron beam was sent over the samples surface, using an extra high tension (EHT) of 3 kV, a working distance (WD) of 2.8 mm and a probe intensity of 120 pA.

Additionally, the composition of the catalysts was determined through EDS analysis (Oxford X-ACT), choosing from two to three zones with a length between 5 and 25  $\mu\text{m}$ , that

were representative of each sample. Having this information, the average atomic composition of the sample was determined.

A representative image of the equipment utilized to perform the technique is showed in the Figure 3.3



**Figure 3.3** Field Emission Scanning Electron Microscope Zeiss Merlin, Gemini-II column [2]

#### 3.2.4.4 Temperature programmed reduction

To study the reducibility of the synthesized samples, temperature-programmed reductions were performed, using hydrogen 5% in argon as the reducing flow. The task was performed using a TPDRO 1100, ThermoQuest Instruments.

The sample was put inside a tubular reactor over a quartz wool bed. Such reactor was then set inside the equipment's oven. Previously to the temperature programmed analysis, the samples were subject to a pretreatment. During the latter, a helium flowrate of 40 mL/min was sent and the heating rate was 10 °C/min, going from room temperature until 550 °C and then dwelling from one hour.

After the pretreatment the sample was cooled down, and the H<sub>2</sub>-TPR was started. During the analysis the sample was subject to a hydrogen 5% in argon flow of 20 mL/min at a heating rate of 10 °C/min, starting from room temperature, until 800 °C and then dwelling for ten minutes.

### 3.4 Catalytic Tests

With the objective of examining the activity of the synthesized catalysts, a set of catalytic tests were performed. These tests consisted in a classical temperature-programmed oxidation (TPO) setup, comprising a fixed-bed Quartz U-tube microreactor. The reactor was set inside a PID-controlled furnace and the temperature was measured using a K-type thermocouple. For every experiment the utilized catalyst mass was of 0.1 g.

The system previously described is shown in the Figure 3.4.

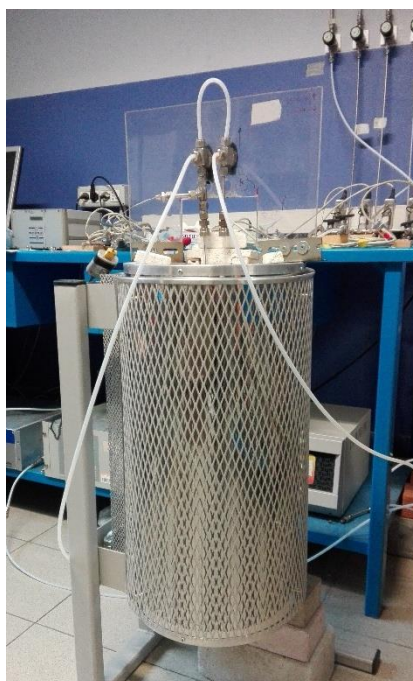


**Figure 3.4** Catalytic test system

Previously to the start of the catalytic test, with the aim of removing humidity and other atmospheric pollutants, a degassing pretreatment was performed. The latter was realized using a helium flow of 15 mL/min, maintaining a constant temperature of 150 °C for 1 hour.

Considering the varying densities of the catalysts set, the reactive mix flow was defined by maintaining an identical gas hourly space velocity (GHSV) of 2000 h<sup>-1</sup> for every test. The VOC quantity sent in the reactor was 500 ppm-vol and the oxygen volume percent was

maintained at 10% in nitrogen. The same conditions were preserved for the catalytic tests performed to the selected set of catalysts that were eventually aged at 750 °C for 4 hours.

The catalytic tests were carried out at a set of temperatures starting from ambient condition, then raising until 50 °C and carrying out an isotherm. Afterwards, temperature steps of 50 °C were performed. At each step, further isothermal conditions were maintained until the thermodynamic equilibrium was reached and the conversion of the volatile organic compound was stable. Such conditions were then repeated until arriving to 350 °C, condition at which the last isotherm was performed. After this the catalytic test were stopped.

Additionally, catalytic tests in low oxygen conditions were realized to the catalyst that showed the highest oxidation activity in the previous phase. During these set of tests, the gas hourly space velocity and the VOC quantity sent in the reactor were still 20000 h<sup>-1</sup> and 500 ppm-vol respectively, but the oxygen volume percent was set to 1% in nitrogen, instead of 10%.

## **CHAPTER IV: RESULTS AND DISCUSSION**

## 4.1 Introduction

During the experimental phase of this work a set of porous binary and ternary (Cu and Mn) cerium mixed catalysts were synthesized through the solution combustion method. Such set was formed by nine samples, each one synthesized with a different Ce-to-metal ratio. The next list shows the synthesized cerium mixed catalysts and the corresponding Ce-to-metal ratio utilized:

- Binary cerium-manganese oxides,  $Ce_xMn_{100-x}O_y$ 
  - Mn doped 5%,  $Ce_{95}Mn_5O_y$
  - Mn doped 15%,  $Ce_{85}Mn_{15}O_y$
  - Mn doped 55%,  $Ce_{55}Mn_{45}O_y$
- Binary cerium-copper oxides,  $Ce_xCu_{100-x}O_y$ 
  - Cu doped 5%,  $Ce_{95}Cu_5O_y$
  - Cu doped 15%,  $Ce_{85}Cu_{15}O_y$
  - Cu doped 55%,  $Ce_{55}Cu_{45}O_y$
- Ternary cerium-manganese-copper oxides,  $Ce_xMn_{(100-x)/2}Cu_{(100-x)/2}O_y$ 
  - Mn+Cu doped 5%,  $Ce_{95}Mn_{2.5}Cu_{2.5}O_y$
  - Mn+Cu doped 15%,  $Ce_{85}Mn_{7.5}Cu_{7.5}O_y$
  - Mn+Cu doped 45%,  $Ce_{55}Mn_{22.5}Cu_{22.5}O_y$

In addition to the previous catalysts the pure oxides of each metal were synthesized. Such synthesis products were the following:

- Cerium (IV) oxide,  $CeO_2$
- Manganese (III) oxide,  $Mn_2O_3$
- Copper (II) oxide,  $CuO$

The performed characterization tests to which the samples were subject showed in general a variation of the main physical, chemical and structural solid's characteristics, according to the doping ratio utilized on each synthesis. Changes in the samples' phases were observed in the diffraction patterns obtained through the X-ray diffraction test verifying the presence of single metal oxide clusters. Also, the samples' morphologies were examined, according to the variation of the doping composition and changes in the structure were

evidenced. Such changes were detected by the field emission scanning electron microscope that showed an evolution of the surface features as a function of the doping metal used in the synthesis.

Pore distributions of every sample showed that the synthesized samples could be categorized as mesoporous and the analysis of the surface area behavior revealed an actual variation of the latter, depending as well on the metal doping percentage.

In the study of the samples' reducibility there was evidenced that, depending on the selected sample, the species present were reduced by hydrogen at varying rates and at different temperatures. The deconvoluted peaks of the pure oxides helped in evidencing when specific reducible species corresponded to pure oxides' clusters, and to discriminate when there were new species formed by mixed metal lattices possibly acting synergistically.

The catalytic performance of the synthesized samples during the temperature programmed oxidations exhibited an evident improvement when the oxidized VOC was the propylene. Then, following the increase of the metal doping the catalytic activity in comparison with pure ceria was also studied, to evidence the rightful integration of the metals in the ceria lattice and a possible synergetic action between them. Additionally, the possibility of a change in the concentration of oxygen in the reactive mix was studied, with the objective of verifying if the catalytic activity would be affected under such conditions.

Finally, catalytic tests were also performed to a selected set of catalysts to evaluate the possible deviation of their catalytic activity, caused by the aging process to which they were submitted. The analysis of these results was realized taking in account the characterization tests that were also performed for this group of samples.

## 4.2 Characterization of catalysts

### 4.2.1 X-ray diffraction

For the synthesized ceria, the gathered diffraction patterns evidenced the Fm3m fluorite structure of cerium (IV) oxide. These peaks correspond to a face-centered-cubic structure (FCC) containing octahedral and hexahedral holes filled with oxygen ions [13].

The gathered diffraction patterns obtained during the experimental phase of this work were organized according to the doping metal and the doping percentage. The Figure 4.1 shows the gathered patterns for the manganese doped catalyst set:

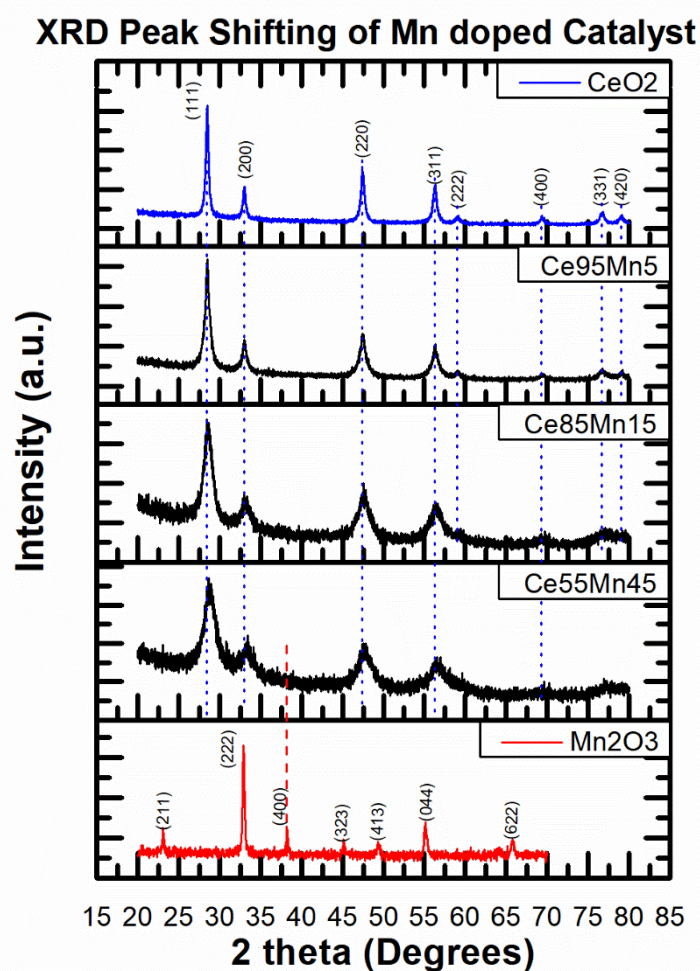


**Figure 4.1** Peak shifting of the manganese doped ceria

In the Figure 4.1 there can be seen that while the metal doping is increased, the most intense peaks remained representative of the crystal structure corresponding to ceria. It was also noticed that the X-ray diffraction lines broadened with the increase of the doping percentage, this behavior could be related to the fact that the content of small and defect-rich crystallites in the sample may have increased [17]. Such factor is also indicative of the possible increase of the sample's oxygen storage capacity [13]

Even if the qualitative evaluation of the gathered diffraction patterns was more complex while the metal doping was increased, a new phase could be retrieved for the catalyst with a 45% content of manganese, which presented a peak at 38.17°. After checking in the Powder Data File Database (PDF 2000, International Centre of Diffraction Data, Pennsylvania), it was found that this new phase may be associated to the plane identified with the miller indices of {400}, corresponding to  $Mn_2O_3$  which could be present in the bulk of the sample.

In the Figure 4.2 the retrieved patterns for the copper doped ceria are shown.

### XRD Peak Shifting of Cu doped Catalysts

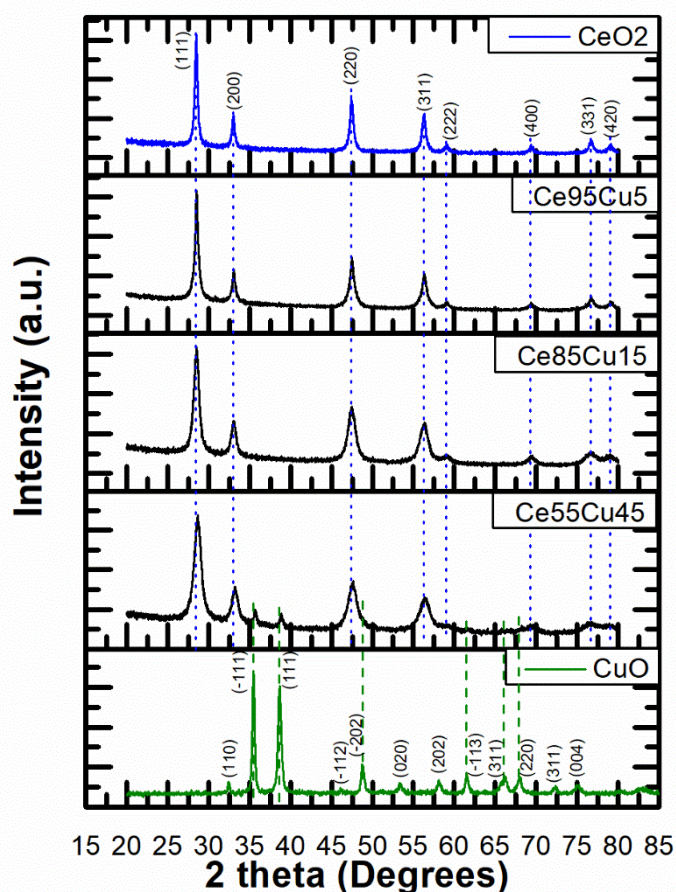
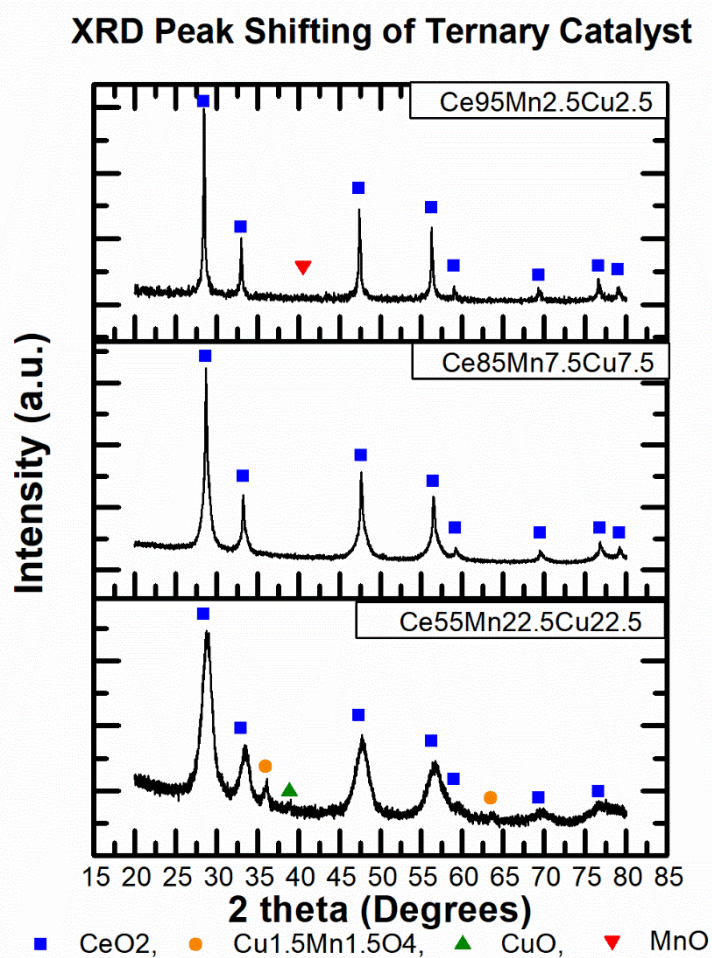


Figure 4.2 Peak shifting of the copper doped ceria

The Figure 4.2 evidences that copper doped solids with copper doping percentage of 5% and 15% are yet characterized by ceria's crystalline structure. Instead for the 45% copper doped catalyst, peaks corresponding of CuO crystals were retrieved, two of them are actually the most intense peaks of the pure copper (II) oxide. This result may evidence that segregation of the copper species have occurred in the bulk.

In the case of the copper doped solids it could also be observed that the diffraction lines broadened when the doping composition was increased as for the manganese doped catalysts.

The Figure 4.3 evidences the diffraction patterns obtained for the ternary catalysts and its corresponding analysis using the PDF 2000.



**Figure 4.3** Peak shifting of the ternary catalysts

In the Figure 4.3 it is possible to notice that for the ternary oxides the situation is more complex in comparison with the binary catalysts. In the 5% Mn+Cu doped catalyst the diffraction pattern shows a crystalline structure corresponding to the fluorite structure of the ceria, however a low intense peak was found, and during the performed analysis using the Database it was found to be characteristic of the manganese (II) oxide, showing that part of the manganese doesn't integrate in the lattice.

The sample with a total mix doping of 15% exhibits the ceria fluorite structure with no other identifiable phases, showing that both dopants are integrated in the lattice. In the case of the 45% doped sample the representative peaks are still the ones corresponding to the ceria structure, however diffraction peaks of other oxides were also found. Peaks correspondent to a mixed oxide of manganese and copper were retrieved at 35.94° and 63.51°, being the first one a representative high intensity peak of the pure copper manganese oxide, such fact shows that manganese and copper are able to oxidize between themselves and not only with cerium. Additionally, a peak at 38.87° was retrieved, and after qualitative analysis using the PDF it was found to be a peak correspondent to copper (II) oxide. This last result suggests that also CuO species may have formed during the synthesis. Instead, the XRD study performed on aged catalyst showed no variation of the phases present in the sample

Using the parameters of the most representative peaks of each sample, the crystallite sizes were calculated through the Scherrer equation. The obtained values are shown in the Table 4.1 as follows.

**Table 4.1** Catalyst's crystallite size

<b>Catalyst</b>	<b>Crystallite Size (nm)</b>
CeO <sub>2</sub>	21
Ce <sub>95</sub> Mn <sub>5</sub>	12
Ce <sub>85</sub> Mn <sub>15</sub>	7
Ce <sub>55</sub> Mn <sub>45</sub>	4
Ce <sub>95</sub> Cu <sub>5</sub>	12
Ce <sub>85</sub> Cu <sub>15</sub>	9
Ce <sub>55</sub> Cu <sub>45</sub>	9
Ce <sub>95</sub> Mn <sub>2.5</sub> Cu <sub>2.5</sub>	40
Ce <sub>85</sub> Mn <sub>7.5</sub> Cu <sub>7.5</sub>	9
Ce <sub>55</sub> Mn <sub>22.5</sub> Cu <sub>22.5</sub>	5

To evidence the behavior of this parameter the Figure 4.4 is presented next:

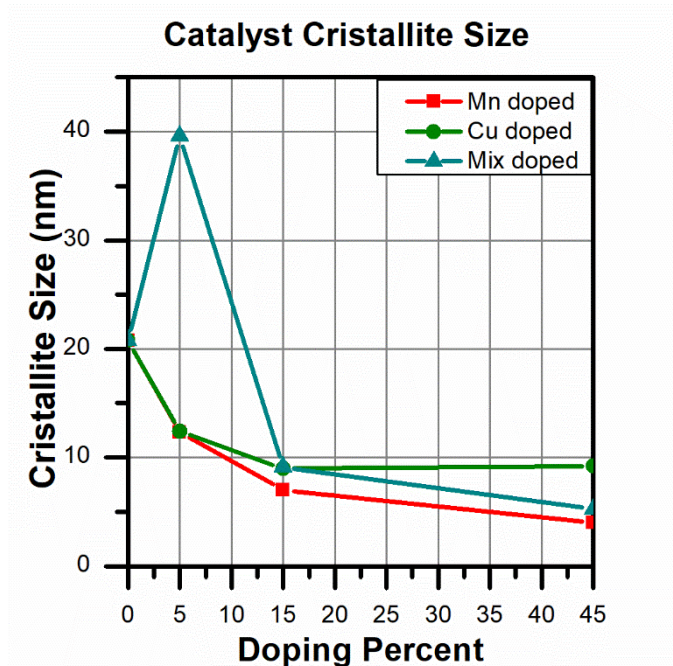
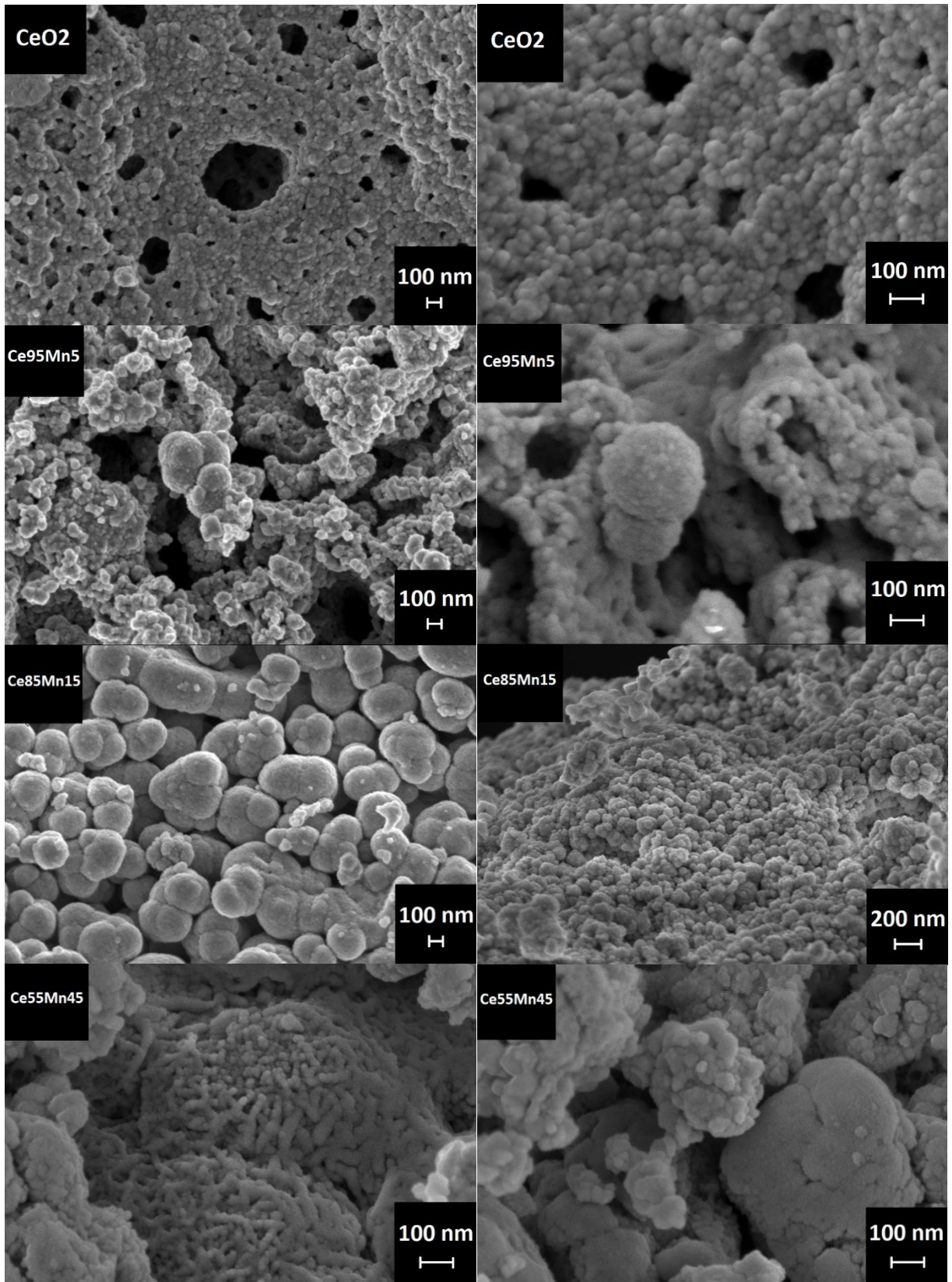


Figure 4.4 Catalyst's crystallite size

Figure 4.4 evidences a general decreasing tendency of the sample's crystallite size when the doping percentage is increased. This behavior, together with the XRD patterns confirm that the individual ions  $\text{Mn}^{+3}$  and  $\text{Cu}^{+2}$  are effectively introduced in the ceria lattice. This could be related to their ionic radii (0.064 nm and 0.073 nm respectively) which are smaller than the  $\text{Ce}^{+4}$  radius (0.114 nm) [23]. However, it can also be seen that when the dopants are coupled at 5% concentration the crystallite size has a behavior out of the general tendency. Such result suggests that when the dopants are coupled at a low percentage and are introduced in the ceria lattice, oxygen defects in the latter are diminished and the crystallinity of the sample may be enhanced at the calcination temperature used for the synthesis [24].

#### 4.2.2 Morphology and energy dispersive X-ray spectrometry

The morphology variations in a group of the synthesized catalysts, according to the present doping percentage, was evidenced in the images obtained using the field emission scanning electronic microscope. The following images are correspondent to pure ceria and the manganese-doped ceria serie.



**Figure 4.5** FESEM images of  $\text{CeO}_2$  and manganese doped samples

Figure 4.5 evidences that the synthesized  $\text{CeO}_2$  has a globular sponge-like shape. The image shows the material's discontinuities and varying size pores, thereby the solid can be classified as a porous structure. The diameter of the globular features present on the solid's surface seem to increase when the manganese doping was increased. Additionally, the image shows that the basic globular structure correspondent to ceria is maintained despite the manganese doping percentage, and only in the case with the highest content of manganese doping the features present in the structure are flatter than the ones with lower content of manganese.

The next figure evidence the morphology found for the 5% copper doped solids, together with the images correspondent to ceria for comparison.

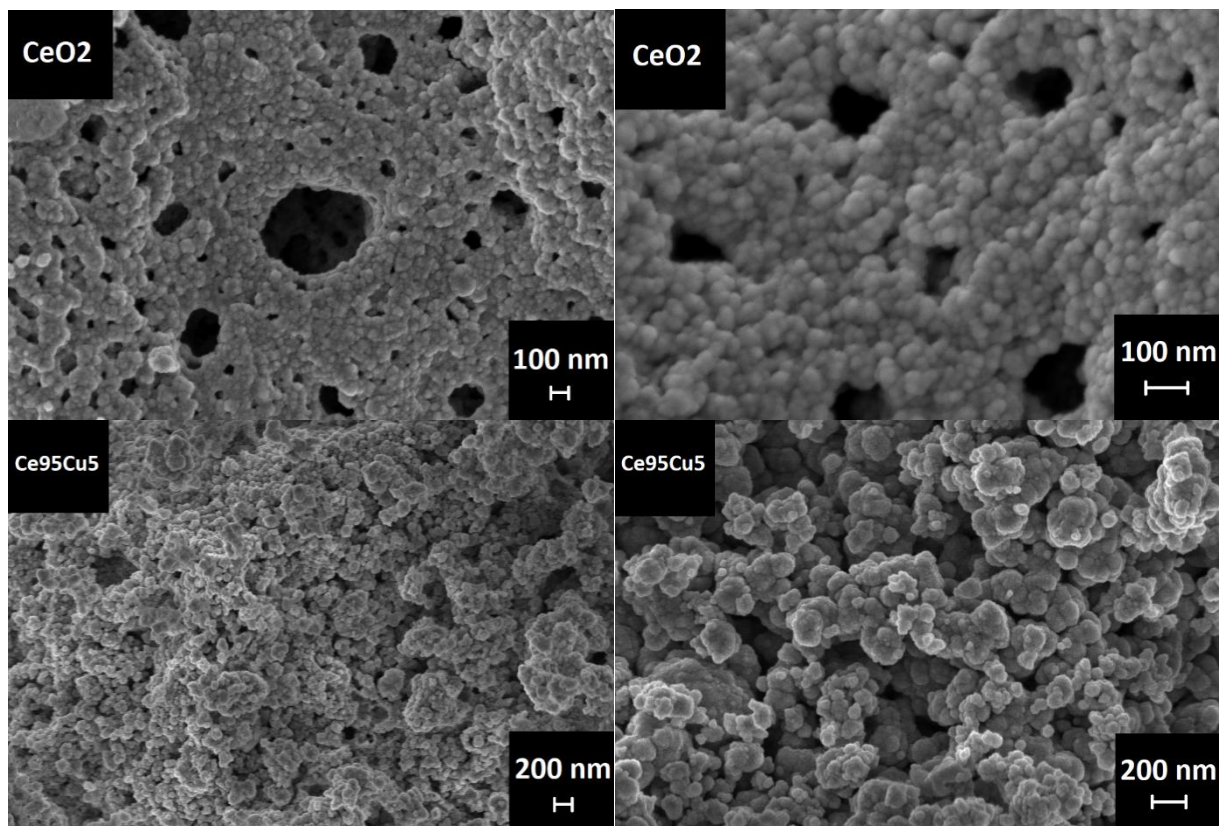


**Figure 4.6** FESEM images of  $\text{CeO}_2$  and 5% copper doped sample

The images of the analyzed copper doped solid shows that the main globular-like structure of ceria is maintained for this dopant as well, and that the features present have also variable diameters, like in the manganese 5% doped ceria. The rest of the copper doped solids

were assumed to keep a characteristic morphology trend similar to the one of the manganese doped solids, and it was confirmed by observation of a structural trend in other consulted research study [25].

For the doped samples that were analyzed, the energy dispersive X-ray spectrometry was also performed during the FESEM session. From this activity the results were the sample's spectrogram and the atomic average composition.

The representative spectrograms of the manganese doped samples are shown in the next figure:

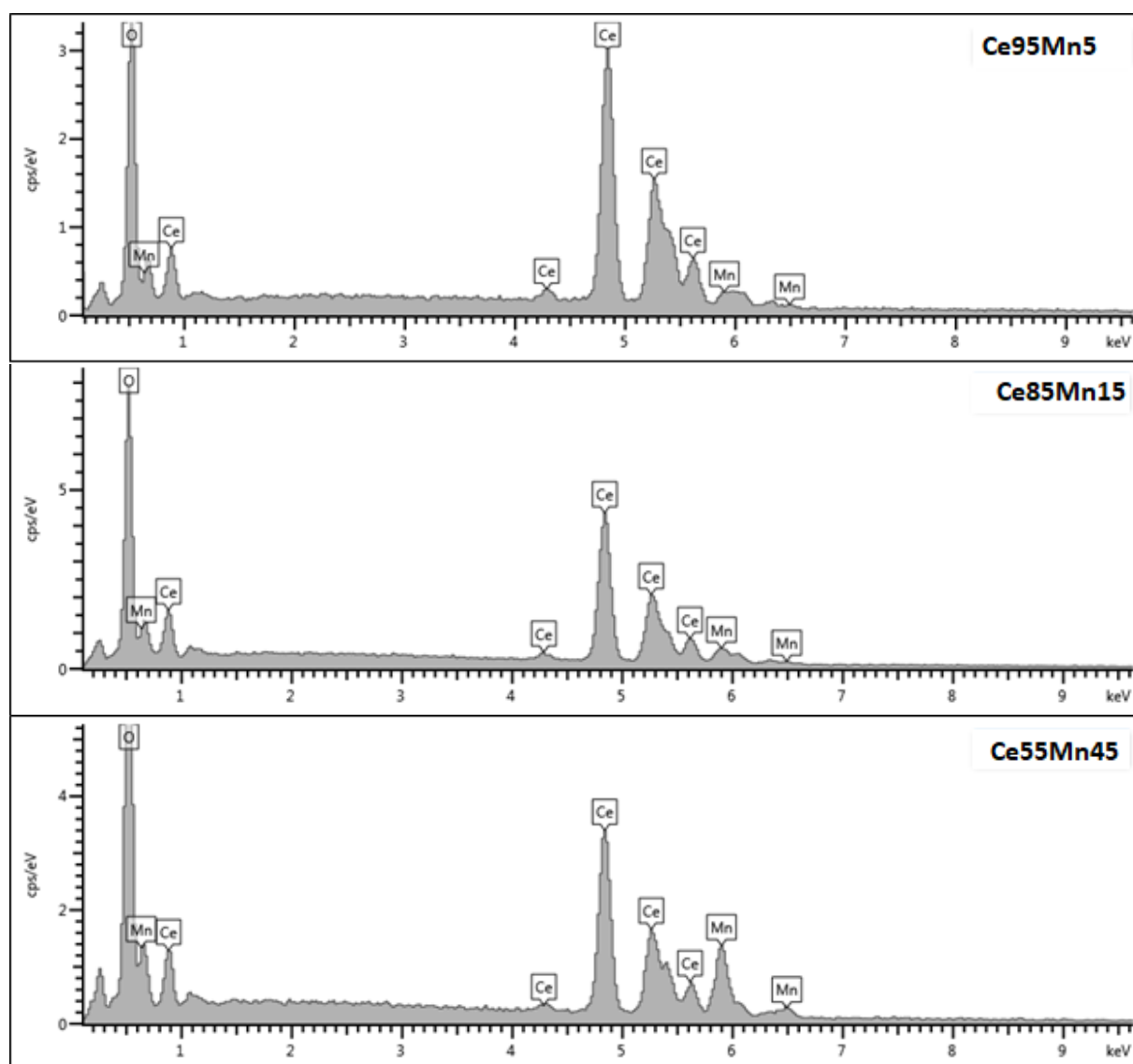


**Figure 4.6** X-ray spectrograms of manganese doped catalysts

In the Figure 4.6 it was observed the increase of the manganese peaks heights according to the increasing doping percentage, confirming the presence of the dopant in the structure. The corresponding zones of each spectrograms are shown in the next figure.

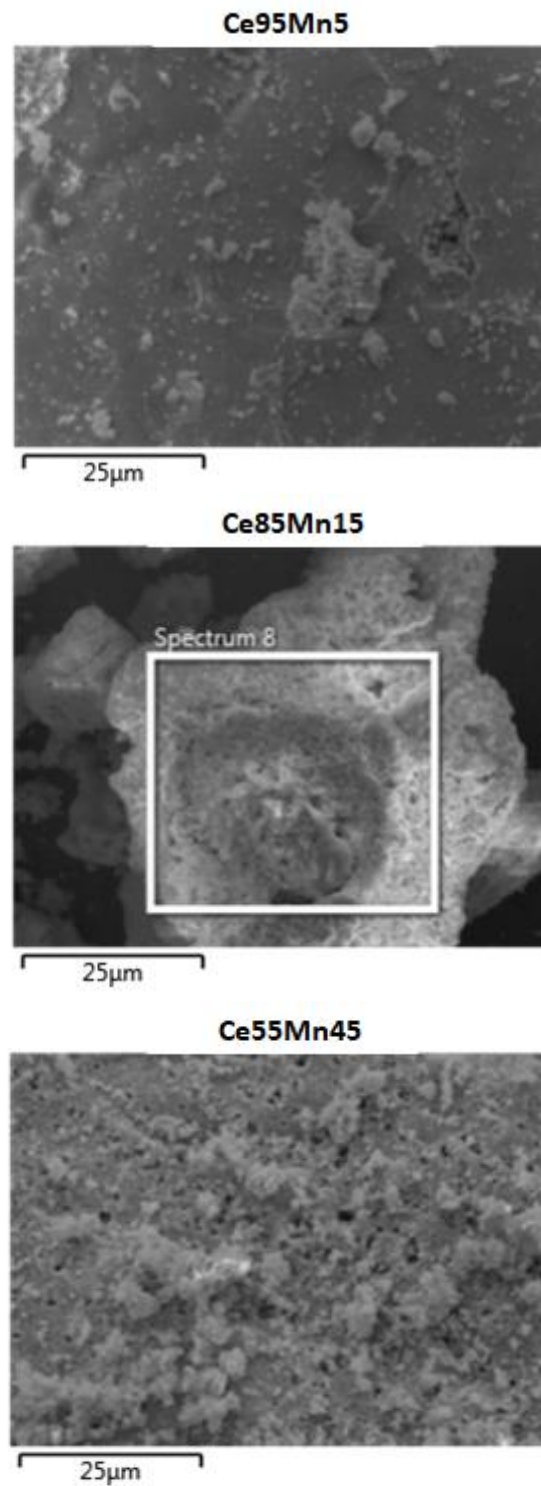


**Figure 4.7** Representative zones taken for manganese doped sample's spectrograms

The zones chosen to perform the spectrograms showed to include the most important characteristics of the studied samples. These zones, together with the other zones considered to calculate the average composition are in the appendices of this work.

The next table summarizes the determined composition of the manganese doped set

**Table 4.2** Average atomic percentage of the manganese doped catalysts

Catalyst	Element	Atomic% Media
Ce95Mn5	Ce	31.20
	Mn	1.83
	O	66.97
Ce85Mn15	Ce	23.88
	Mn	3.67
	O	72.46
Ce55Mn45	Ce	18.07
	Mn	12.10
	O	69.64

The average compositions obtained from the performed analysis show the effective increase of the manganese content in the samples. The calculated ratio between the metals confirmed that the content of dopant in the sample is consistent to the wished composition defined during the synthesis phase.

The next figure corresponds to the representative spectrogram obtained from the copper 5% doped catalyst.

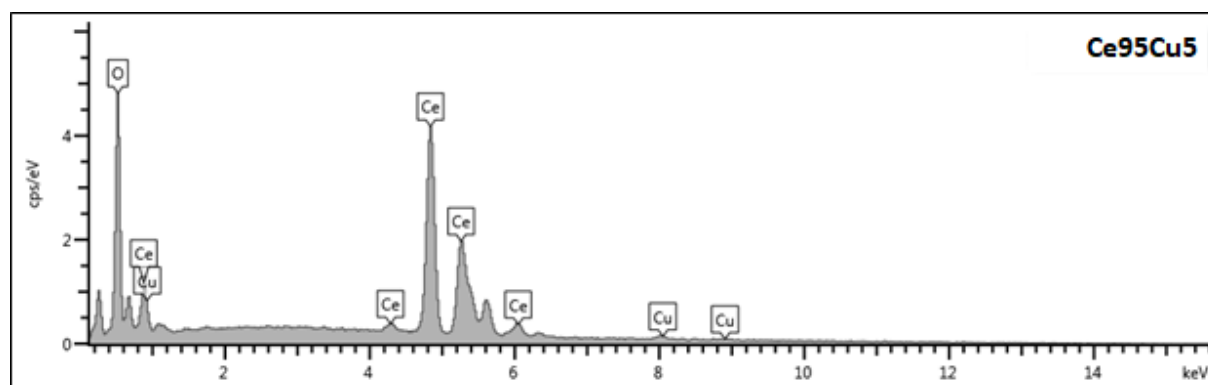


**Figure 4.8** X-ray spectrograms of copper 5% doped catalyst

In the Figure 4.8 it can be observed the typical peaks corresponding to cerium and oxygen also seen in the previous spectrograms, with the addition of the peaks correspondent to the copper present in the sample.

The zone of the copper doped solid over which this analysis was performed is the following.

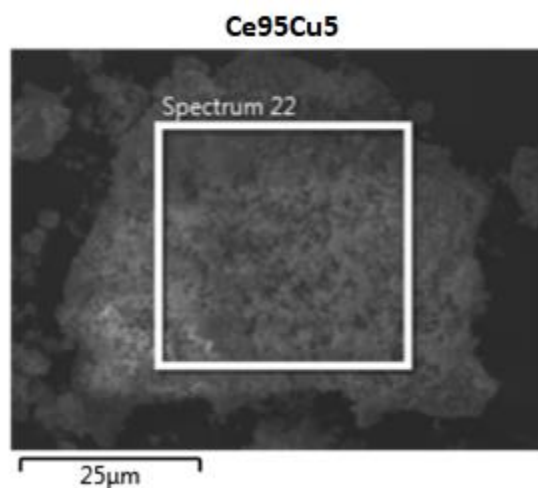


**Figure 4.9** Representative zone taken for the 5% copper doped sample spectrogram

The Figure 4.9 considers the principal features of the copper doped sample and was selected as representative of the set of zones studied with the energy dispersive X-ray spectrometry.

The determined composition for the copper doped sample analyzed is shown in the next table.

**Table 4.3** Average atomic percentage of the copper doped catalyst

Catalyst	Element	Atomic% Media
Ce95Cu5	Ce	31.45
	Cu	2.08
	O	66.47

As well for the copper doped sample, in the results evidenced in the Table 4.3 the ratio between the metals corresponds to the desired composition defined in the sample's synthesis.

### 4.2.3 Surface area and porosity

The results obtained through the surface area and porosity analysis include the nitrogen adsorption isotherms (conducted at  $-196\text{ }^{\circ}\text{C}$ ) and the pore distribution of the catalysts. From this information it was obtained as well, the BET surface area, total cumulative pore volume of the pores between 17 and  $3000\text{ \AA}$  and the average pore width.

The following figure includes the adsorption isotherm and the pore distribution of the synthesized  $\text{CeO}_2$ .

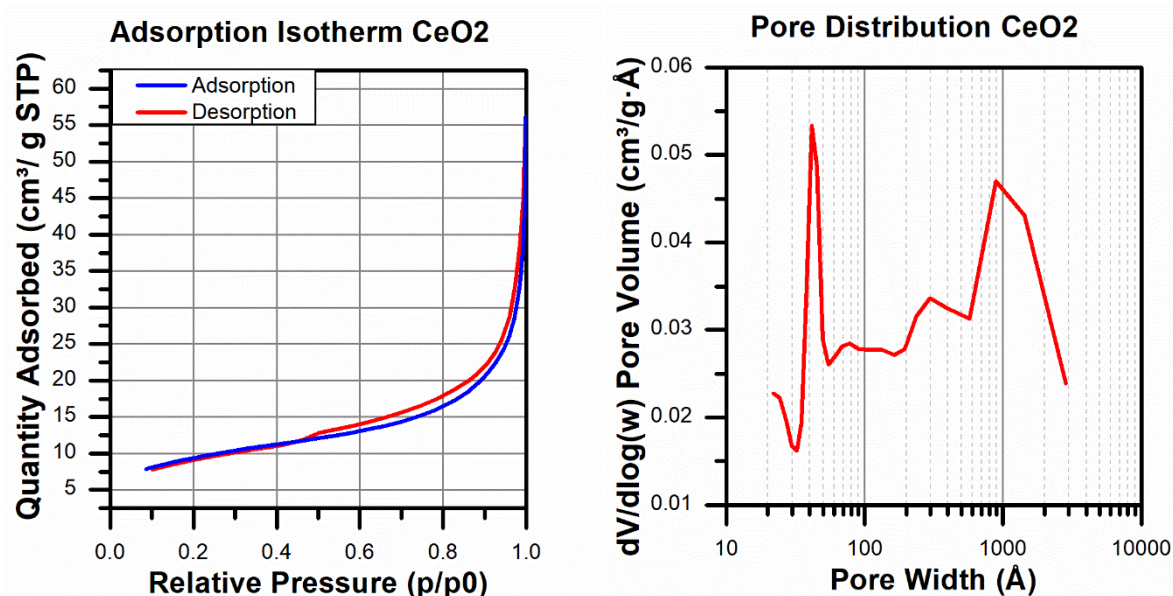


**Figure 4.10** Adsorption isotherm and pore distribution of ceria

The Figure 4.10 shows that the synthesized ceria has a type IV adsorption isotherm. This type corresponds to mesoporous adsorbents, for which the first adsorption occurs on the mesopore walls and then capillary condensation occurs as well [17]. Additionally, the isotherm adsorption is not limited when the pressure equals the vapor pressure, behavior characteristic of plate like particles with pores that are slit shaped. From the pore distribution the seen behavior corresponds to an uneven pore distribution, confirming that the solid possesses pores with a variable pore width.

For  $\text{CeO}_2$ , the determined BET surface area after the analysis was of  $32\text{ m}^2/\text{g}$ , a cumulative volume of pores of  $0.09\text{ cm}^3/\text{g}$  and that the average pore width is equal to  $15\text{ nm}$ .

The following figure shows the obtained adsorption isotherms and pore distribution for the manganese doped solids.

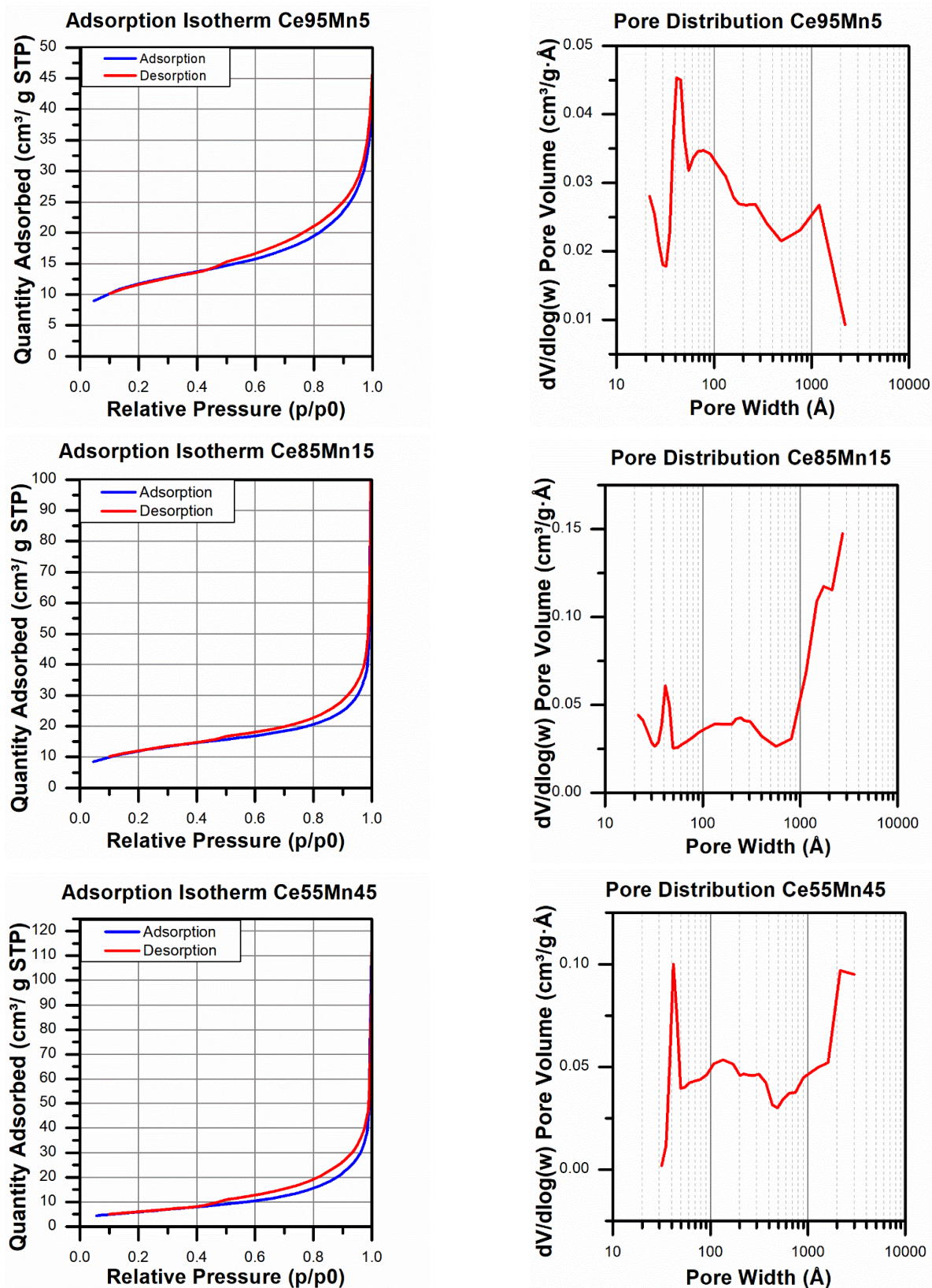


Figure 4.11 Adsorption isotherms and pore distributions of Mn doped catalysts

In the Figure 4.11 it can be seen that the characteristic type IV adsorption isotherm is representative for the manganese doped set of catalysts as for ceria, evidencing non-significant difference in the amounts of nitrogen adsorbed during the test. Yet, these behavior shows that the manganese samples maintain the identical adsorptive properties of ceria.

The next table shows the main characteristics determined through the surface area analysis for the manganese doped solids and the cerium (IV) and manganese (III) oxides synthesized as the reference oxides through the same synthesis method.

**Table 4.4** Surface area, pore volume and average pore width of the Mn doped set

<b>Catalyst</b>	<b>BET Surface Area (m<sup>2</sup>/g)</b>	<b>BJH Pore Volume (cm<sup>3</sup>/g)</b>	<b>BJH Average Pore Width (nm)</b>
CeO <sub>2</sub>	32	0.090	15
Ce <sub>95</sub> Mn <sub>5</sub>	39	0.070	11
Ce <sub>85</sub> Mn <sub>15</sub>	41	0.120	15
Ce <sub>55</sub> Mn <sub>45</sub>	21	0.110	17
Mn <sub>2</sub> O <sub>3</sub>	15	0.109	28

The information in the Table 4.4 evidences a trend of the catalyst's surface area, which is enhanced when the manganese doping is increased, but then when the doping meets its highest value, the surface area decreases even under the value obtained for the ceria.

The pore volume has an uneven trend, which seems to stabilize at the pore volume of the pure manganese oxide while the doping is increased. Finally, for the pore width the samples show no significant variation, and the value is yet between 2 and 50 nm, confirming that the pores present in the solid can be classified as mesopores.

The information of the copper doped catalysts, obtained through the surface and porosity analysis, is shown in the following figure.

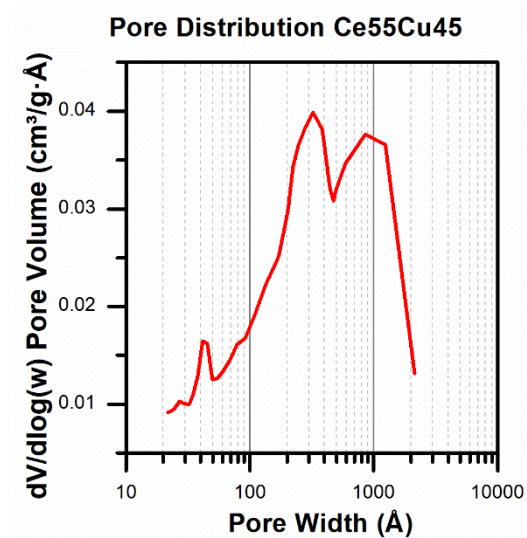
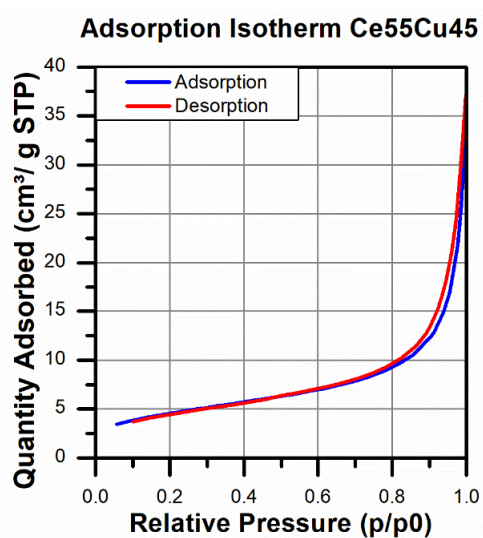
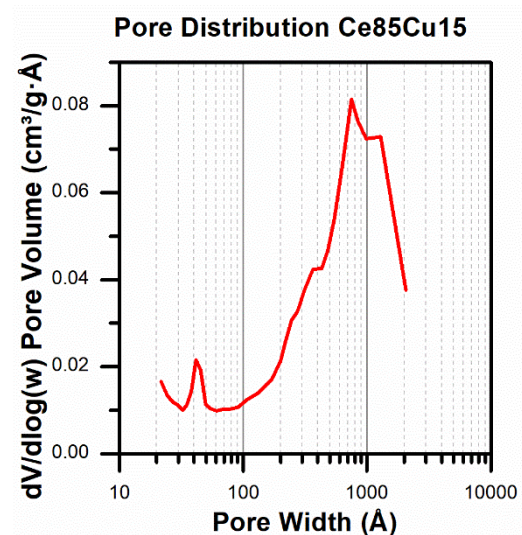
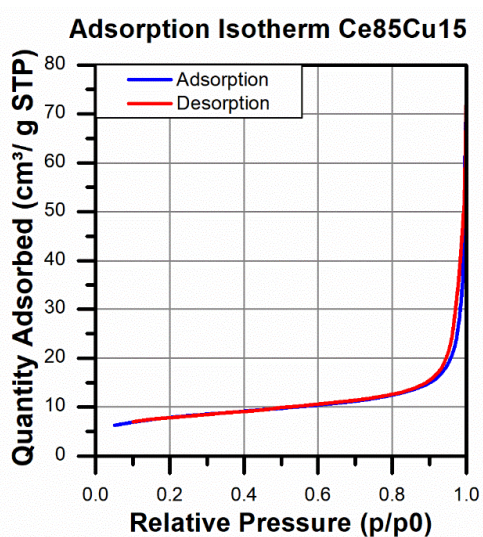
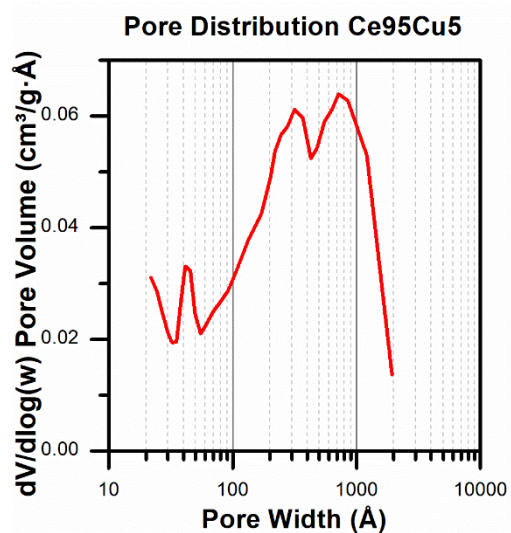
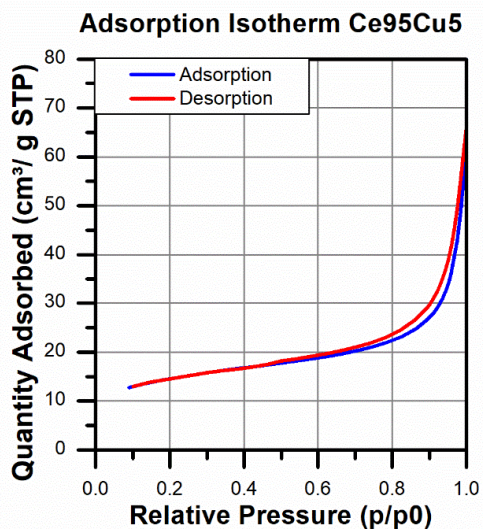


**Figure 4.12** Adsorption isotherms and pore distributions of Cu doped catalysts

The figure 4.12 shows that the copper doped catalysts present a type IV isotherm as well. The adsorbed quantity of nitrogen seems to decrease when the copper doping is increased. The pore distributions of the samples show an even quantity of pores of high and low width, instead the copper 15% doped shows an apparent increase in the number of larger pores, stabilising a normal distribution centered at 70 nm.

In the next table for the copper doped catalysts, and the copper (II) oxide, are evidenced the surface area and other relevant parameters that were determined in the performed analysis.

**Table 4.5** Surface area, pore volume and average pore width of the Cu doped set

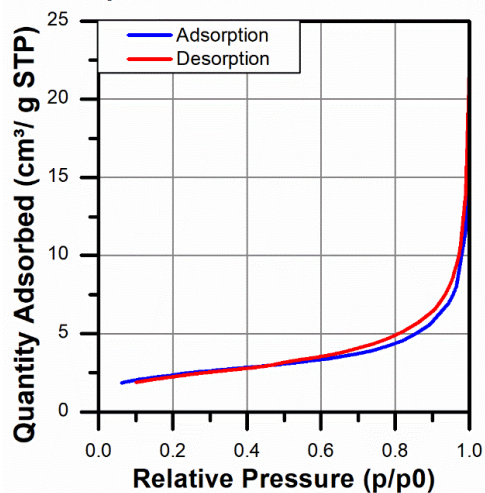
<b>Catalyst</b>	<b>BET Surface Area (m<sup>2</sup>/g)</b>	<b>BJH Pore Volume (cm<sup>3</sup>/g)</b>	<b>BJH Average Pore Width (nm)</b>
CeO <sub>2</sub>	32	0.090	15
Ce <sub>95</sub> Cu <sub>5</sub>	48	0.090	14
Ce <sub>85</sub> Cu <sub>15</sub>	26	0.080	22
Ce <sub>55</sub> Cu <sub>45</sub>	16	0.060	17
CuO	1	0.003	18

The BET surface areas reported in the Table 4.5 show that at the lowest copper doping the surface area is enhanced, but when such content seems to decrease when the copper doping is increased.

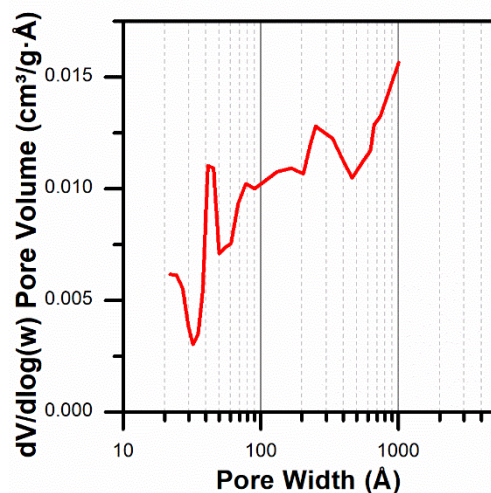
The pore volume shows a decreasing trend when the doping is increased. Only for the 5% copper doped catalyst the pore volume remains identical to the one of ceria, but when such percentage is increased the pore volume of the samples seem to decrease systematically. The information related to the average pore width confirms the behavior seen in the pore distributions, that when the copper content is equal to 15% the number of pores present in the structure are bigger than the ones of the 5% and 45% copper catalysts.

The data obtained from the surface area and porosity analysis performed to the trinary catalysts of cerium, manganese and copper is shown in the following figure.

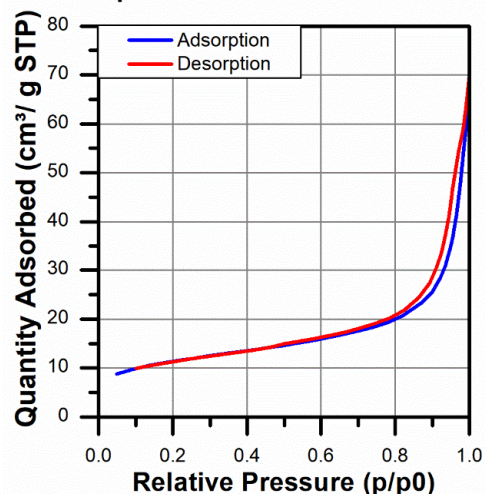
**Adsorption Isotherm Ce95Mn2.5Cu2.5**



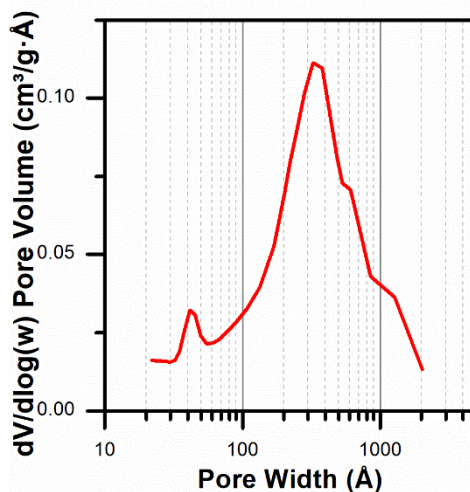
**Pore Distribution Ce95Mn2.5Cu2.5**



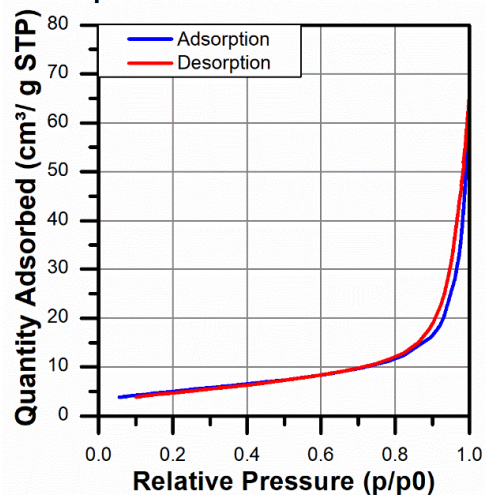
**Adsorption Isotherm Ce85Mn7.5Cu7.5**



**Pore Distribution Ce85Mn7.5Cu7.5**



**Adsorption Isotherm Ce55Mn22.5Cu22.5**



**Pore Distribution Ce55Mn22.5Cu22.5**

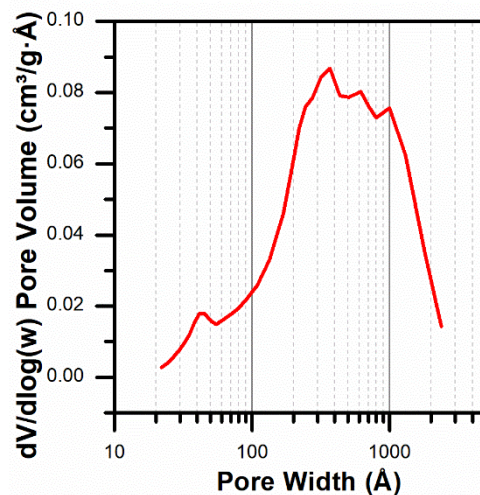


**Figure 4.13** Adsorption isotherms and pore distributions of ternary Ce-Mn-Cu catalysts

The isotherms in the Figure 4.13 evidence that also the ternary catalysts have identical adsorbate-adsorbent interactions of pure ceria, by sharing the same ceria type IV adsorption isotherm with no adsorption limit at pressure equal to the vapor pressure, having then slit type cavities. Such isotherms also show a variation in the nitrogen quantity adsorbed, which is lower for the 5% total doped sample, and for the other two samples (15% and 45%).

The pore distribution in the case of the 5% doped ternary catalyst shows that the number of pores have uneven width, besides the samples with higher content of manganese and copper present normal pore distributions, being the 45% doped the one containing a bigger number of larger pores.

The next table summarizes the determined information in the surfaces area and porosity analysis performed to the ternary catalysts.

**Table 4.6** Surface area, pore volume and average pore width of the ternary catalyst set

<b>Catalyst</b>	<b>BET Surface Area (m<sup>2</sup>/g)</b>	<b>BJH Pore Volume (cm<sup>3</sup>/g)</b>	<b>BJH Average Pore Width (nm)</b>
CeO <sub>2</sub>	32	0.090	15
Ce <sub>95</sub> Mn <sub>2.5</sub> Cu <sub>2.5</sub>	8	0.022	13
Ce <sub>85</sub> Mn <sub>7.5</sub> Cu <sub>7.5</sub>	38	0.100	17
Ce <sub>55</sub> Mn <sub>22.5</sub> Cu <sub>22.5</sub>	18	0.100	24

The information shown in the Table 4.6 evidences that the surface area doesn't follow any specific trend respect to the total content of dopants in the samples but presents a significant variation in the case of the sample with 5% doping. Such behavior may be related to the possibility that the sample is highly crystalline as it was discussed in the section 4.2.1, where the crystallite size of the sample was found to be extraordinary bigger than the ones of the other samples.

In the case of the average pore width, an increasing trend can be seen when the total doping is bigger, confirming the behavior previously seen in the pore distribution of these samples.

The general trend of the BET surface area for every catalyst, shown in the previous tables is resumed in the next figure.

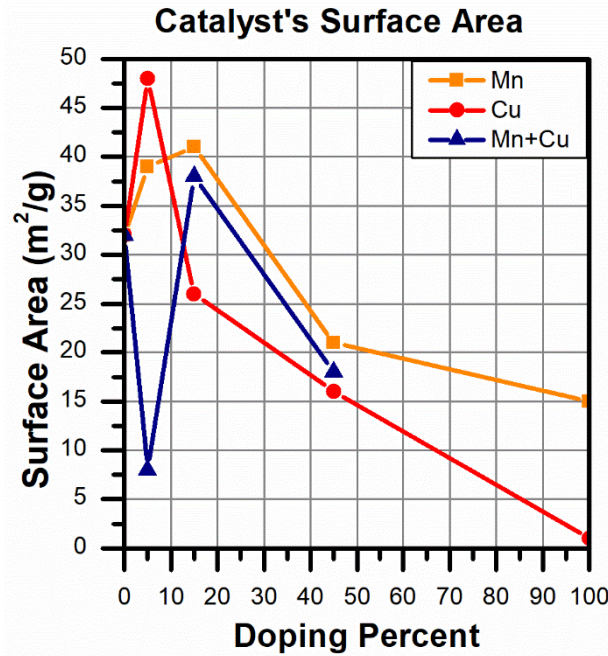


Figure 4.14 Catalyst's surface area

As it can be seen in the Figure 4.14 the binary oxides follow a general trend, at which a little quantity of dopant enhances a higher surface area respect to ceria, and while the dopant percentage is increased the SSA seems to reach a maximum and starts decreasing. The general behavior seems to be applied for the trinary oxides, except for the 5% sample, which surface area is lower than the one of ceria.

This test was also performed to the aged catalysts with a doping percentage of 45% of each series, to evidence an eventual variation of the specific surface area caused by high temperatures for a long time (750 °C, 4 hours). Such results are shown in the next table.

Table 4.7 Specific surface area of fresh and aged 45% doped binary and trinary catalysts

Catalyst	BET Surface Area (m <sup>2</sup> /g)	
	Fresh	Aged
Ce55Mn45	21	8
Ce55Cu45	16	7
Ce55Mn22.5Cu22.5	18	8

The information in the Table 4.7 confirms that the catalysts' surface area may reduce when these are subject to elevated temperatures for long times.

#### 4.2.4 Temperature programmed reduction ( $H_2$ -TPR)

The results obtained from the  $H_2$ -temperature-programmed reduction includes the value of the intensity measured by the thermal conductivity detector (TCD) in function of the temperature and the total or partial consumption of hydrogen according to species that were reduced. The samples chosen for testing were the ones that resulted to be the most active in the catalytic oxidation tests, therefore the 45% doped sample of each series.

The next figure shows the reduction peaks obtained for the manganese doped sample and the reference samples, ceria and manganese (III) oxide.

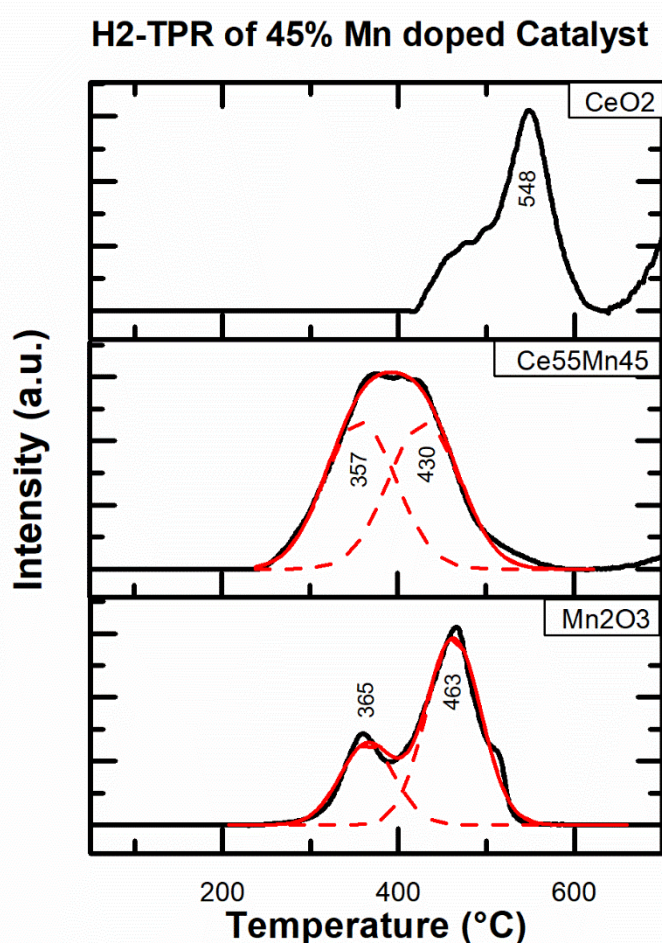


**Figure 4.15**  $H_2$ -Temperature programmed reduction of the 45% manganese doped ceria

The Figure 4.15 evidences the hydrogen consumption of three samples. The first is the consumption corresponding to the reduction of ceria. This sample exhibits a wide reduction peak centered at 548 °C, which is attributed to reduction of surface oxygen, subsurface oxygen

and the surface cerium reduction ( $\text{Ce}^{4+} \rightarrow \text{Ce}^{3+}$ ) [26], while the increasing peak located over 700 °C is attributed to the reduction of the bulk cerium.

In the case of the manganese (III) oxide the characteristic peak is deconvoluted in two peaks, the first one occurring at 365 °C attributed to the reduction of  $\text{Mn}_2\text{O}_3 \rightarrow \text{Mn}_3\text{O}_4$ , and the second centered at 463 °C corresponding to the reaction  $\text{Mn}_3\text{O}_4 \rightarrow \text{MnO}$  [27]

The statistical deconvolution made for the manganese 45% doped ceria's peaks shows two peaks. The first peak is centered at 357 °C and may be attributed to the reduction of the surface adsorbed oxygen of the mixed Mn-Ce oxide, and the second which is centered at 430 °C may correspond to the reduction of the surface lattice oxygen of the mixed oxide. Additionally, over 700 °C there is evidenced a developing reduction peak, such reduction is attributed to the reduction of the bulk oxygen. [28]

The next figure evidences the reduction peaks obtained for the 45% copper doped ceria, together with the relevant reference pure oxides.

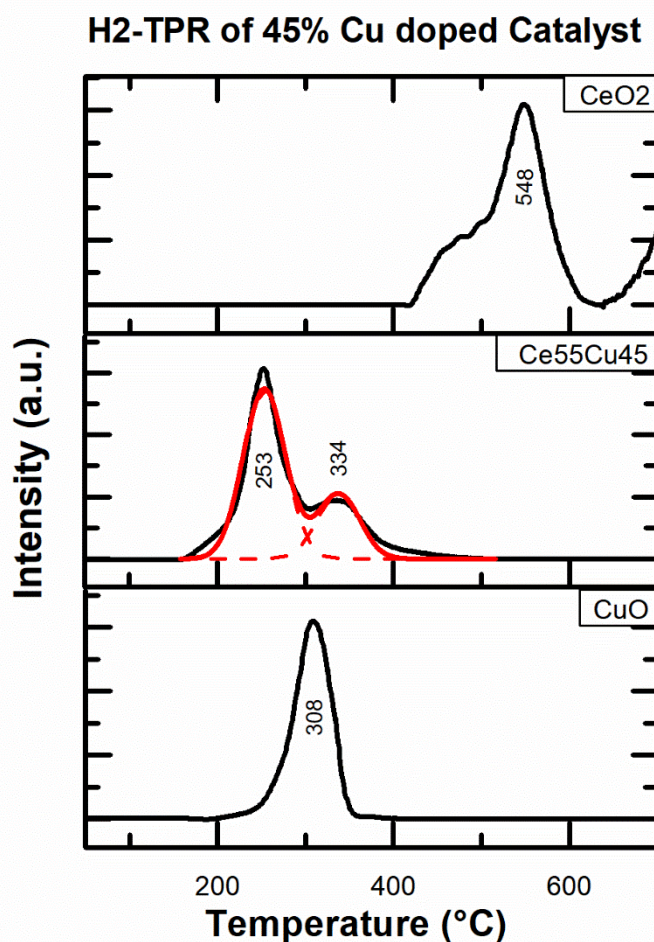


**Figure 4.16** H<sub>2</sub>-Temperature programmed reduction of the 45% copper doped ceria

The Figure 4.16 evidences the reduction peak of the pure copper (II) oxide centered at 308 °C, while for the 45% copper doped catalyst, the statistical approximation shows two interacting peaks at 253 °C and at 334 °C. The low temperature peak may be related to the reduction of CuO clusters interacting with ceria, while the second peak occurring at a higher temperature is attributed to the copper oxide well dispersed in the oxide. By watching the area of the copper oxide clusters' peak, it is noticeable that their hydrogen consumption is higher than the one related to the reduction of the lattice oxygen [25].

The next figure evidences the measured reduction capacity of the 45% doped trinary catalyst.

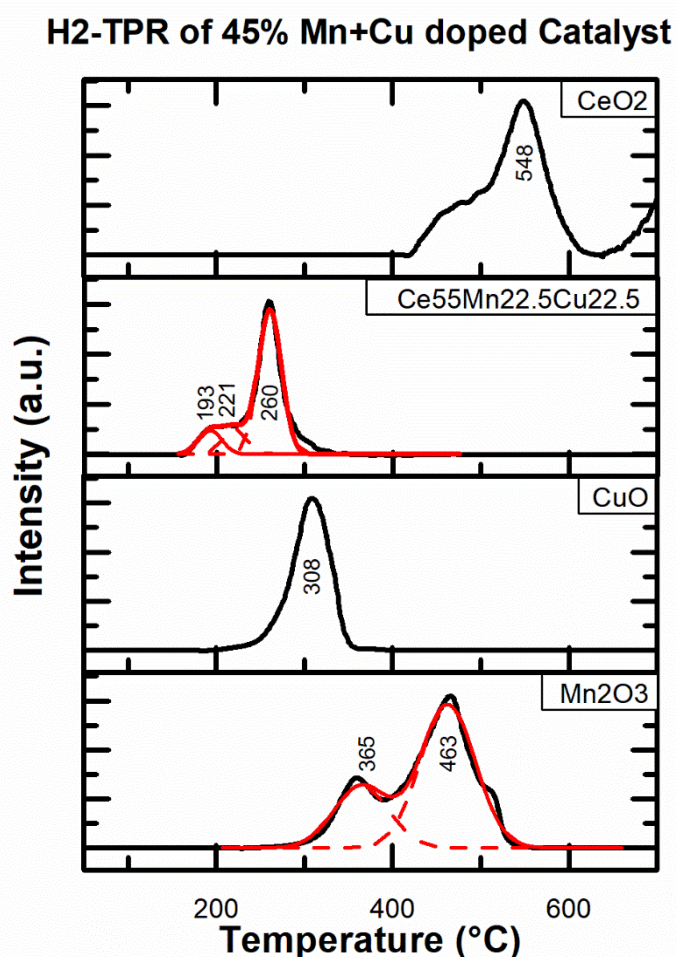


**Figure 4.17** H<sub>2</sub>-Temperature programmed reduction of the 55% Mn+Cu doped ceria

The reduction profiles seen in the Figure 4.17 for the mixed doped ceria shows an ensemble of peaks at around 200 °C. After deconvolution, the peak was divided in three, the

low temperature one that occurs at 193 °C may be attributed to the presence of copper oxide clusters interacting with the species present in the sample, what makes them be reduced at a lower temperature respect to the pure oxide [25]. The second peak can be attributed to the presence of copper-manganese oxide ( $\text{Cu}_{1.5}\text{Mn}_{1.5}\text{O}_4$ ) clusters present in the sample, this specie interacting with the mixed ceria structure is reduced at around 221 °C [29]. Finally, the peak centered at 260 °C may be attributed to the reduction of the lattice oxygen of the mixed ceria structure.

The next table evidences the hydrogen consumption correspondent to the species present in the studied samples.

**Table 4.8** H<sub>2</sub>-TPR catalysts' hydrogen uptake

Catalyst	Temp. Peak 1 (°C)	Peak 1 H <sub>2</sub> -Uptake (mmol/gcat)	Temp. Peak 2 (°C)	Peak 2 H <sub>2</sub> -Uptake (mmol/gcat)	Temp. Peak 3 (°C)	Peak 3 H <sub>2</sub> -Uptake (mmol/gcat)	Total H <sub>2</sub> -uptake (mmol/gcat)
CeO <sub>2</sub>	548	0.18					0.18
Ce <sub>55</sub> Mn <sub>45</sub>	357	0.93	430	0.93			1.86
Ce <sub>55</sub> Cu <sub>45</sub>	253	2.17	334	0.83			3.01
Ce <sub>55</sub> Mn <sub>22.5</sub> Cu <sub>22.5</sub>	193	0.29	221	0.31	260	1.74	2.33
Mn <sub>2</sub> O <sub>3</sub>	365	1.81	463	4.17			5.98
CuO	308	12.57					12.57

Table 4.8 shows the hydrogen consumption correspondent to the 45% doped sample of each set, and their base oxides. It evidences the reducibility order of the bulk oxygen of the samples, which according to the type of doping follows the following reduction trend: Trinary catalyst > Mn doped catalyst > Cu doped catalyst.

Additionally, it shows the reducibility of oxygen from eventual oxides clusters in the trinary and in the copper doped ceria, being the latter the one with the highest hydrogen uptake among these two. This indicates that copper may induce the mixed ceria structure to release oxygen easily, or at least more than manganese.

### 4.3 Catalytic oxidation tests

In the following section are presented the results obtained from the thermal catalytic tests performed with the synthesized samples. Such tests were performed either with the fresh and aged catalysts and in two different oxygen concentration conditions.

#### 4.3.1 Temperature programmed oxidation at 10%-vol of $O_2$

##### 4.3.1.1 “Fresh” catalysts

The performed tests were organized according to the oxidized VOC and to the doping element, therefore these were classified as follows:

- Oxidation of propylene

The next figure shows the propylene conversion of the manganese doped catalysts and the respective reference oxides.

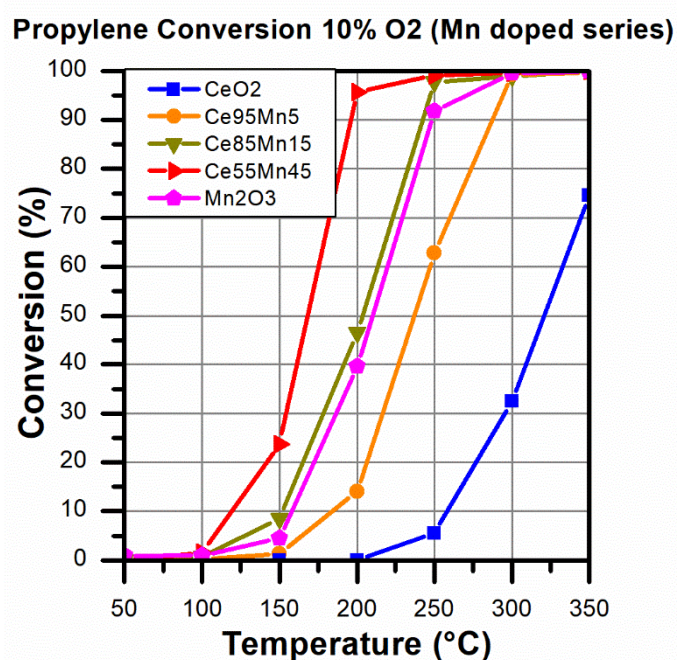


**Figure 4.18** Propylene conversion on Mn-doped catalysts in 10%  $O_2$  concentration

The Figure 4.18 evidences an increasing trend of the oxidative activity when the manganese doping content is increased, reaching the highest activity when the manganese doping percentage is equal to 45%. The 5% doped catalyst conversion shows that little quantities of manganese dispersed in the ceria structure improve the catalytic activity, reaching to convert all the propylene by 300 °C and thereby showing an evident synergy between cerium and manganese ions. Such fact may be related to the enhancing of oxygen release and storage characteristic of ceria when the metals are introduced in the lattice [30].

The next figure shown the conversion of propylene over the copper doped catalysts and the correspondent references.

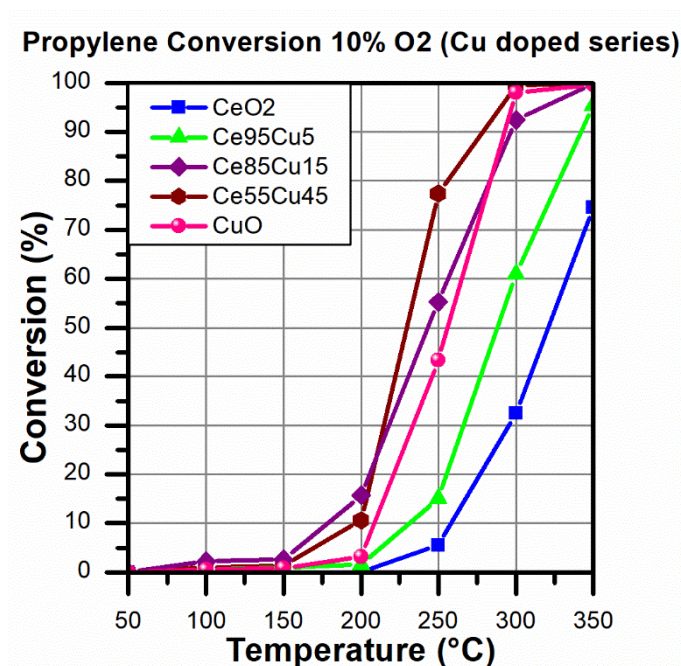


**Figure 4.19** Propylene conversion on Cu-doped catalysts in 10% O<sub>2</sub> concentration

In the Figure 4.19 it can be observed that as well for the copper doping, the catalytic activity of ceria is enhanced by the addition of copper atoms in the sample's lattice, favoring a synergetic activity between the present metal ions. Such activity improves to the point that the 45% doped sample converts the total amount of propylene by 300 °C. This may be attributed to the effectiveness of the Mars-van Krevelen reaction mechanism that occurs between the interacting phases of copper and cerium [25].

The next figure shows the catalytic performance of the trinary samples in the realized tests.

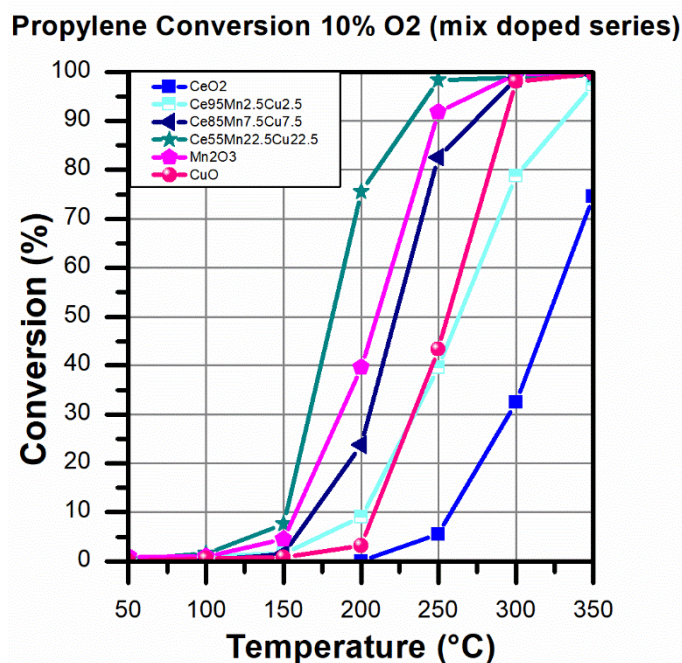


**Figure 4.20** Propylene conversion on trinary catalysts in 10% O<sub>2</sub> concentration

The Figure 4.20 evidences for the mixed doped ceria, that the catalytic activity is improved when the doping percentage is increased, being the 45% doped more active than pure CuO and the manganese (III) oxide. This fact indicates that also in this case the species present in the catalyst interact among themselves and improve the oxidative performance.

A detail that can be observed through further analysis is the fact that when ceria is doped at 15% with a single or coupled metals, the catalytic activity is either paired or very close to the one of the pure oxides.

From the analysis of the Figures 4.18, 4.19 and 4.20, it can be noticed that the most active catalyst in the oxidation of propylene is the binary sample Ce-Mn, followed by the trinary catalyst. Merging the information, it can be said that the manganese species may enhance more the catalytic activity of ceria, respect to copper species, when oxidizing propylene.

- Oxidation of ethylene

When ethylene was used as the VOC probe molecule the catalytic performance of the samples was qualitatively similar to the oxidation of propylene, but in general the performance of the catalysts was reduced because of the chemical nature of ethylene, that gives the molecules a lower reactivity compared to propylene.

The next figure shows the ethylene conversion of the manganese doped catalysts and the respective reference oxides.

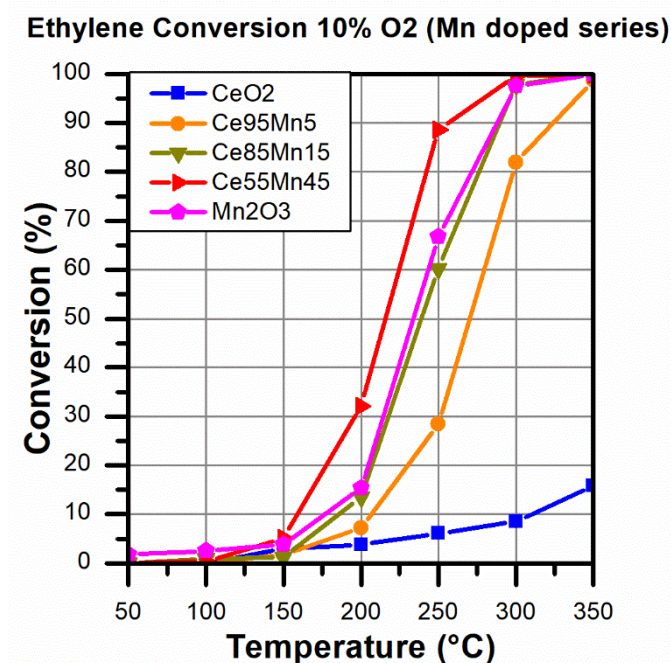


**Figure 4.21** Ethylene conversion on Mn-doped catalysts in 10% O<sub>2</sub> concentration

The catalytic behavior seen in the Figure 4.21 shows an increasing trend when the manganese doping percentage is risen. Showing that the doping of manganese also improves ceria catalytic activity towards ethylene's oxidation, reaching 100% conversion at 350 °C with only 5% of doping percentage. This behavior indicates that the occurring synergy between the metals also takes place when the VOC is changed, thereby indicating that this improved performance may take place with different types of VOC.

In comparison with Figure 4.18, the lowest temperature at which the VOC conversion is total has increased of at least 100 °C, always for the 45% manganese doped

ceria and also in this case the oxidative activity of the manganese 15% doped ceria is paired to the one of pure manganese (III) oxide.

The following figure shows the catalytic performance of the Cu-doped samples towards ethylene oxidation.

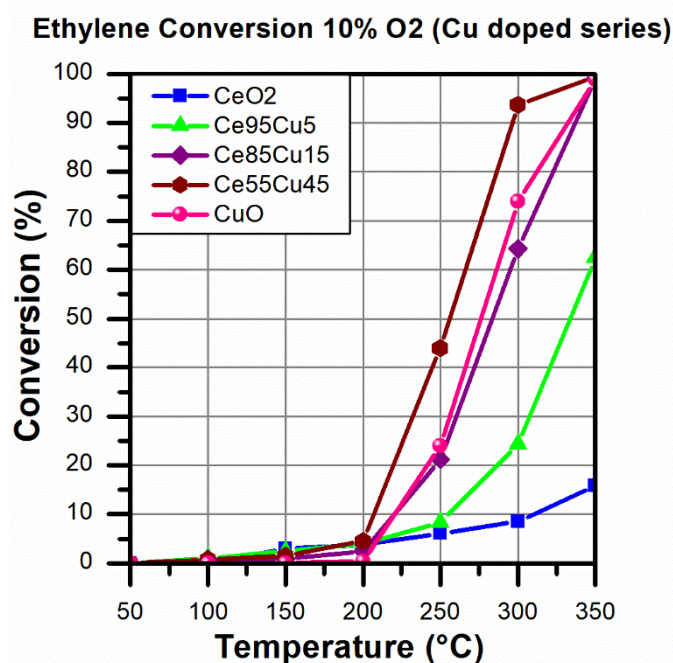


**Figure 4.22** Ethylene conversion on Cu-doped catalysts in 10% O<sub>2</sub> concentration

In the Figure 4.22 it is evidenced the previous increasing behavior of the oxidative activity when the copper content is increased, like in the case of propylene oxidation, with the difference that the total VOC conversion for the best catalyst is reached at 300 °C instead of 250 °C.

Additionally, it can be noticed that, as it has been seen for previous tests, only when the copper doping percentage is higher than 15% the catalytic behavior of the sample is better than the one of pure copper (II) oxide.

The next figure shows the catalytic performance of the ternary catalysts when the temperature programmed oxidation of ethylene was performed.

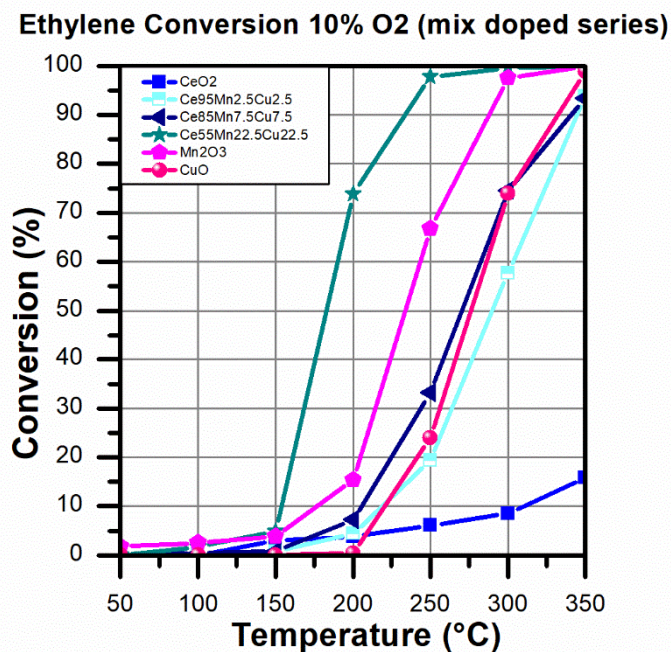


**Figure 4.23** Ethylene conversion on trinary catalysts in 10% O<sub>2</sub> concentration

The Figure 4.23 shows that also in the case of the trinary catalysts, the catalytic oxidation of ethylene is also enhanced when the doping percentage is higher. The 45% doped catalysts show to be the most active between this set of samples, being more active than the pure manganese oxide. Such behavior indicates that the species present in the 45% doped sample may enhance the catalytic activity, by the interactions that take place among them and the mixed ceria lattice.

In this case, and in the catalytic oxidation of propylene as well, the trinary catalyst with 15% doping the ceria lattice reaches an intermediate catalytic activity between the one of manganese (III) oxide and copper (II) oxide.

After further analysis of the Figures 4.21, 4.22 and 4.23, it was observed that the most active catalyst in the oxidation of ethylene is the 45% trinary Ce-Mn-Cu doped sample, followed by the Ce-Mn binary catalyst, also this at 45% doping. Realized this, it can be said that the species present in the ternary catalyst enhance the catalytic oxidation of ethylene, thereby the coupled presence of manganese-copper oxide crystals, together with copper oxide clusters enhance the activity of ceria towards the oxidation of ethylene.

To resume the most relevant details of the catalytic activity, the next figure shows the temperatures at which the conversion is approximately 10%, 50% and 90%, for the most active sample of each set, so the 45% doped in the oxidation of ethylene and propylene.

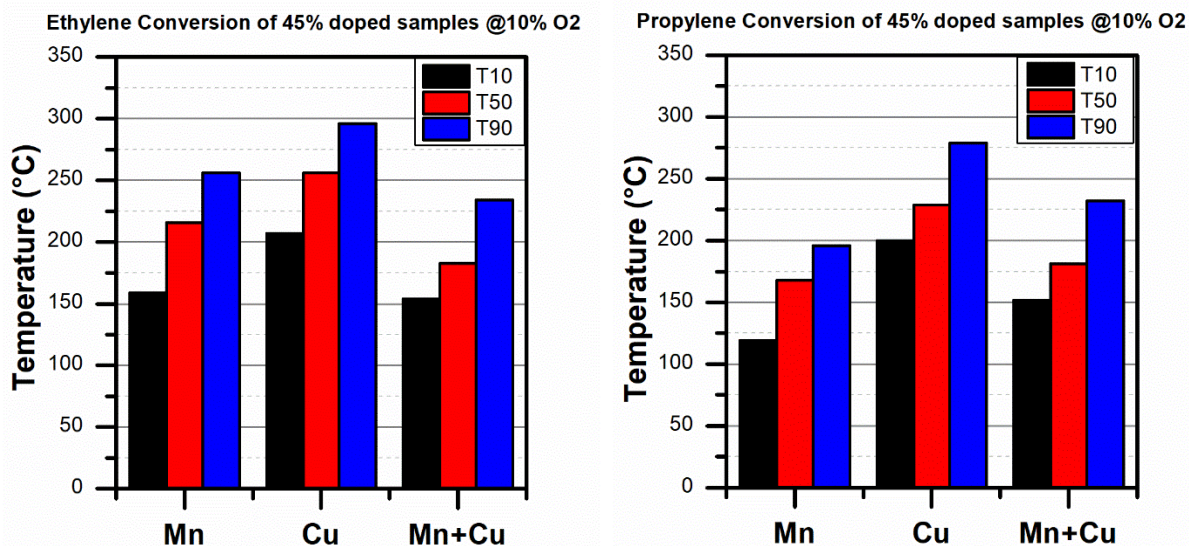


**Figure 4.24** T<sub>10%</sub>, T<sub>50%</sub> and T<sub>90%</sub> of the 45% at. doped catalysts in VOC oxidation

Figure 4.24 evidences that the most active catalysts are the ones containing manganese oxides species, because manganese manages to increase the catalytic activity of the ceria lattice when they are coupled, and also when it interacts with copper and/or cerium when they are all together in a single structure.

Additionally, the performance of the best catalysts was studied and the reaction rates per unit of surface area were calculated. These are presented in the next table.

**Table 4.9** Average reaction rates of the most active catalysts for VOC oxidation

Catalyst	r (mmol/h*m <sup>2</sup> )
	Ethylene
Ce55Mn45	0.53
Ce55Cu45	0.24
Ce55Mn22.5Cu22.5	0.69

The reaction rates shown in the Table 4.9 evidence the average reaction rates of the synthesized powders, normalized according to their surface area. Taking ethylene as a representative molecule for most VOCs, it can be said that the presence of manganese species in the lattice of ceria enhances the catalytic activity, and when it forms mixed species with copper, these improve even more the redox capacity of the catalyst [25,27,29].

### 4.3.1.1 “Aged” catalysts

The following figure shows the catalytic activity of the most active catalysts during the performance of the thermal catalytic oxidation.

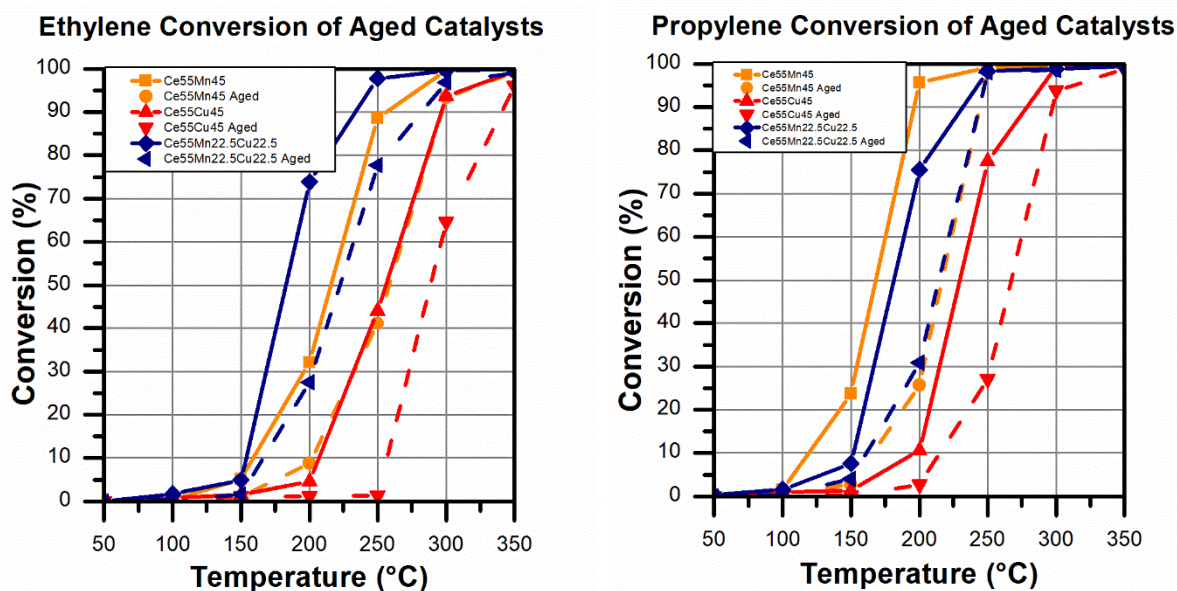


**Figure 4.25** Conversion comparison of the 45% at. doped aged catalysts, during VOC oxidation test at 10% O<sub>2</sub> volume-concentration

The catalytic behaviors seen in the Figure 4.25 evidence that after the catalysts were subject to aging at 750 °C for 4 hours their activity for the VOC catalytic oxidation is reduced. All the catalysts evidenced an important decrease in the conversions reached at the same temperatures either for ethylene or propylene oxidation.

This worsening of the samples' activity may be attributed to the reduction of the specific surface area after the aging treatment. These areas were reduced at least in a 56%, as it was evidenced in the section 4.2.3 of this work. Such reduction diminishes the active sites disposed in the sample to perform the oxidation of the VOC.

The evidenced behavior can also be related to a sintering process that may have taken place by the elevated temperature during the aging process. This would cause an increase of the crystallinity and a reduction of the oxygen defects, as it indicates the narrower peaks seen in the XRD studies performed to the aged samples, and thereby cause the reduction of the oxygen storage capacity of the catalyst as well [13,24].

### 4.3.2 Temperature programmed oxidation at 1%-vol of O<sub>2</sub>

The resulting conversions obtained during the catalytic oxidations performed with an oxygen volume-concentration of 1% are shown in the following figure.

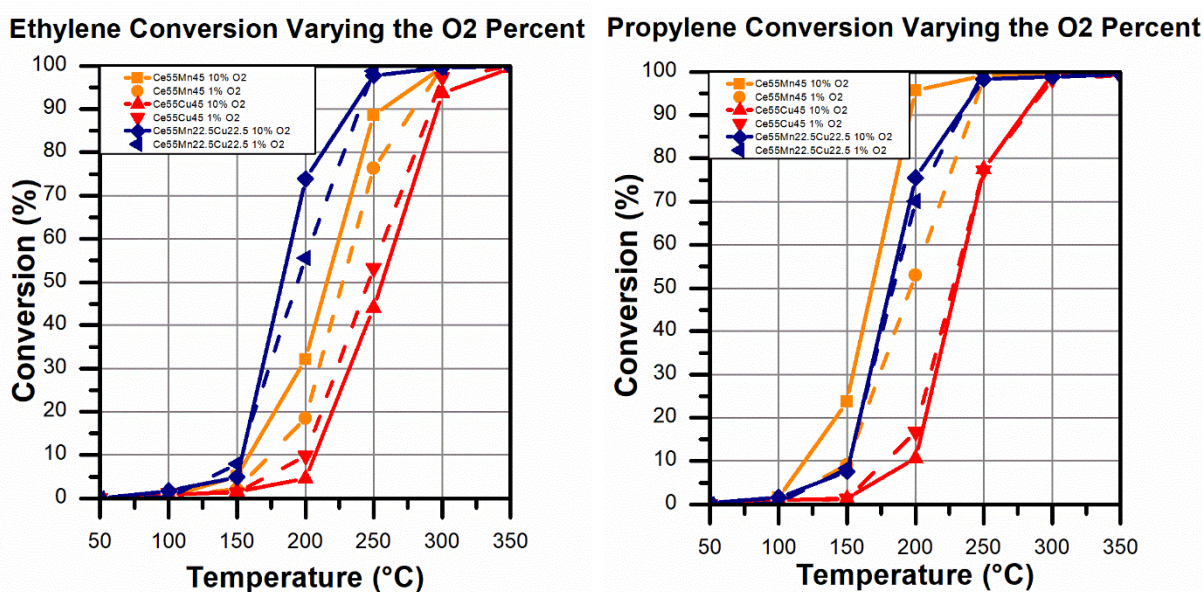


**Figure 4.26** Conversion comparison of the 45% at. doped aged catalysts, during VOC oxidation test at 1% O<sub>2</sub> volume-concentration

The conversions shown in the Figure 4.26 evidences a general trend, at which the activity of the catalysts is slightly reduced when the available oxygen in the reactive mix is reduced to 1%-vol. This results open a wide range of possibilities, for example it may indicate that under this conditions the VOC reaction rate may depend on the partial pressure of oxygen in the reaction mix, and consequently that the rate determining step might be or the adsorption of oxygen of the sample if this followed a Lagnmuir-Hinshelwood mechanism, or the surface reaction if the mechanism was Eley-Rideal type. To determine the veracity of such affirmations, it would be necessary to perform a kinetic study under this particular condition. However, since the mechanism reaction for ceria and doped ceria has been found to follow the one proposed by Mars-van Krevelen in previous research studies and bibliography [25,28,29], another possibility would be that the specific partial pressure of oxygen in the system affects its incorporation in the crystal structure [13], thereby reducing its oxygen storage capacity and eventually its later release when the catalytic oxidation is carried on.

In the case of propylene's oxidation, a substantial activity change is verified only for the manganese doped ceria, while for the other catalysts the activity remains virtually unchanged. Therefore, the analysis of the oxygen concentration's effect, as for VOCs in general was based on the results obtained for ethylene's oxidation.

Analyzing the results of the catalytic activity it can be noticed that only in one case there is a slightly improvement of the catalytic activity when the volume concentration of oxygen in the reaction flow is reduced, this is for the copper doped sample. This fact indicates that under lean oxygen conditions the copper-cerium mixed lattice may be able to release oxygen easier, in comparison to oxygen rich conditions. Such behavior could be associated with the results obtained in the temperature programmed reduction studies, where the copper doped sample showed to be the one most reducible among the tested catalysts under reducing conditions.

## CONCLUSIONS

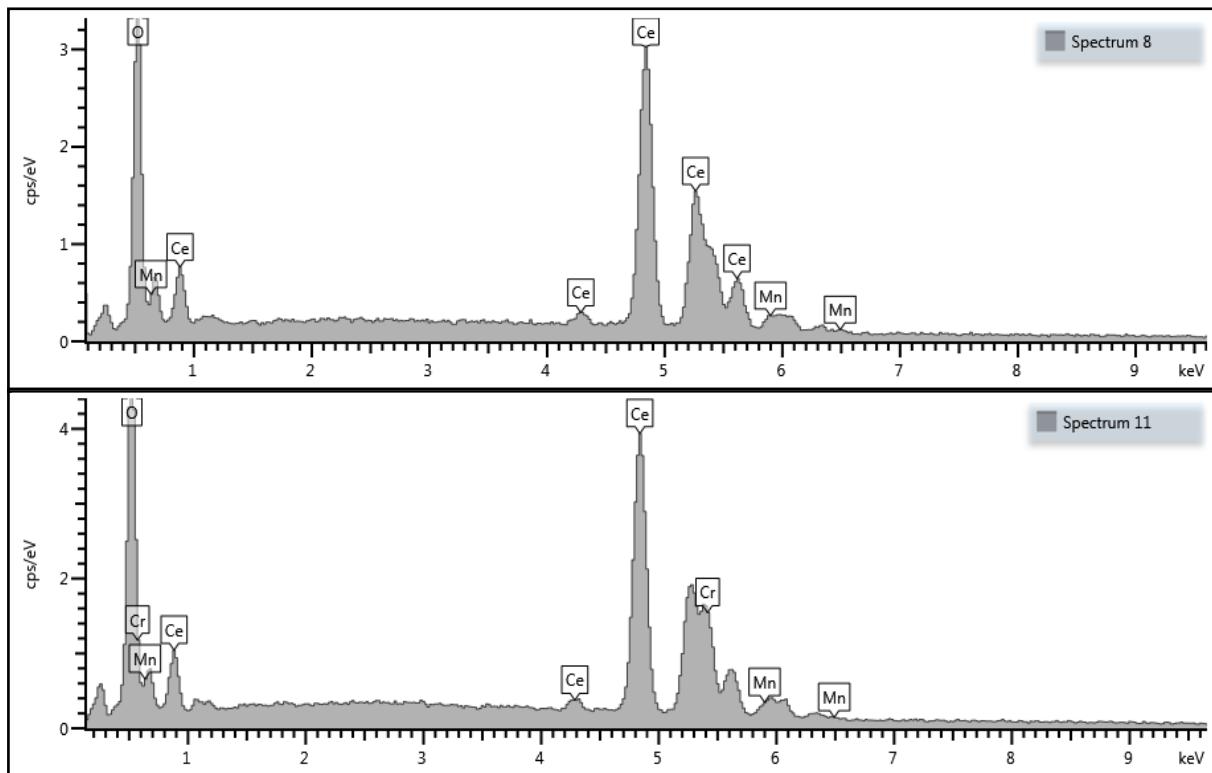
In this thesis work there was realized the study of the performance of binary and ternary (Cu and Mn) cerium mixed oxides with different Ce-to-metal ratios synthesized through solution combustion method, in the catalytic oxidation of ethylene and propylene. After study, research, and analysis over such catalytic performance and its relationship to the main physicochemical characteristics of the catalysts, the conclusions of this experimental thesis work are the following:

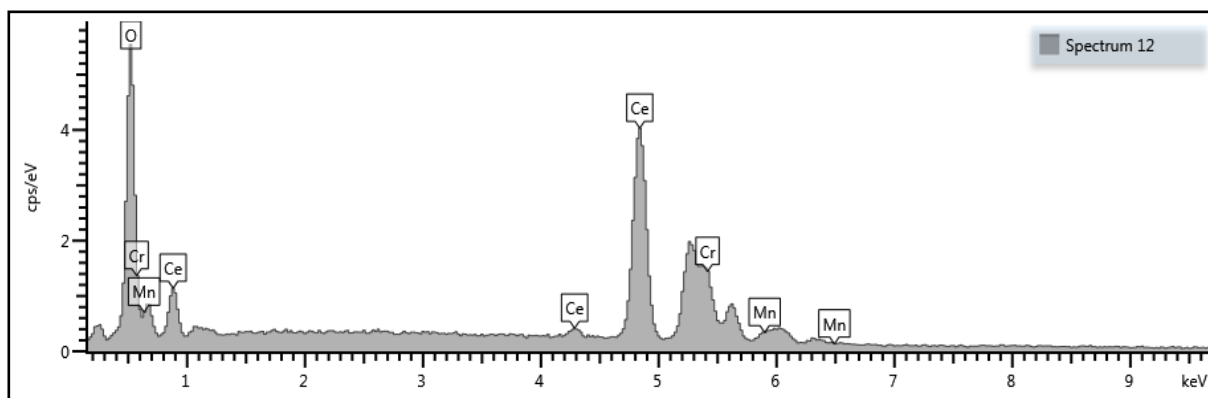
- Manganese and/or copper were effectively introduced in the ceria lattice through the solution combustion synthesis.
- The addition of manganese and/or copper in ceria's lattice may decrease the crystallite size of the catalyst and increase its quantity of oxygen defects.
- The increase of copper and/or manganese doping percentage may promote the formation of pure and mixed metal clusters during the synthesis.
- Manganese and/or copper doping improves the reducibility of ceria's structure.
- The increase of the doping metal percentage enhances the activity of ceria in the catalytic oxidation of VOCs.
- According to the doping percentage, binary Ce-Mn catalysts showed to be the most active in the oxidation of propylene.
- According to the doping percentage, ternary Ce-Mn-Cu catalysts showed to be the most active in the oxidation of ethylene.
- Manganese containing catalysts showed the best catalytic performances respect to the one doped with copper.
- The synthesized mixed oxides may not be stable in high temperatures environments for prolonged times.
- The catalytic activity of the manganese doped catalysts can be reduced in lean oxygen conditions.
- The activity of copper doped catalysts may to improve in lean oxygen conditions

## APPENDIX

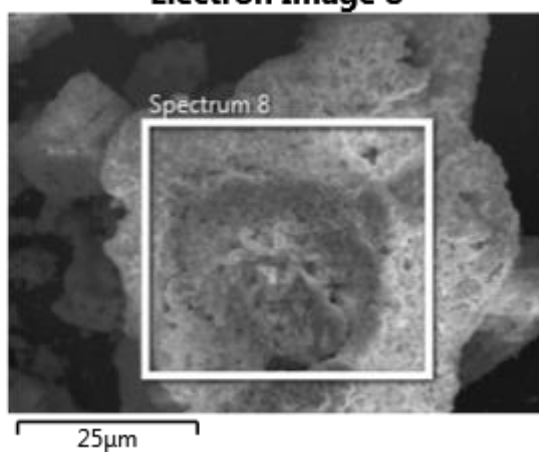
In this appendix the most important physical characteristics of the synthesized catalysts are listed, together with the complete zones studied in the EDS analysis.

- CeO<sub>2</sub>
  - Surface Area Analysis
    - BET surface area: 32 m<sup>2</sup>/g.
    - BJH desorption cumulative volume of pores (between 17 and 3000 Å width): 0.09 cm<sup>3</sup>/g.
    - BJH desorption average pore width (4V/A): 15 nm.
    - Type IV adsorption isotherm
    - Structure type: Slits
- Mixed oxide of Ce<sub>95</sub>Mn<sub>5</sub>
  - Surface Area Analysis
    - BET surface area: 39 m<sup>2</sup>/g.
    - BJH desorption cumulative volume of pores (between 17 and 3000 Å width): 0.07 cm<sup>3</sup>/g.
    - BJH desorption average pore width (4V/A): 11 nm.
    - Type IV adsorption isotherm
    - Structure type: Slits
  - EDS

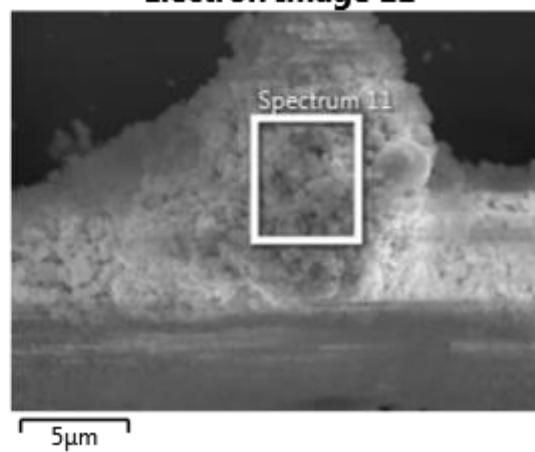




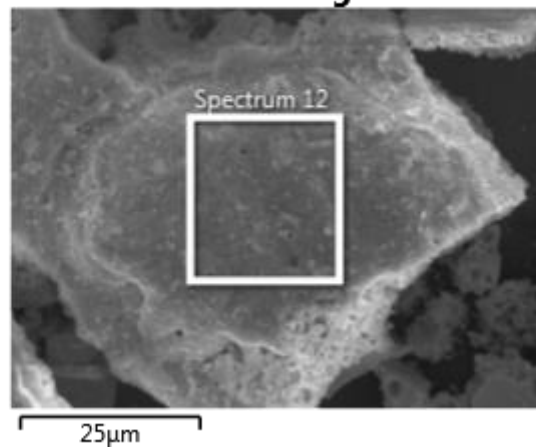
**Electron Image 8**



**Electron Image 11**

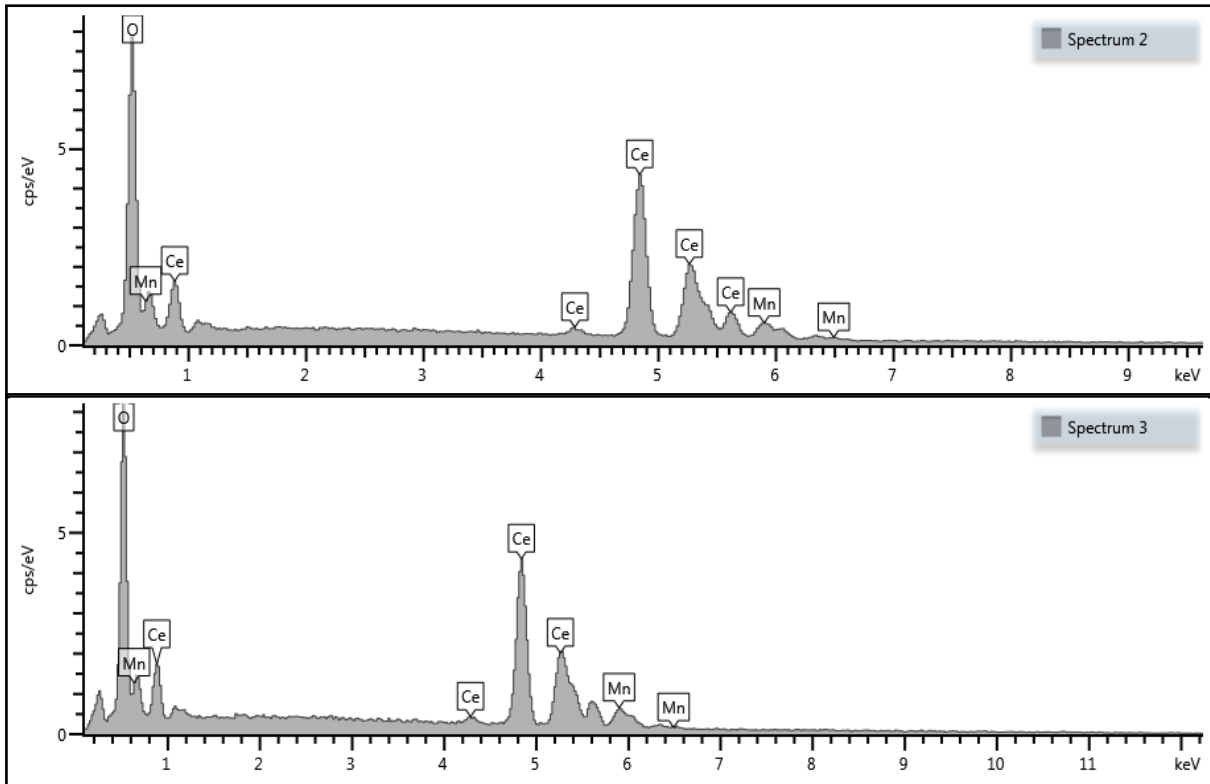


**Electron Image 12**

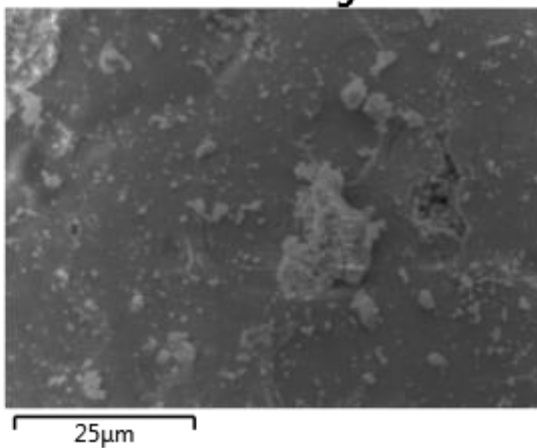


Catalyst	Element	Atomic% Media
Ce95Mn5	Ce	31.20
	Mn	1.83
	O	66.97

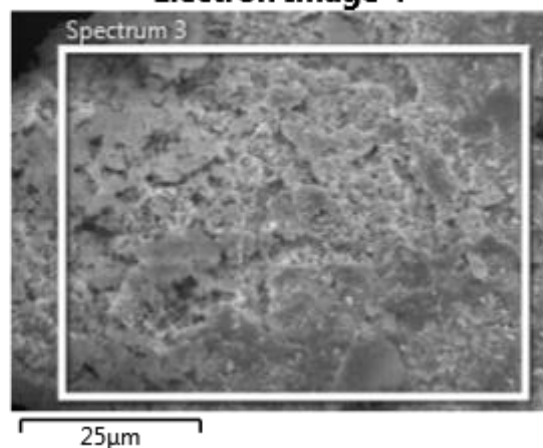
- Mixed oxide of  $\text{Ce}_{85}\text{Mn}_{15}$ 
  - Surface Area Analysis
    - BET surface area:  $41 \text{ m}^2/\text{g}$ .
    - BJH desorption cumulative volume of pores (between 17 and  $3000 \text{ \AA}$  width):  $0.12 \text{ cm}^3/\text{g}$ .
    - BJH desorption average pore width ( $4V/A$ ): 15 nm.
    - Type IV adsorption isotherm
    - Structure type: Slits
  - EDS



**Electron Image 3**

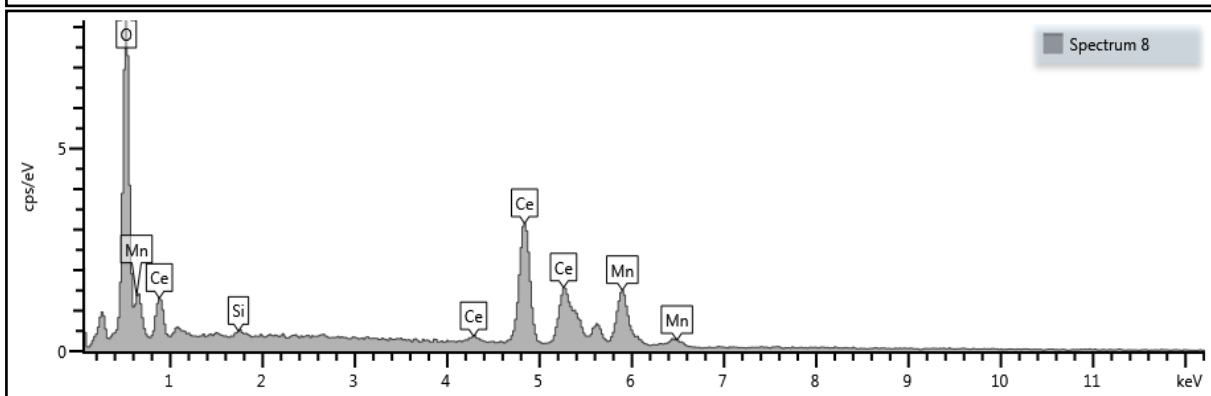
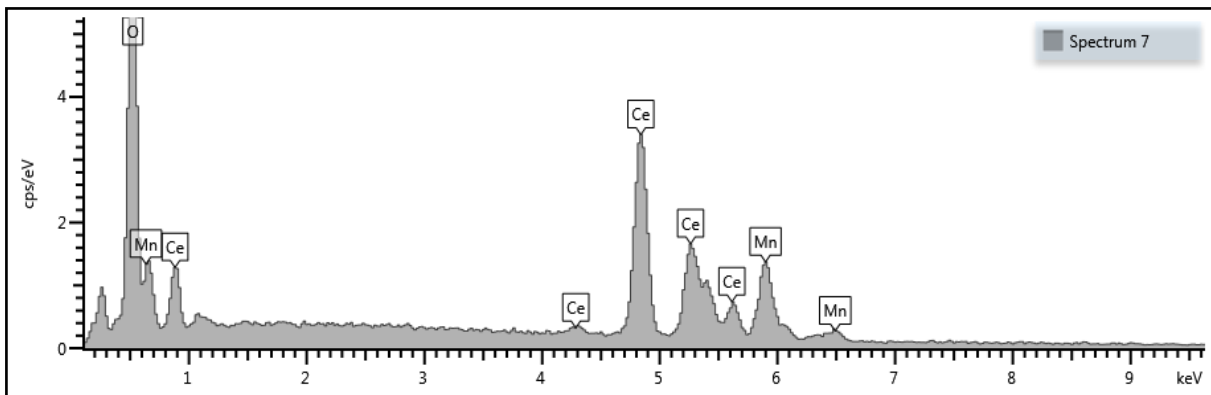


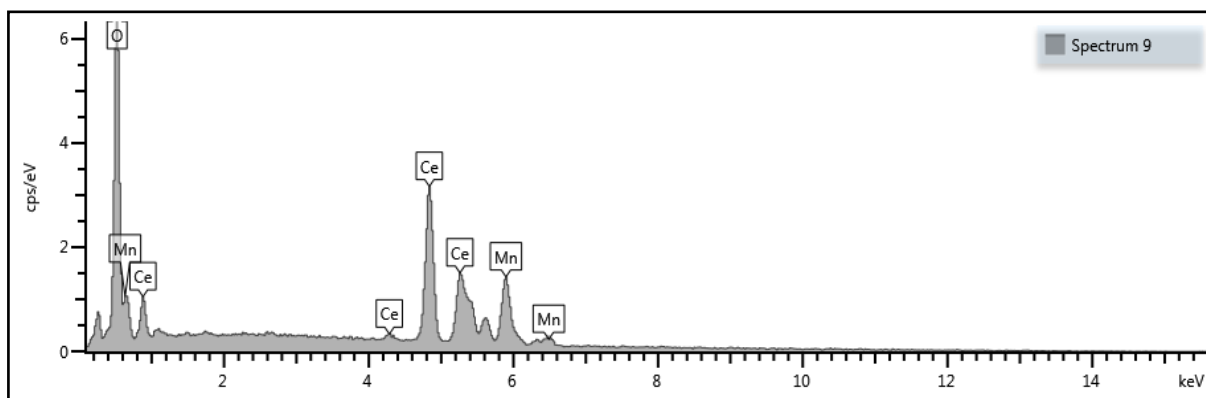
**Electron Image 4**



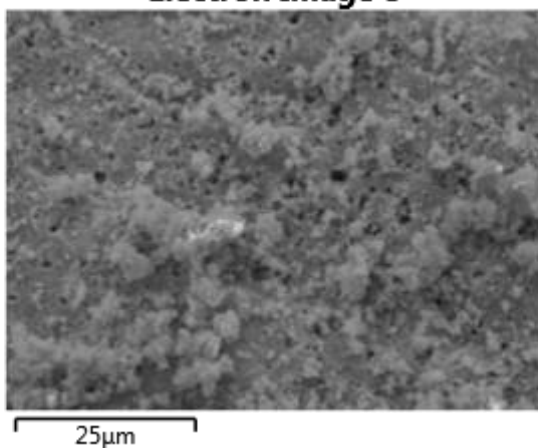
Catalyst	Element	Atomic% Media
Ce85Mn15	Ce	23.88
	Mn	3.67
	O	72.46

- Mixed oxide of Ce<sub>55</sub>Mn<sub>45</sub>
  - Surface Area Analysis
    - BET surface area: 21 m<sup>2</sup>/g.
    - BJH desorption cumulative volume of pores (between 17 and 3000 Å width): 0.11 cm<sup>3</sup>/g.
    - BJH desorption average pore width (4V/A): 17 nm.
    - Type IV adsorption isotherm
    - Structure type: Slits
- EDS

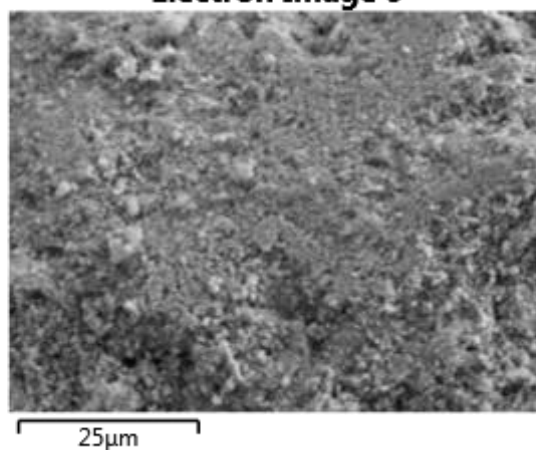




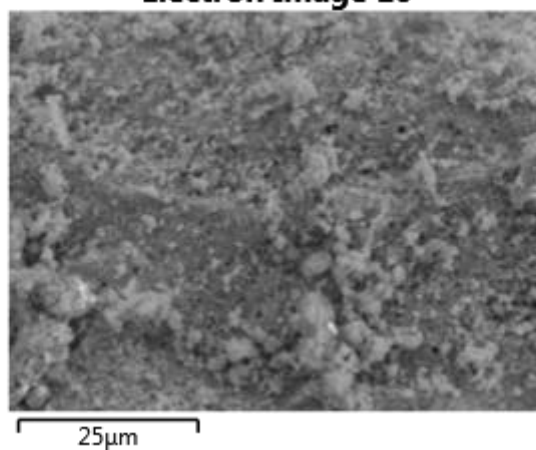
**Electron Image 8**



**Electron Image 9**

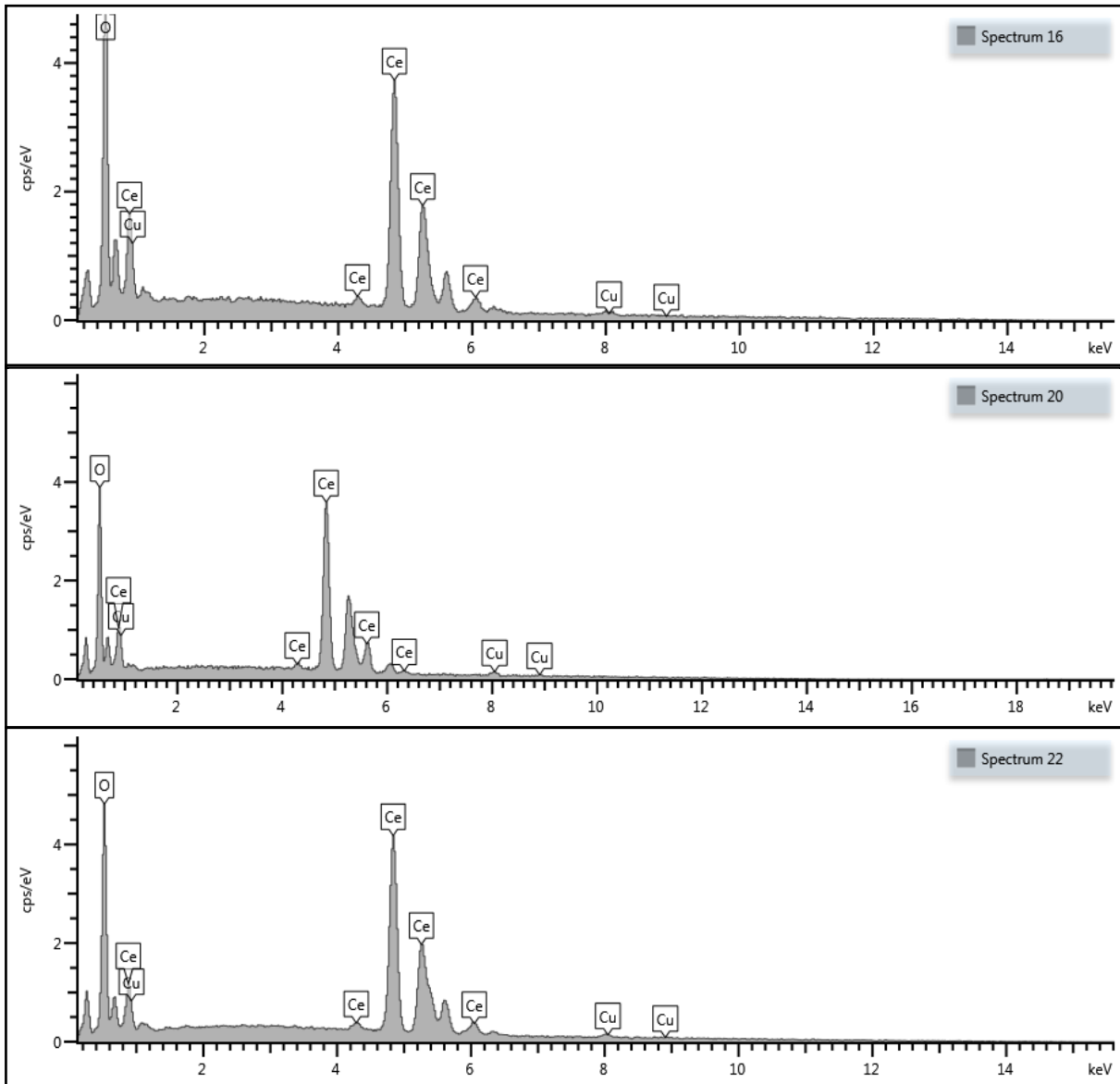


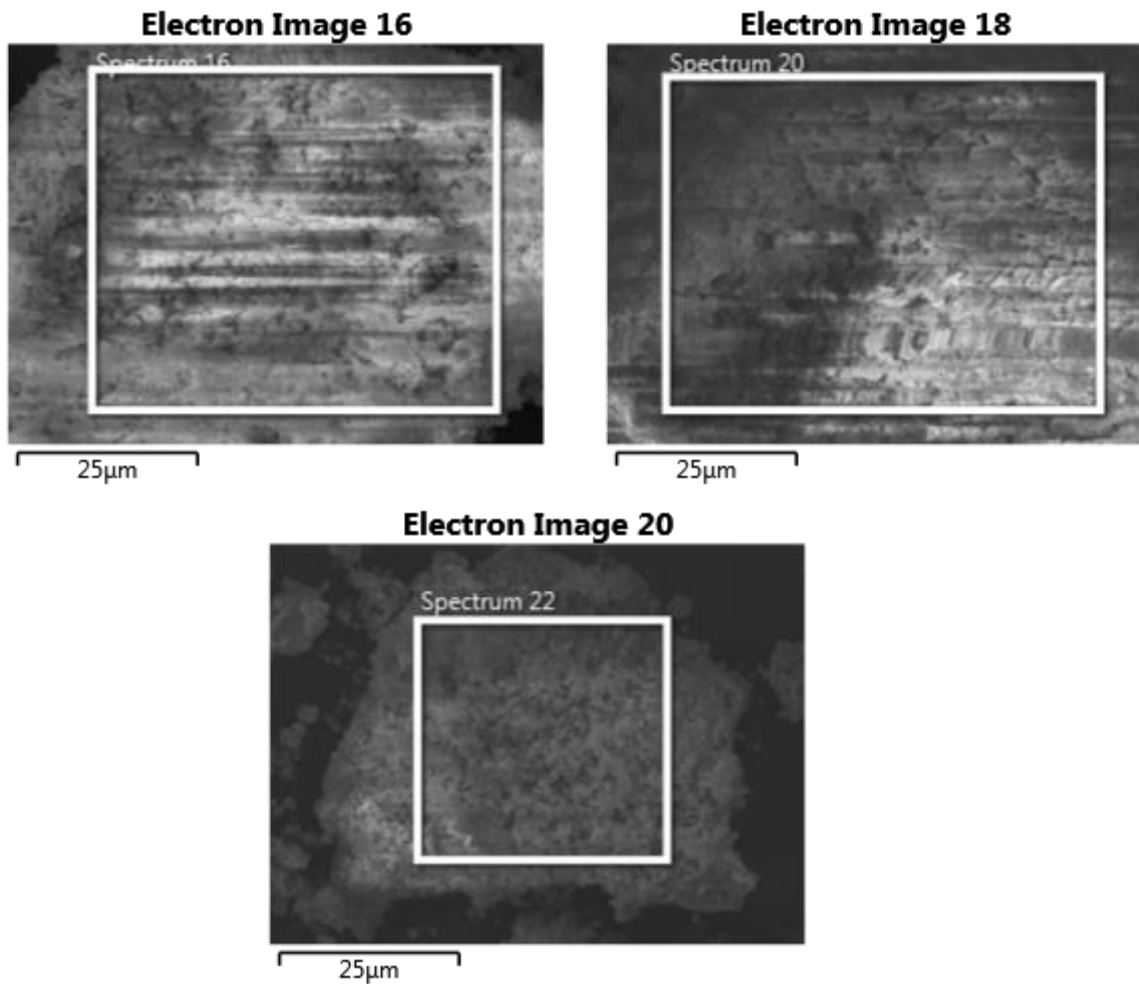
**Electron Image 10**



Catalyst	Element	Atomic% Media
Ce55Mn45	Ce	18.07
	Mn	12.10
	O	69.64

- Mixed oxide of  $Ce_{95}Cu_5$ 
  - Surface Area Analysis
    - BET surface area:  $48 \text{ m}^2/\text{g}$ .
    - BJH desorption cumulative volume of pores (between 17 and  $3000 \text{ \AA}$  width):  $0.09 \text{ cm}^3/\text{g}$ .
    - BJH desorption average pore width ( $4V/A$ ): 14 nm.
    - Type IV adsorption isotherm
    - Structure type: Slits
  - EDS





Catalyst	Element	Atomic% Media
Ce95Cu5	Ce	31.45
	Cu	2.08
	O	66.47

- Mixed oxide of  $Ce_{85}Cu_{15}$ 
  - Surface Area Analysis
    - BET surface area:  $26 \text{ m}^2/\text{g}$ .
    - BJH desorption cumulative volume of pores (between 17 and  $3000 \text{ \AA}$  width):  $0.08 \text{ cm}^3/\text{g}$ .
    - BJH desorption average pore width ( $4V/A$ ): 22 nm.
    - Type IV adsorption isotherm
    - Structure type: Slits
- Mixed oxide of  $Ce_{55}Cu_{45}$ 
  - Surface Area Analysis
    - BET surface area:  $16 \text{ m}^2/\text{g}$ .

- BJH desorption cumulative volume of pores (between 17 and 3000 Å width): 0.06 cm<sup>3</sup>/g.
  - BJH desorption average pore width (4V/A): 17 nm.
  - Type IV adsorption isotherm
  - Structure type: Slits
- Mixed oxide of Ce<sub>95</sub>Mn<sub>2.5</sub>Cu<sub>2.5</sub>
  - Surface Area Analysis
    - BET surface area: 8 m<sup>2</sup>/g.
    - BJH desorption cumulative volume of pores (between 17 and 3000 Å width): 0.022 cm<sup>3</sup>/g.
    - BJH desorption average pore width (4V/A): 13 nm.
    - Type IV adsorption isotherm
    - Structure type: Slits
- Mixed oxide of Ce<sub>85</sub>Mn<sub>7.5</sub>Cu<sub>7.5</sub>
  - Surface Area Analysis
    - BET surface area: 38 m<sup>2</sup>/g.
    - BJH desorption cumulative volume of pores (between 17 and 3000 Å width): 0.10 cm<sup>3</sup>/g.
    - BJH desorption average pore width (4V/A): 17 nm.
    - Type IV adsorption isotherm
    - Structure type: Slits
- Mixed oxide of Ce<sub>55</sub>Mn<sub>22.5</sub>Cu<sub>22.5</sub>
  - Surface Area Analysis
    - BET surface area: 18 m<sup>2</sup>/g.
    - BJH desorption cumulative volume of pores (between 17 and 3000 Å width): 0.10 cm<sup>3</sup>/g.
    - BJH desorption average pore width (4V/A): 24 nm.
    - Type IV adsorption isotherm
    - Structure type: Slits

## BIBLIOGRAPHY

- [1] Electronic Code of Federal Regulations, <https://www.ecfr.gov/cgi-bin/text-idx?SID=9f2ffa73f1b399778c0c38af954be221&mc=true&node=sp40.2.51.f&rgn=div6>, e-CFR data is current as of January 25, 2018, Visited on 29/01/18
- [2] Official Journal of the European Communities, <http://eur-lex.europa.eu/legal-content/EN/TXT/PDF/?uri=CELEX:32004L0042&from=EN>, 30/04/2004. Visited on 01/02/18
- [3] Koppmann, R (2007). *“Volatile Organic Compounds in the Atmosphere”*. Oxford. Blackwell Publishing Ltd.
- [4] Control Techniques for Volatile Organic Compound Emissions from Stationary Sources. U.S. Environmental Protection Agency. Office of Air and Radiation. North Carolina 1992
- [5] Moretti, E.C. (June 2002), *“Reduce VOC and HAP Emissions”*. CEP Magazine.
- [6] Chorkendorff, I. and Niemantsverdriet, J. W (2003). *“Concepts of Modern Catalysis and Kinetics”*. Weinheim. WILEY-VCH Verlag GmbH & Co. KGaA.
- [7] Piumetti, M and Russo, N. (2017) *“Notes on Catalysis for Environment and Energy”*. Turin. C.L.U.T.
- [8] Scott Fogler, H (1999). *“Elements of Chemical Reaction Engineering”*. Third edition. New Jersey. Prentice-Hall, Inc.
- [9] IUPAC (1982). *“Reporting Physisorption Data for Gas/Solid Systems”*. Great Britain. K.S.W. Sing. Pergamon Press.
- [10] David Jackson, S and Hargreaves, Justin S. J. (2009). *“Metal Oxide Catalysis”*. Weinheim. WILEY-VCH Verlag GmbH & Co. KGaA.
- [11] Sheldon, R.A. and van Santen, R.A. (1995). *“Catalytic Oxidation Principles and Applications”*. Singapore. World Scientific Publishing Co. Pte. Ltd.
- [12] Study and modelling of kinetics of the oxidation of VOC catalyzed by nanosized Cu–Mn spinels prepared via an alginate route. S. Behar, et al., Appl. Catal. A: Gen. (2014), <http://dx.doi.org/10.1016/j.apcata.2014.12.021>.
- [13] Trovarelli, A (2002). *“Catalysis by Ceria and Related Materials”*. London. Imperial College Press.
- [14] Manganese oxide catalysts synthesized by exotemplating for the total oxidation of ethanol. S.S.T. Bastos et al., Appl. Catal. B: Env. (2009).
- [15] Catalytic oxidation of toluene over binary mixtures of copper, manganese and cerium oxides supported on  $\gamma$ -Al<sub>2</sub>O<sub>3</sub>. S. Saqer et. al., Appl. Catal. B: Env. (2011).
- [16] Burton, J and Garten, R. (1977). *“Advanced Materials in Catalysis”*. U.S.A. Academic Press, Inc.
- [17] Ertl, G, Knoezinger, H, Schueth, F. and Weitkamp, J. (2008). *“Handbook of Heterogeneous Catalysis”*. Weinheim. WILEY-VCH Verlag GmbH & Co. KGaA.

- [18] Corain, B, Schmid, G and Toshima, N. (2008) *“Metal Nanoclusters in Catalysis and Materials Science: The Issue of Size Control”*. Amsterdam. Elsevier B.V.
- [19] Kazmiruk, V. (2012). *“Scanning Electron Microscopy”*. Rijeka. InTech Europe.
- [20] Novel Synthesis and Characterization of Nanostructured Materials. A. Kopp Alves et. al. Springer-Verlag Berlin. Heidelberg 2013.
- [21] Solution combustion synthesis of nanomaterials. A. Mukasyan et. al. Elsevier. Science Direct. Notre Dame 2007.
- [22] Fundamentals, properties and applications of solid catalysts prepared by solution combustion synthesis (SCS). S. Gonzalez-Cortes et. al. Appl. Catal. A: Gen. (2013).
- [23] Effect of doping rare earth oxide on performance of copper-manganese catalysts for water-gas shift reaction. R. He, et al. Elsevier. Science Direct. (2013).
- [24] Relationship between surface area and crystal size of pure and doped cerium oxides. C. Bueno-Ferrer, et al. Elsevier. Science Direct. (2010).
- [25] Cerium-copper oxides prepared by solution combustion synthesis for total oxidation reactions: From powder catalysts to structured reactors. M. Piumetti et al. Appl. Catal. B: Env. (2016).
- [26] A new insight into morphology effect of ceria on CuO/CeO<sub>2</sub> catalysts for CO selective oxidation in hydrogen-rich gas. X. Guo, R. Zhou. Catal. Sci. Technol. (2015).
- [27] Mesoporous manganese oxides prepared by solution combustion synthesis as catalysts for the total oxidation of VOCs. M. Piumetti et al. Appl. Catal. B: Env. (2015).
- [28] Effects of Mn-doped ceria oxygen-storage material on oxidation activity of diesel soot. Huang et al. RSC Adv. (2017).
- [29] Cu-Mn-Ce ternary mixed-oxide catalysts for catalytic combustion of toluene. H. Lu et al. Elsevier. Science Direct. (2015).
- [30] Abatement of toluene from polluted air over Mn/clinoptilolite-CeO<sub>2</sub> nanopowder: Impregnation vs. ultrasound assisted synthesis with various Mn-loading. L. Yosefi et al. Advanced Powder Technology (2015)

## Figures

- [1] Micromeritics. <http://www.micromeritics.com/Product-Showcase/TriStar-II-Series/TriStar-II-Series2.aspx>
- [2] New Atlas. <https://newatlas.com/merlin-electron-microscope/12145/>